"SELF-CLEANING" HYDROGEL MEMBRANES FOR FULLY IMPLANTABLE GLUCOSE BIOSENSORS

A Dissertation

by

PING DONG

Submitted to the Graduate and Professional School of
Texas A&M University
in partial fulfillment of the requirements for the degree of

DOCTOR OF PHILOSOPHY

Chair of Committee,	Melissa A. Grunlan
Committee Members,	Akhilesh K.Gaharwar
	Daniel L. Alge
	Victor Ugaz
Head of Department,	Michael J. McShane

December 2021

Major Subject: Biomedical Engineering

ABSTRACT

Continuous glucose monitors (CGMs) that permit real-time tracking of glucose levels have the potential to vastly improve diabetes management. The membrane used to construct an optical glucose sensor must address challenges related to assay retention, glucose diffusivity, and minimizing the foreign body reaction (FBR). In this work, thermosensitive, double network (DN) hydrogel membranes based on *N*-isopropyl-acrylamide (NIPAAm) were designed. With a tuned volume phase transition temperature (VPTT), membranes are expected to "self-clean" via cyclical deswelling/reswelling with body temperature fluctuations.

In a first study, the membrane mesh size was reduced with a comb architecture, towards eventual formation of a biosensor with a förster resonance energy transfer (FRET)-based glucose sensing assay. A tightly cross-linked first network was comprised of NIPAAm copolymerized with negatively charged 2-acrylamido-2-methylpropane sulfonic acid (AMPS), and a loosely cross-linked second network was formed from NIPAAm copolymerized with *N*-vinylpyrrolidone (NVP). Combs of varying charges, lengths, and concentrations were introduced to the first network. Able to achieve the targeted mesh size (~1-3 nm), negatively charged combs were the most effective in reducing mesh size, attributed to electrostatic repulsive forces.

In a second study, a membrane was customized to directly embed a phosphorescence sensing assay based on an oxygen-sensitive metalloporphyrin (HULK) and glucose oxidase (GOx). The membrane's first network was prepared from NIPAAm

and cationic (3-acrylamidopropyl)trimethylammonium chloride (APTAC). The second network was formed with NIPAAm copolymerized with acrylamide (AAm). Anionic HULK was retained via electrostatic attractive forces while the GOx was covalently bonded via a glutaraldehyde linker. A membrane achieved the desired increase in phosphorescence lifetime with increasing glucose concentrations from 50 to 200 mg/dL. A lack of sensitivity at higher glucose levels was attributed to membrane oxygen depletion.

In a final study, to improve the glucose sensitivity of the phosphorescence assay at higher glucose levels, a membrane with improved oxygen permeability was prepared by incorporation of silicone microdroplets. A ultrasonicate processor was used to disperse the silicone phase during formation of the first network and the second network was comprised of P(NIPAAm-*co*-AAm). With the optimal concentration of silicone microdroplets, glucose sensitivity was observed for concentrations from 100 to 300 mg/dL.

DEDICATION

To My Parents

Thank you for all the love & support as always.
And bearing the hysterical me.

ACKNOWLEDGEMENTS

I would like to, firstly and mostly, thank my chair Prof. Melissa Grunlan for bearing with me for 5 years. Just kidding, it's been a great journey with her, for all the encouragements, advices and cheers when I was feeling like nothing. It's incredibly lucky to work in this lab under her mentorship for 5 years. She helped me put myself together, and inspired me to pursue my career in academia.

Thanks to all my committee members, Prof. Daniel Alge, Prof. Akhilesh Gaharwar and Prof. Victor Ugaz, and my collaborators Prof. Gerard Coté and Prof. Mike McShane, for all the advices. Thanks to Prof. Daniel Alge and Prof. Mike McShane for letting me borrow their lab instruments. Thanks to Prof. Akhilesh Gaharwar and his student Abhay for assisting me with cell studies.

Lastly, I would like to thank my co-workers. It's been nice working with y'all! Thanks to Kristen who supported me when I was fresh here, and to Michaela who has been a great friend and supporter in graduate school! Thanks to all my undergraduate students, Bradley, Emily, Kayllie and Amelia for the hard works! Thanks to my friends, Abhay, Dandan, Yong-Yu, Yangling, Gong Jun and Zhang Zhehan, for all the supports. Great, great thanks to my family who are thousands of miles away but still make me feel strongly supported, without it, I won't get to this point!

CONTRIBUTORS AND FUNDING SOURCES

Contributors

This work was supervised by a dissertation committee consisting of Professor Melissa Grunlan [advisor] and Professors Daniel Alge and Akhilesh Gaharwar of the Department of Biomedical Engineering, and Professor Victor Ugaz of the Department of Chemical Engineering.

In Chapter III, the Figure 6 was collected with the assist of Biran Ko under the supervision of Prof. Mike McShane of the Biomedical Engineering Department at Texas A&M. In Chapter IV, the cell studies were performed by Kanwar Abhay Singh under the supervision of Prof. Akhilesh Gaharwar. Figure 3 was collected by Dr. Stanislav Vitha from the Microscopy and Imaging Center at Texas A&M. The use of the Microscopy and Imaging Center at Texas A&M is acknowledged for use of the Tescan Vega SEM, EDS analyses, and the Olympus FV 1000 confocal microscope for imaging used in Chapters IV.

All other work for the dissertation was completed by the student, under the advisement of Professor Melissa Grunlan of the Department of Biomedical Engineering.

Funding Sources

This work was made possible in part by the NSF Engineering Research Center for Precise Advanced Technologies and Health Systems for Underserved Populations (PATHS-UP) under Award Number 1648451, the Robert J. Kleberg, Jr. and Helen C.

Kleberg Foundation and the Texas A&M Engineering Experiment Station (TEES). Its contents are solely the responsibility of the authors and do not necessarily represent the official views of the institutions.

TABLE OF CONTENTS

Page

ABSTRACT ii

DEDICATION iv

ACKNOWLEDGEMENTS v

CONTRIBUTORS AND FUNDING SOURCES vi

TABLE OF CONTENTS viii

LIST OF FIGURES xi

LIST OF TABLES xvi

1. INTRODUCTION 1

1.1. Overview 1
1.2. Current CGMs on-the-market 1
1.3. Hydrogels used to build implantable glucose biosensors 7
1.3.1. Hydrogel coatings 7
1.3.2. Hydrogel matrix 8
1.4. Conclusion 10

2. A COMB ARCHITECTURE TO CONTROL THE SELECTIVE DIFFUSIVITY O A DOUBLE NETWORK HYDROGEL 12

2.1. Overview 12
2.2. Introduction 13
2.3. Experimental 17
2.3.1. Material 17
2.3.2. Comb macromer synthesis 18
2.3.3. Hydrogel fabrication 19
2.3.4. Mesh size 21
2.3.5. Glucose diffusion coefficient 22
2.3.6. Volume phase transition temperature (VPTT) 23
2.3.7. Equilibrium water content 23
2.3.8. Mechanical properties 24
2.3.9. Cytocompatibility 24

2.3.10. Statistical Analysis 25
2.4. Results and discussion 25
2.4.1. Design and fabrication of comb hydrogels 25
2.4.2. Hydrogel diffusivity 26
2.4.3. Water content, mechanical properties and non-cytotoxicity 33
2.5. Conclusion 35
2.6. Supplement 37

3. A GLUCOSE BIOSENSOR BASED ON PHOSPHORESCENCE LIFETIME SENSING AND A SELF-CLEANING MEMBRANE 41

3.1. Overview 41
3.2. Introduction 42
3.3. Experimental 47
3.3.1. Materials 47
3.3.2. Fabrication of DN membranes containing $[PdPh_4(SO_3Na)_4TBP]_3$ (i.e., "HULK") 48
3.3.3. HULK absorbance profile and leaching study 50
3.3.4. HULK concentration 51
3.3.5. Sol content 52
3.3.6. Volume phase transition temperature (VPTT) 52
3.3.7. Swelling and deswelling kinetics 52
3.3.8. Equilibrium water content 53
3.3.9. Glucose diffusion coefficient 53
3.3.10. Mechanical properties 54
3.3.11. Incorporation of GOx 54
3.3.12. GOx enzyme activity test 55
3.3.13. Glucose sensing based on phosphorescence intensity 56
3.3.14. Glucose sensing based on phosphorescence lifetime 56
3.3.15. Statistical analysis 57
3.4. Results and discussion 57
3.5. Conclusion 67
3.6. Supplement 68

4. A SELF-CLEANING SILICONE CONTAINING DOUBLE NETWORK HYDROGEL MEMBRANE TO ENHANCE GLUCOSE SENSING 75

4.1. Overview 75
4.2. Introduction 76
4.3. Experimental 81
4.3.1. Materials 81
4.3.2. Fabrication of DNs 82
4.3.3. Characterization of microdroplet size 84
4.3.4. Sol content 85

4.3.5. Volume phase transition temperature (VPTT) 85
4.3.6. Equilibrium water content 86
4.3.7. Attenuated total reflectance-Fourier transform infrared spectroscopy (ATR-FTIR) 86
4.3.8. Morphology of the DNs 86
4.3.9. Confocal laser scanning microscope (CLSM) 87
4.3.10. Hydrophilicity 87
4.3.11. Mechanical properties 88
4.3.12. Glucose diffusion coefficient 88
4.3.13. Fabrications of DNs containing HULK 89
4.3.14. Fabrications of hydrogel glucose sensors 90
4.3.15. Oxygen permeability 91
4.3.16. Glucose sensitivity 92
4.3.17. Cytocompatibility 92
4.4. Results and discussion 93
4.5. Conclusion 105
4.6. Supplement 106

5. CONCLUSIONS AND FUTURE WORK 111

5.1. Conclusion 111
5.2. Future works 114

REFERENCES 116

LIST OF FIGURES

Page

Figure 1.1 Foreign body responses after the biosensor implantation. 5

Figure 2.1 (a) Chemical structures of monomers and their comb macromers used in fabrication of comb-type double network (DN) hydrogels. (b) Fabrication process wherein a comb architecture was incorporated into the 1st network. (c) Comb macromer variables studied in this work, including charge, concentrations and length. 16

Figure 2.2 (a) Size exclusion study of *DN-25%* and *PEG* hydrogels. (b) Calculated mesh sizes (ξ) of these compositions. [*Note: The dash line represents a negligible concentration of FITC-dextran (≤ 0.00005 mg/mL).*] 27

Figure 2.3 Size exclusion study of *comb-DN-25%* prepared with PAMPS-MA combs (negatively charged) (a) of the same length (n = 5) at different concentration (5, 15, 25 and 50%); (b) of the same lengths (n = 10) at different concentration (5, 15 and 25%); (c) of the same lengths (n = 20) at different concentration (5 and 15%); (d) of different lengths (n = 5, 10 and 20) at different concentration (15, 25 and 50%, respectively); (e) Calculated mesh sizes (ξ) of these compositions. [*Note: The dash line represents a negligible concentration of FITC-dextran (≤ 0.00005 mg/mL).*] 29

Figure 2.4 (a) Size exclusion study of *comb-DN-25%* hydrogels prepared combs of the same length (*n = 10*) and concentration (25%), including PAMPS-MA (negatively charged), PEG-A (neutral charge) and PAPTAC-MA (positively charged). (b) Calculated mesh sizes (ξ) of these compositions. [*Note: The dash line represents a negligible concentration of a FITC-dextran (≤ 0.00005 mg/mL).*] 31

Figure 2.5 Measured glucose diffusion coefficient (D_{eff}) values of *PEG*, *DN*-25% and *PAMPS-c*-25% (n = 10) hydrogels. $^{\#}p > 0.05$ 32

Figure 2.6 Measured glucose diffusion coefficient (D_{eff}) values of *PEG, DN*-25% and *PAMPS-c*-25% (n = 10) hydrogels. $^{\#}p > 0.05$. 34

Figure 2.7 For *PEG*, *DN-25%*, *PAMPS-c*-25% (n = 10), *PEG-c*-25% (n = 10) and *PAPTAC-c*-25% (n = 10), values for: (a) water content, (b) compressive modulus, and (c) compressive strength .$^{\#}p > 0.05$; $^{*}p < 0.05$ vs. PEG; $^{\$}p <$ 0.05 vs. *DN-25%* 35

Figure 2.8 ^{1}H NMR spectra of PAMPS-MA macromers *(n* = 5, 10 and 20). Peaks labelled (a-g) correspond to protons noted on structure. The peak integration values are noted beneath each spectra. 37

Figure 2.9 ^{1}H NMR spectrum of the PAPTAC-MA (*n* = 10). Peaks labelled (a-k) correspond to protons noted on structure. The peak integration values are noted beneath the spectrum. 38

Figure 2.10 Size exclusion diffusion using neutral TRITC-dextran and negatively charged FITC-dextran of the *PEG* hydrogel, *DN-25%* and *comb-DN-25%* hydrogels prepared combs of the same length (*n = 10*) and concentration, including PAMPS-MA (negatively charged), PEG-A (neutral charge) and PAPTAC-MA (positively charged). $^{*}p < 0.05$ vs. TRITC-dextran. [*Note: The dash line (- - -) represents a negligible concentration of a FITC-dextran (≤ 0.00005 mg/mL). The dash line (---) represents a negligible concentration of a TRITC-dextran (≤ 0.00002 mg/mL).*] 38

Figure 2.11 Cytocompatibility evaluated with LDH assay (PS culture dish control, *PEG*, *DN*-25% and *PAMPS-c*-25% (*n* = 10). $^{\#}p > 0.05$.....39

Figure 3.1 Towards a subcutaneous implanted CGM, glucose biosensors were constructed with a metalloporphyrin [$PdPh_4(SO_3Na)_4TBP$] (i.e., "HULK") and glucose oxidase (GOx) embedded in a self-cleaning membrane disc. The phosphorescence lifetime response of HULK to oxygen can be correlated to glucose concentrations. The cyclical deswelling/reswelling of the thermoresponsive membrane due to body temperature fluctuations reduces biofouling and, hence, the foreign body reaction (FBR) for an extended the biosensor lifetime. 47

Figure 3.2 (a) Fabrication of double network (DN) membranes containing "HULK" [i.e., $PdPh_4(SO_3Na)_4$] using a two-step UV-cure process. (b) Subsequent incorporation of GOx enzyme into HULK-containing DN membranes with a glutaraldehyde linker.....49

Figure 3.3 (a) Photo image of *DN-0*, *DN-0.1*, *DN-0.3*, and *DN-0.5* discs (i.e., increasing amounts of HULK). (b) Absorbance spectra [350-900 nm] of 0.1 mM HULK (i.e., $[PdPh_4(SO_3Na)_4TBP]_3$) aqueous solution, *DN*-0.3, and the supernatant of a *DN-0.3* slab following equilibration for 3 days. (c) Absorbance of *SN-x* and *DN-x* at 460 and 640 nm (\$: $p \leq 0.05$, significantly different versus corresponding *SN-x*). (d) Calculated concentration of HULK in *DN-x* membranes. 59

Figure 3.4 (a) Deswelling/swelling kinetics, in which the weight changes of the *DN-x* were recorded when the DN membranes were subjected to temperature changes between 36 °C and 38 ºC while submerged in water. The results at

20 min and 30 min were isolated and plotted into bar graphs. (b) Glucose diffusion coefficient (D_{eff}) values of *DN-x* at RT and 37 °C. (#: $p > 0.05$, no significant difference) 60

Figure 3.5 (a) Compressive modulus (E), and (b) strength (CS) of the *DN-x* membranes. ($: $p \leq 0.05$, significantly different versus *DN-0*. #: $p > 0.05$, no significant difference) 62

Figure 3.6 (a) Photo image of *DN-x-G0.5* hydrogel discs (x = 0, 0.1, 0.3, and 0.5). (b) GOx concentration based on its enzyme activity (unit/mL) for aqueous GOx fabrication solution (0.5 mg/mL) and *DN-x-G0.5* (x = 0, 0.1, 0.3, and 0.5). (c) Preliminary glucose sensing test based on the phosphorescence intensity of *DN-x-G0.5* (x = 0, 0.1, 0.3, and 0.5). ($: $p \leq 0.05$, significantly different; #: $p > 0.05$, no significant difference) 63

Figure 3.7 For *DN-0.3-Gy* membranes (y = 0.05, 0.1, and 0.5): (a) GOx activity, and (b) glucose sensing based on phosphorescence intensity. ($: $p \leq 0.05$, significantly different) 65

Figure 3.8 Glucose sensing test based on the phosphorescence lifetime of *DN*-0.3-*G*0.05. (#: $p > 0.05$, no significant difference) 66

Figure 3.9 Calibration curves for absorbance at (a) 460 nm and (b) 640 nm versus the concentration of HULK absorbed into *DN-0* membranes. From these calibration curves, the actual concentration of HULK within *DN-x* membranes was calculated (Figure 3.3 d). 69

Figure 3.10 (a) Sol content of *SN-0* and *DN-0* membranes fabricated with 30 min or 10 min UV-cure. (b) Water content of *DN-0* membranes cured for 30 min and 10 min. (c) Compressive strength of *DN-0* cured for 30 min and 10 min. (d) Photo image of *SN-0.3* membrane cured for 14 min. ($: $p \leqslant 0.05$, significantly different versus 'UV: 30 min'; #: $p > 0.05$, no significant difference) 69

Figure 3.11 Photo image of an empty vial previously used to contain the precursor solution of *SN-0.5*. Visible aggregation was observed on the bottom of the glass vial, attributed to the high HULK concentration. 70

Figure 3.12 (a) VPTT (T_o and T_{max}), and water content of *DN-x* and *DN*-x-*G*0.5 (x = 0, 0.1, 0.3, and 0.5). (b) Compressive mechanical properties of DN-x and *DN-x-G*0.5 (x = 0, 0.1, 0.3, and 0.5). There were no significant changes between *DN*-x and the corresponding *DN*-x-*G*0.5 (i.e., same value of *x*). ($: $p \leqslant 0.05$, significantly different versus corresponding *DN-x*). Data also shown in Tables S4a and S4b. 70

Figure 4.1 (a) An illustration of sensing mechanism of HULK/GOx, after the introduction of glucose, the oxygen in the membrane can be consumed via glucose oxidation, resulting in increased phosphorescence signals. The phosphorescence intensity was directly linked to the oxygen concentration in the membrane, which was determined by the oxygen consumption and oxygen diffusion. (b) An illustration of three possible sensing profile between the interested glucose concentration range (50 - 500 mg/dL). The three profiles were determined by the relationship between oxygen diffusion and oxygen consumption. 81

Figure 4.2 (a) a scheme showing the UV-curing fabrication for the DN hydrogels containing the silicone microdomains. (b) a scheme showing the incorporation of HULK and GOx post UV-curing. 84

Figure 4.3 (a) Distribution of microdroplet in the 1st network precursor emulsion of *SiHy*-0.25 diameter (μm) measured by image J. (b) Distribution of microdroplet in the 1st network precursor emulsion of *SiHy*-0.5 diameter (μm) measured by image J. (c) Representative SEM image of *SiHy*-0.25 microdroplet in the 1st network precursor emulsion (scale bar: 2 μm). (d) Representative SEM image of *SiHy*-0.5 microdroplet in the 1st network precursor emulsion (scale bar: 20 μm). 94

Figure 4.4 (a) Representative photo image of *SiHy*-x (x = 0, 0.25 or 0.5) disc samples immersed in DI or IPA. (b) Sol content of both SNs and DNs for all compositions (*SiHy*-0, *SiHy*-0.25, and *SiHy*-0.5). (c) Representative ATR-FTIR curves of *SiHy*-x (x = 0, 0.25 and 0.5), peaks of Si-CH3 (~1250 nm), Si-O-Si (~1050 nm) and Si(CH3)2 (~ 840 nm) were labeled. (#: $p > 0.05$, no significant difference).....96

Figure 4.5 Representative CLSM image of (a) *SiHy*-0, (b) *SiHy*-0.25 and (c) *SiHy*-0.5. (Scale bar: 10 μm) 97

Figure 4.6 (a) Representative SEM image of *SiHy*-0 cross-section (scale bar: up – 20 μm, down – 10 μm). (b) Representative SEM image of *SiHy*-0.25 cross-section (scale bar: up – 20 μm, down – 10 μm). (c) Representative SEM image of *SiHy*-0.5 cross-section (scale bar: up – 20 μm, down – 10 μm).....99

Figure 4.7 Physical properties of *SiHy*-x (x = 0, 0.25 or 0.5) (a) Contact angel. (b) H-index. (c) Glucose diffusion coefficient. (*: $p < 0.05$, significantly different from each other sample at the same condition; $: $p < 0.05$, *SiHy*-x (x = 0, 0.25 or 0.5) is significantly different from its own at different condition.)....100

Figure 4.8 Mechanical properties of *SiHy*-x (x = 0, 0.25 or 0.5) (a) Compressive strain (ε). (b) Compressive modulus (*E*). (c) Compressive strength (*CS*). (d) Toughness. (*: $p < 0.05$, significantly different from each other).....102

Figure 4.9 (a) Calculated concentration of HULK loaded in the hydrogel discs (Ø = 6 mm, thickness = 0.5 mm, *SiHy*-0, 0.25 or 0.5). (b) GOx activity of the hydrogel discs (Ø = 6 mm, thickness = 0.5 mm, *SiHy*-0, 0.25 or 0.5, loaded with ~0.3 mM HULK). (c) Phosphorescence intensity changing rate within the first minute when the hydrogel discs were first exposing to oxygen (Ø = 6 mm, thickness = 0.5 mm, *SiHy*-0, 0.25 or 0.5, loaded with ~0.3 mM HULK and ~100 unit/mL GOx). (#: $p > 0.05$, not significantly different from each other) ($: $p < 0.05$, significantly different from each other).....103

Figure 4.10 (a-d) Fluorescence imaging of cells seeded on *SiHy*-0. 0.25 or 0.5 and tissue culture plates (TCPs) after 24 hr. (e) Normalized cell viability of *SiHy*-0. 0.25 or 0.5 and tissue culture plates (TCPs). (#: $p > 0.05$, not significantly different from each other).....105

Figure 4.11 (a) Photo image of 1st network precursor emulsion for *SiHy*-0.25 and *SiHy*-0.5 took on first day. (b) Photo image of 1st network precursor emulsion for *SiHy*-0.25 and *SiHy*-0.5 took after sitting for 30 days.....106

Figure 4.12 (a) Representative SEM and EDS images of *SiHy*-0. (b) Representative SEM and EDS images of *SiHy*-0.25. (c) Representative SEM and EDS images of *SiHy*-0.5. (d) Average elements percentages of *SiHy*-x (x = 0, 0.25 or 0.5) characterized with SEM-EDS. 107

Figure 4.13 Calibration curves for absorbance at (a, c, e) 460 nm and (b, d, f) 640 nm, plotting with absorbance of HULK in DNs (SiHy-x, x = 0, 0.25 and 0.5) versus HULK concentrations in DNs (~ 0.05 mM, ~0.1 mM, ~0.45 mM, ~0.65 mM, and ~1 mM).....108

Figure 4.14 Calibration curves for absorbance at (a) 460 nm and (b) 640 nm, plotting with absorbance of HULK IPA solution versus HULK concentrations (0.01 mM, 0.05 mM, 0.1 mM and 0.2 mM).....109

LIST OF TABLES

Page

Table 1.1 A brief summary of the major CGMs on-the-market.....2

Table 2.1 *DN-25%* (i.e. no combs) and *comb-DN-25%* hydrogel compositions and their VPTT values.....20

Table 2.2 Water content of *PEG*, *DN*-25%, *PAMPS-c*-25% (*n* = 10), *PEG-c*-25% (*n* = 10) and *PAPTAC-c*-25% (*n* = 10) (Data corresponds to that reported in Figure 2.7a.).....39

Table 2.3 Compressive modulus of PEG, DN-25%, PAMPS-c-25% (n = 10), PEG-c-25% (n = 10) and PAPTAC-c-25% (n = 10) (Data corresponds to that reported in Figure 2.7b.).....39

Table 2.4 Compressive strength of *PEG*, *DN*-25%, *PAMPS-c*-25% (*n* = 10), *PEG-c*-25% (*n* = 10) and *PAPTAC-c*-25% (*n* = 10) (Data corresponds to that reported in Figure 2.7c.).....40

Table 3.1 Compositions, VPTTs, and water contents of *DN-x* membranes prepared with different concentrations of HULK.....50

Table 3.2 Absorbance of *SN-x* and *DN-x* membranes at 460 nm & 640 nm. (Data corresponds to that reported in Figure 3.3c.).....71

Table 3.3 Calculated concentration of actual amount of HULK in *DN-x* membranes. (Data corresponds to that reported in Figure 3.3d.).....71

Table 3.4 Sol content (%) of *SN-0* and *DN*-0 membranes fabricated with 10 min or 30 min UV-cure. (Data corresponds to that reported in Figure 3.10a.).....71

Table 3.5 Water content (%) of *DN-0* membranes fabricated with 10 min or 30 min UV-cure. (Data corresponds to that reported in Figure 3.10b.).....72

Table 3.6 Compressive modulus (E) and strength (CS) and of *DN-0* membrane fabricated with 10 min or 30 min UV-cure. (Data corresponds to that reported in Figure 3.10c.).....72

Table 3.7 Deswelling/swelling kinetics at 20 min and 30 min of *DN-x* membranes. (Data corresponds to that reported in Figure 3.4a.).....72

Table 3.8 Glucose diffusion coefficient (D_{eff}) values of *DN-x* membranes at RT and 37 °C. (Data corresponds to that reported in Figure 3.4b.).....72

Table 3.9 Mechanical properties of *DN-x* membranes. (Data corresponds to that reported in Figure 3.5.).....73

Table 3.10 VPTT and water content of DN membranes before (*DN-x*, x = 0.1, 0.3 & 0.5) and after incorporation of GOx (*DN-x-G0.5*, x = 0.1, 0.3, & 0.5). (Data corresponds to that reported in Figure 3.12a.).....73

Table 3.11 Mechanical properties of DN membranes before (*DN-x*, x = 0.1, 0.3 & 0.5) and after incorporation of GOx (*DN-x-G0.5*, x = 0.1, 0.3, & 0.5). (Data corresponds to that reported in Figure 3.12b.).....73

Table 3.12 GOx concentration based on its enzyme activity (unit/mL) for aqueous GOx fabrication solution (0.5 mg/mL) and *DN-x-G0.5*. (Data corresponds to that reported in Figure 3.6b.).....74

Table 3.13 GOx concentration based on its enzyme activity (unit/mL) for *DN-0.3-Gy*. (Data corresponds to that reported in Figure 3.7a.).....74

Table 3.14 Glucose sensing based on phosphorescence lifetime of *DN-0.3-G0.05*. (Data corresponds to that reported in Figure 3.8.).....74

Table 4.1 Compositions, VPTTs, and water contents of DN membranes prepared with different concentrations of silicones.....84

Table 4.2 Sol content of both SNs and DNs for all compositions (*SiHy*-0, *SiHy*-0.25, and *SiHy*-0.5). (Data corresponds to that reported in Figure 4.4b.).....109

Table 4.3 Contact angle (°) of *SiHy*-0, *SiHy*-0.25, and *SiHy*-0.5. (Data corresponds to that reported in Figure 4.7a.).....109

Table 4.4 H-index of *SiHy*-0, *SiHy*-0.25, and *SiHy*-0.5. (Data corresponds to that reported in Figure 4.7b.).....109

Table 4.5 Glucose diffusion coefficient ($\times 10^{-6}$ cm^2s^{-1}) of *SiHy*-0, *SiHy*-0.25, and *SiHy*-0.5. (Data corresponds to that reported in Figure 4.7c.).....110

Table 4.6 Compressive mechanical properties of *SiHy*-0, *SiHy*-0.25, and *SiHy*-0.5. (Data corresponds to that reported in Figure 4.8.).....110

1. INTRODUCTION

1.1. Overview

Although positive outcomes have been reported with continuous uses, the adoption of CGMs were limited by the user-experience, functionality and lifetime of the implantable biosensor. This paper discussed the common CGMs on-the-market, and their limitations affected by the foreign body responses. In addition, hydrogel material owing to the high hydration, similar mechanical properties toward ECM and hydrophilic surfaces, have been a good candidate as biocompatible interface between biosensor implant and the host. A brief review on using hydrogels either as a biocompatible coating for the biosensor, or as a matrix to incorporate the sensing assay was presented in this paper. Some studies were discusses based on utilizing the unique properties of hydrogels, such as diffusivity, wide-range of modification capacity, and various fabrication capability, to construct the implantable glucose sensor, with mechanism such as electrochemical sensing and optical sensing.

1.2. Current CGMs on-the-market

Diabetes have been a world-wide chronic disease with one of the fastest growing patients' population. Estimated in 2014, There were 422 million adults affected by diabetes worldwide. The global prevalence of diabetes grew from 4.7% to 8.5% in adult population (1980 - 2014).[1-3] In particular to US, there were estimated 34.1 adult diabetes mellites in 2018, which is 13% of the US adult population. The total cost related to diabetes in US was ~$ 327 billion in 2017.[4]

Table 1.1 A brief summary of the major CGMs on-the-market

	Guardian	FreeStyle Libre	Dexcom G6	Eversense
Sensor type	Transcutaneous Electrochemical sensor	Transcutaneous Electrochemical sensor	Transcutaneous Electrochemical sensor	Fully implantable Optical hydrogel sensor
Replacement frequency	7 days	14 days	10 days	90 days
Calibration frequency	Twice per day	No	No	Twice per day
Annual cost*	~ $7000	> ~ $2000	~ $5000	~ $600
Accuracy	9%	9%	10%	9%
Implant site	Abdominal region	Abdominal region / Upper arm	Abdominal region	Upper arm
Data collecting	Skin-attach transmitter (chargeable) App	Skin-attach transmitter (non-reusable) App & reader	Skin-attach transmitter (up to 3 month) App	Skin-attach transmitter (chargeable) App

People with diabetes are not able to maintain their blood glucose levels (BGs) in normal physiological ranges (70 - 120 mg/dL, or 4 - 7 mM), either due to insufficient insulin production (type) or response (type 2), leading to a widely swinging blood glucose range between 35 - 550 mg/dL (2 - 30 mM).[5-7] Without the efficient glucose regulation, constant hyperglycemia events can lead to various long-term complications, such as blindness, heart diseases or tissue failures.[8, 9] Moreover, hypoglycemia occurs from inadequate intake or response to medicine (e.g. insulin or glinides), which can result in mortality.[10, 11] Diabetes patients are highly encouraged to perform self-monitoring of blood glucose (SMBG), which is commonly done by a "finger-prick" test, drawing a small amount of blood from a fingertip and testing it on a non-reusable enzymatic assay strip. Besides the user comfort and convenience, the SMBG is undesirable because its outcome is linked to administration, specifically the number of tests performed throughout a day.[12]

Apparently, even with recommended testing frequency (4 - 7 times per day), the odds to catch and stop hyper- / hypo-glycemia with SMBG depends on luck.

A concept to monitor patients' glucose levels in real-time, 24 / 7, was raised in 1970s.[13] Continuous glucose monitors (CGMs) allow better assisted adjustment of BGs, avoiding hyper- / hypo-glycemia, and establish an overview of BGs fluctuating with patients' lifestyles. The first commercial CGM was launched in 1990s.[14] Recent years, this market has been competing among four major companies, Medtronic (Guardian), Abbot (FreeStyle Libre), Dexcom (Dexcom G6) and Senseonics (Eversense).[12, 14-16] **(Table 1.1)**[17-19] The first three products (Guardian, FreeStyle Libre and Dexcom G6) all designed with a electroenzymatic biosensor "needle", which will be inserted transcutanteously under skin monitoring the fluctuations of glucose in interstitial fluid (ISF), a transmitter connect to the "needle", attaching to the skin, and a smart device / app collecting the data. The electroenzymatic sensor ("the needle"), consisted with an electrode layer, an enzyme layer (glucose oxidase, GOx) and a semi-permeable membrane layer, measures the glucose indirectly by detecting the hydrogen peroxide generated from glucose oxidation.[20, 21] **(Equation 1)**

$$\beta\text{-D-Glucose} + O_2 + H_2O \xrightarrow{GOx} D\text{-}Glucono\text{-}1,5\text{-}Lactone + H_2O_2 \quad (1)$$

With years of development, the current products have acquired great features and eased a lot of concerns, including easy insertion by the patients themselves, minimized irritation allowing carriers doing all types of activities, and minimized infections.[22] Still, there are three major barriers limit the adoption of those transcutaneous CGMs.[23] First, the frequent replacement of the "needle" sensor generating reoccurring cost (also on the

transmitters), as the sensing components can be damaged by the molecules from the inflammation responses and the sensing results can be drifted from the fibrous capsule.[13, 24-27] Second, to avoid tissue fibroses caused by repeated insertion, the installing site need to avoid last insertion site and any areas with tattoo, scaring or irritation.[15] Third, the uncomfortable skin-attach transmitter design, which has causing irritations and fallouts.[28] Recent years, Senseonics launched a CGM (Eversense) with the first and the only fully implantable sensor, which have been FDA approved for 90-day operation.[16, 29-31] The implant [diameter (d) ~3.5 mm × length (l) ~13.5 mm] is comprised with electronics and optics hardware included in a poly(methyl methacrylate) (PMMA) case, and with a small piece of hydrogel sensor coated on the PMMA cylinder, covering on top of the photonics. Unlike the previous mentioned products, the hydrogel sensors contain fluorescent indicators functionalized with boronic acid groups. Thus, the fluorescence signal fluctuates directly with the reversible binding of glucose to the boronic acid. To minimize the influence from the inflammation responses, a silicone drug release collar was also incorporated to the PMMS case, eluting dexamethasone and extending the lifetime (90 days with FDA approval or 180 days stability studies)[32] of the implants. Undoubtedly, Eversense is a big breakthrough in state-of-the-art CGM. The rapid technology development allows the optics and electronic been fabricated in such small sizes which was unimaginable 20 years ago. However, the bulky skin-attach transmitters are still required. The relatively large implants limit insertion to specific location (upper arm) and require the procedure to be done by a medical specialist, which generating a big portion

of the cost.[18] A recent FDA recall was issued due to manufacture misconduct due to inappropriate hydration of the hydrogel sensor, resulting in shortened lifetime < 3 weeks.[33]

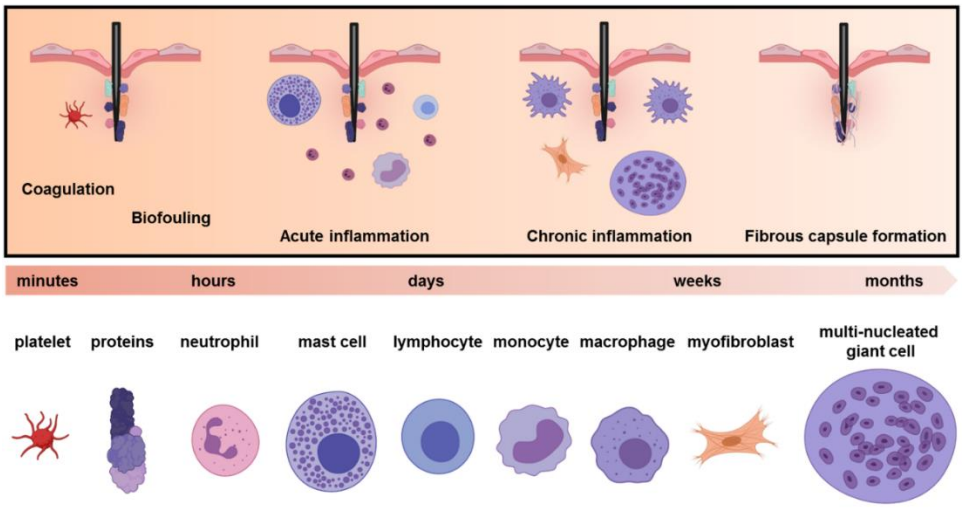

Figure 1.1 Foreign body responses after the biosensor implantation.

After introducing the CGMs to the market over 20 years, studies have shown positive outcomes including reduced hypoglycemia events and glycated hemoglobin, and also increased time in range.[34] The improvements indicated that patients' blood glucose level were better controlled with the adoption of CGMs. To encourage the adoption of CGMs, development of biosensor implants has been conducted toward better functionality and long lifetime. Various sensing mechanism has been applied to glucose sensing, including aforementioned electrochemical sensing and optical sensing, and novel methods such as semiconductor-based field effect transfer (FET), microelectromechanical systems (MEMS) and quartz crystal microbalance (QCM). Nonetheless, for all the sensing methods, after implantation, the foreign body responses are the bottlenecks for the current researches.[13, 24, 26, 35, 36] After the implantation (minutes), tissue damages initiate the wound

healing cascade, starting with platelets adhesion. Non-specific protein adhesion (e.g. fibrinogens) also quickly occurs on the implant surfaces (minutes). Later, acute inflammation is activated (hours to days), with inflammatory cells (e.g. neutrophils, leukocytes and mast cells) infiltrating on site attempting to "clean" the bacteria and injured tissue or cell debris. chronic inflammation starts from days and lasts for weeks, with active inflammatory cells (e.g. macrophages, myofibroblast and multi-nucleated giant cells) presented on site. At late stage, proliferation of myofibroblast activities generating fibrous capsule to insulate the implant, or phagocytosis activities by the multi-nucleated giant cells to further digest or damage the implant. There are few major influences generated from the foreign body responses, (1) active inflammatory cells (e.g. macrophages) consume local glucose and oxygen, affecting the sensor functionality,[37, 38] (2) interference molecules generated from inflammation [e.g. acidic molecules or reactive oxygen species (ROS)], which could lead to implant damage or sensing assay degradation,[25, 39] and (3) thick fibrous capsule around the sensor, results to additional diffusion barriers, influencing the readings.[26] In order to achieve better sensor functionality after implanted, minimized inflammatory response, fast healing and thin fibrous capsule are expected. Common approaches to enhance the implant biocompatibility include refining implant shape, size and stiffness,[40-42] anti-inflammatory drug elution,[43, 44] surfaces modifications to prevent biofouling,[45-47] and mostly the consideration of better biocompatible materials.[31, 48, 49] Among those materials, hydrogels are emerged as particularly intriguing options to fabricate the implant sensors, not only as surface coatings[47, 50, 51] but also as bulk matrix to accommodate the assay.[31, 52, 53]

1.3. Hydrogels used to build implantable glucose biosensors

Hydrogels are three-dimensional (3D) crosslinked polymer networks with well-recognized excellent biocompatibility.[54-59] Structurally, hydrogels highly resemble to extracellular matrix (ECM), which is generally crosslinked natural macromolecules such as proteins and glycans. The mechanical properties of hydrogels could be adjusted to closely matching to the soft tissue, allowing for good biomechanical biocompatibility. Additionally, the hydrophilic polymers allow water molecules filling the 3D networks, retaining these materials high water content (> ~70%), which is a critical property contributing to their biocompatibility. Besides the natural advantages, hydrogels have been explored for enhanced biocompatibility, such as enhancing the surface hydrophilicity by using charged polymers[60] or biomimicry polymers[61], consideration of macro-porous constructions,[62] and stimuli-responsive hydrogels which dynamically prevent the biofouling[63]. A "self-cleaning" double network hydrogel (denoted as *DN*-25%) was reported from our lab, which was comprised with a poly(*N*-isopropylacrylamide-*co*-2-acrylamido-2-methylpropane sulfonic acid) [P(NIPAAm-co-AMPS), 75 wt% NIPAAm vs. 25 wt% AMPS] 1st network and a poly(*N*-isopropylacrylamide-*co*-*N*-vinylpyrrolidone) [P(NIPAAm-*co*-NVP)] 2nd network.[64] *DN*-25% exhibited self-cleaning properties *in vitro*,[65] releasing adhered cells with temperature fluctuations between its volume phase transition temperature (VPTT), and excellent biocompatibility *in vivo*,[48] with minor inflammation, fast healing and ultra-thin fibrous capsule formation.

1.3.1. Hydrogel coatings

As early in the 90s, poly(ethylene glycol) (PEG) hydrogels and poly(2-hydroxyethyl methacrylate) PHEMA hydrogels were shown to be good biocompatible interfaces for glucose biosensors .[66, 67] Later, various of hydrogels were used to coat the electrochemical sensor electrodes. A 2,3-dihydroxypropyl methacrylate (DHPMA) hydrogel coating showed reduced fibrosis and reduced inflammation *in vivo*,[68] a PHEMA hydrogel coating improved the sensor lifetime to at least 21 days *in vivo*,[69] and a poly(2-methacryloyloxyethyl phosphorylcholine) PMPC hydrogel coating improved the sensor (from Medtronic) accuracy.[70] A series of composite poly(vinyl alcohol) PVA hydrogels coatings showed great control toward inflammations and fibrosis, with the addition of poly(lactic-co-glycolic acid) (PLGA) microspheres loaded with dexamethasone or/and vascular endothelial growth factor (VEGF).[71-73] Other than the electrochemical sensors, in our lab, a hollow cylindrical capsule was reported to house a förster resonance energy transfer (FRET) based assay.[74] In order to achieve the small assay components (d ~3 nm), layer-by-layer membranes were coated on the inside of the hollow cylindrical membrane, providing additional diffusion barreris,[52] and comb-type architectures were incorporated in the DN networks, adding steric barriers to the 3D mesh.[53] Functional coatings were also fabricated with hydrogels containing glucose receptor molecules (such as boronic acid). Those membranes showed glucose responsive behaviors such as with volumetric changing, weight changing or electron density changes that would be sensed by the devices under the coatings.[75-77]

1.3.2. Hydrogel matrix

By adjusting polymer chemistry or network architectures, hydrogels can be modified to incorporate various sensing assays. For the electrochemical sensors, conductive hydrogels combining with nanoparticles and GOx, were explored as affordable, soft and flexible sensor electrodes.[78] A highly sensitive biosensor electrode was fabricated with a porous polyaniline (PANi) hydrogel containing Pt nanoparticles. The porous structure allowed high GOx enzyme loading and the Pt nanoparticles helped preserve the GOx longterm functionality.[79] A conductive hydrogel based on polyacrylic acid (PAA), PANi and iron phthalocyanine functionalized graphene nanoplatelets (GPL-FePc) were fabricated, showing remarkable sensitivity.[80] A self-healing electrode designed with chitosan and dextran hydrogel containing CeO_2 / MnO_2 hollow nanospheres, was proved to continuously function over 30 days *in vitro*.[81] Those hydrogel electrode were further developed with fabrication methods, such as an nanofibrous hydrogel based on guanosine can be used to print flexible glucose electrode sensor[82], and an injectable glucose sensor was designed based on collagen-poly(pyrrole) hydrogels[83]. For some of the electrode design, a more stable molecules to catalyze glucose oxidation were incorporated comparing the GOx enzyme. A graphene oxide hydrogels were used in combination of Co_3O_4 nanoflowers, the lateral served as electrocatalysts for glucose oxidation.[84] Gelatin methacryloyl (GelMa) hydrogels containing Ni nanoparticles (catalyzing the glucose oxidation) and reduced graphene oxide exhibited high electrochemical performance.[85] Optical assays were another common sensing mechanism incorporating into the hydrogels matrix. Fluorescence assays such as phenylboronic acid[86-88] or FRET fluorophore pairs[89]. For example, recently, a GelMa hydrogel containing

boronic acid-fluorophore pairs were recently reported for its potential for 3D-printing,[90] and a polysulfobetaine based hydrogel biosensor was fabricated containing glucose-binding proteins attached with FRET fluorophore pairs[91]. Assays based on lifetime sensing was also explored on hydrogel biosensor. A highly sensitive senor was fabricated based on a PAA hydrogel containing GOx and CdTe quantum dots (QDs), which exhibited a quenching rate linear to the glucose concentration.[92] Grunlan lab has attempted to incorporate metalloporphyrin molecules coupled with GOx into the self-cleaning hydrogel matrix.[93] Moreover, its sensing behavior was adjusted with the addition of silicone microdomains increasing the oxygen permeability.[94] Multi-valent sensing can be achieved when two or above sensing assays were incorporated into the matrix, such as the combination of lifetime assay and surface-enhanced raman spectroscopy (SERS) assay.[95] Additionally, the hydrogels can be fabricated into minimized size, microsphere hydrogels, enable for injection implantation. PEG hydrogel microparticles coated with silvers were studied for the SERS sensing,[96] PAA hydrogel microdroplets immobilized with carbon dots (CDs) and GOx were used for glucose biosensor based on the CDs quenching,[97] and a alginate microgels combining the peroxyoxalate chemiluminesence and GOx were used to imaging the local oxygen concentration in tumors.[98]

1.4. Conclusion

As illustrated above, hydrogels have been widely used as biosensor implant coatings or as matrix to build biosensor implants. This material is not only a great biocompatible interface between the sensor and the host, but also exhibited tunable diffusivity allowing adequate diffusion of glucose, can be easily modified toward various

sensing mechanism, can be adapted to various fabrication methods and can be fabricated into multiple platforms. With the assist of hydrogel, the CGM implant sensors will be developed toward better accuracy, longer lifetime and minimized implant size.

2. A COMB ARCHITECTURE TO CONTROL THE SELECTIVE DIFFUSIVITY O A DOUBLE NETWORK HYDROGEL*

2.1. Overview

Limiting the diffusion of small-sized substances (D_h < 5 nm) through hydrogels is particularly difficult to achieve. Herein, we demonstrate the utility of a comb architecture to systematically reduce the mesh size of a double network (DN) hydrogel to between ~1 and 3 nm, without loss of hydration. Combs of varying charge, length and concentration were introduced during formation of the 1st network of the DN hydrogel based on of thermoresponsive *N*-isopropylacrylamide and negatively charged 2-acrylamido-2-methylpropane sulfonic acid. The resulting hydrogels' mesh sizes were characterized with a size exclusion test. Negatively charged combs were the most effective in reducing mesh size, attributed to electrostatic repulsive forces with the DN. Due to a lack of interaction and attractive forces to the 1st network, respectively, neutral and particularly positively charged combs were less effective.

---

* Reprinted with permission from "Comb Architecture to Control the Selective Diffusivity of a Double Network Hydrogel" by Dong, P., Schott, B.J., Means, A.K., and Grunlan, M.A., 2020. *ACS Appl. Polym. Mater.*, 2, 5269-5277. Copyright [2020] by American Chemical Society. (http://pubs.acs.org/articlesonrequest/AOR-VFU5JBRCMXCZ64VHTRKZ)

2.2. Introduction

The semi-permeable diffusivity of hydrogels has led to their extensive use in numerous biomedical applications, including drug delivery, regenerative medicine and biosensing.[54, 56, 99-104] Tailoring hydrogel diffusivity to achieve desired retention or release profiles is highly complex but necessary to the specific application. The diffusion of substances through the hydrogel matrix may be entirely passive or may be triggered by a stimulus. Ranging in size and chemical nature, these substances include therapeutic agents (e.g. small-molecule drugs and macromolecular proteins),[54, 56, 105, 106] growth factors,[107-109] metabolic nutrients[102, 110, 111] and biomarkers (e.g. glucose).[100, 112] Advanced hydrogel designs that leverage novel chemistries and architectures to tailor diffusion add further complexity. In particular, methods that precisely limit diffusion of very-small-sized substances (< 5 nm), without compromising other properties, are generally lacking but are essential to certain applications.[54, 103, 113, 114]

Hydrogel diffusivity is inextricably linked to its structural features.[54, 115-117] The 3D structure is generally viewed as a mesh created by crosslinked polymer chains, wherein the crosslinks are formed via chemical bonds (i.e. covalent) or physical interactions (e.g. ionic interactions and crystalline lamellae). Diffusion is regulated by the size exclusion through the mesh, with free water that fills the mesh facilitating hydrodynamic movement of the substances.[114, 116-122] Thus, mesh size (ξ) (i.e. the distance between crosslinks) is often used to quantitatively describe selective diffusivity.[114, 122, 123] Most highly hydrated hydrogels have been reported with mesh sizes ranging from ~5 to ~100 nm.[54, 106, 113, 124, 125] Because of the lower limit in mesh size, small-sized molecules (< 5 nm) are generally

insufficiently encapsulated, resulting in their poor retention or an undesirable burst release. Several strategies have been leveraged to decrease hydrogel mesh size, in particular, increasing crosslink density or polymer concentration. However, those typically result in an undesirable decrease in hydration and associated brittleness and diminished biocompatiblity.[126-128] Towards decreasing mesh size while reducing impact on these properties, hyperbranched or multi-arm polymer architectures that introduce pendant side chains to the 3D network have been reported.[124, 129] However, these did not produce mesh sizes below 5 nm. Selective diffusion may also be refined by introducing physicochemical interactions between the hydrogel mesh and targeted substances.[105, 106, 130] These implement cleavable covalent bonds[131], hydrophobic interactions[132, 133] and electrostatic interactions.[134, 135] Herein, we describe the use of a comb architecture to decrease the mesh size of a double network (DN) hydrogel towards enabling the retention of small-sized molecules such as those used in optical glucose-responsive assays.

Previously, we have reported a thermoresponsive, electrostatic DN hydrogel whose "self-cleaning" property was anticipated to minimize the foreign body reaction (FBR) of a subcutaneously implanted glucose biosensor and subsequently extend its lifetime.[48, 52, 64, 65] The DN membrane was based on *N*-isopropylacrylamide (NIPAAm) and negatively charged 2-acrylamido-2-methylpropane sulfonic acid (AMPS). Denoted as *DN-25%*, a tightly crosslinked 1st network was comprised of NIPAAm copolymerized with AMPS at (75:25 wt% of NIPAAm:AMPS) and a loosely crosslinked 2nd network was comprised of NIPAAm copolymerized with NVP to adjust the volume phase transition temperature (VPTT) [onset (T_o) ~38 °C and maximum (T_{max}) ~42 °C]. In this way, the

hydrogel would undergo dynamic self-cleaning via cyclical deswelling and reswelling, triggered by natural body temperature fluctuations in the subcutaneous tissue.[64, 65] Attributed to their electrostatic and DN nature, the *DN-25%* cylindrical implants were more mechanically robust versus a poly(ethylene glycol) diacrylate hydrogel (*PEG-DA*, 10 % wt/vol, 3.4 k g/mol), having well-established biocompatibility.[136-138] Moreover, *DN-25%* hydrogels subcutaneously implanted in rats produced milder inflammation and exhibited accelerated healing and ultimately formed an extremely thin fibrous capsule of only ~20–25 μm (90 days).[48] The *DN-25%* self-cleaning membrane, if able to adequately house (i.e. retain) an optical liquid glucose-responsive assay in a central cavity, could be used to form an electronics-free, subcutaneously implantable glucose biosensor. One such glucose-responsive assay is a FRET-based, competitive-binding assay comprised of fluorescently labelled PEGylated Concanavalin A (mPEG-TRITC-ConA) and mannotetraose (APTS-MT).[52, 139-141] However, the mesh size of the *DN-25%* was experimentally determined to be ~7 to 10 nm. Thus, as anticipated based on known hydrodynamic diameter (D_h) values, it would permit the desired diffusion of glucose (D_h ~ 0.8 nm)[142] and retention of mPEG-TRIC-ConA (D_h ~ 30 nm)[140, 141] but will fail to retain APTS-MT (D_h ~ 2-4 nm).[140, 141] Indeed, this selective diffusion behavior was confirmed for *DN-25%*.[52]

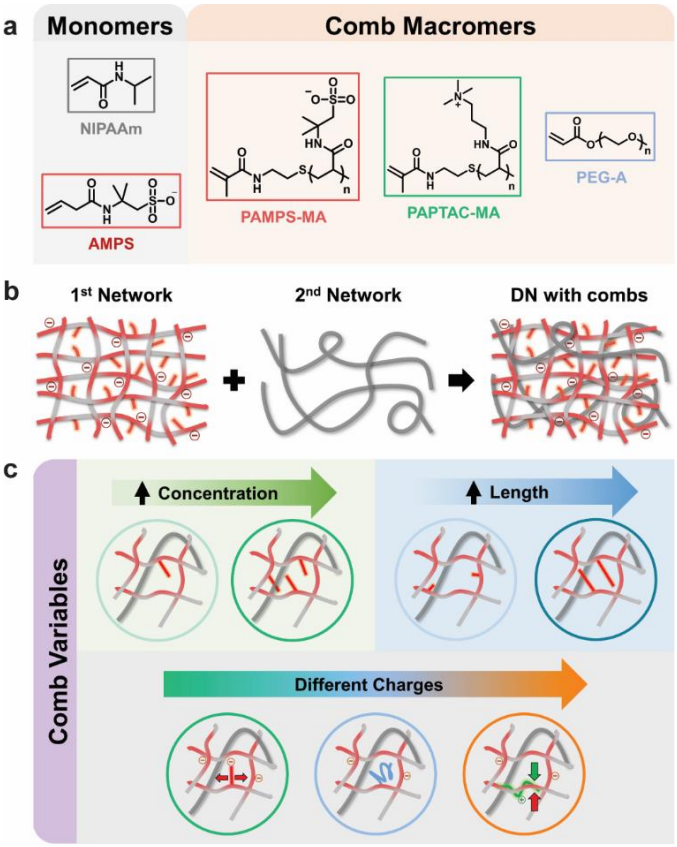

Figure 2.1 (a) Chemical structures of monomers and their comb macromers used in fabrication of comb-type double network (DN) hydrogels. (b) Fabrication process wherein a comb architecture was incorporated into the 1st network. (c) Comb macromer variables studied in this work, including charge, concentrations and length.

Herein, a comb architecture was used to precisely control and reduce the mesh size of this thermoresponsive, electrostatic DN hydrogel (**Figure 2.1**). The mobility of combs, characterized by grafts tethered to backbones, has been leveraged to create polymer electrolytes and antifouling coatings.[143, 144] PNIPAAm comb hydrogels were shown to exhibit enhanced thermosensitivity owing to the mobility of the grafts.[145, 146] For such PNIPAAm comb hydrogels, a reduction in mesh size was inferred from the relative reduction in the diffusion of various probe molecules but quantified mesh sizes were not determined.[147, 148] In this work, we sought to reduce the mesh size of the *DN-25%*

hydrogel using comb architectures, particularly towards achieving a mesh size between approximate 1 and 3 nm. In this way, the resulting *comb-DN-25%* hydrogels may permit glucose diffusion but retain a small-sized glucose sensing assay component. Combs of varying charge, concentration and length (*n*) were introduced the DN's negatively charged 1st network. Specifically, negatively charged PAMPS-methacrylate (PAMPS-MA) combs were incorporated at varying concentration (up to 50 mol%) and degrees of polymerization (n = 5, 10, 20). Combs (n = 10) of different charges were also explored at 25 mol%, including PAMPS-MA (negatively charged), PEG-A (neutral), and poly((3-acrylamido-propyl)trimethylammonium chloride)-MA (PAPTAC-MA) (positively charged). Mesh size was experimentally measured via FITC-dextran permeability studies. Other key properties of the *comb-DN-25%* hydrogels were also quantified and related to comb features, including thermosensitivity, hydration, and mechanical behavior.

2.3. Experimental

2.3.1. Material

NIPAAm (97%), AMPS (97%), NVP (≥99%), (3-acrylamido-propyl)trimethylammonium chloride solution (APTAC, 75 wt% in H_2O), poly(ethylene glycol) methyl ether acrylate (PEG-A, 480 g/mol), *N,N'*-methylenebisacrylamide (BIS, 99%), 2-hydroxy-4'-(2-hydroxyethoxy)-2-methylpropiophenone (Irgacure 2959, 98%), cysteamine hydrochloride (AET, ≥ 98%), ammonium persulfate (APS, ≥ 98%), methacrylic anhydride (MA, 94%), sodium hydroxide (NaOH, ≥ 97%), hydrochloric acid (HCl, 37%), acryloyl chloride, trimethylamine (Et_3N), poly(ethylene glycol) (PEG, molecular weight = 3000 – 3700 g/mol), 2,2-dimethyl-2-phenyl-acetophenone (DMAP),

potassium carbonate (K_2CO_3), magnesium sulfate ($MgSO_4$), sodium bicarbonate ($NaHCO_3$), fluorescein isothiocyanate-dextran (FITC-dextran, 4k, 10k, 20k and 40k g/mol), tetramethylrhodamine isothiocyanate–dextran (TRITC-dextran, 4.4k g/mol), antibiotic solution (100X) (stabilized bioreagent sterile filtered with 10000 units of penicillin and 10 mg of streptomycin per mL), Dulbecco's Modified Eagle's Medium (DMEM) (1000 mg/dL glucose and L-glutamine without Na_2CO_3 and phenol red), ethanol (HPLC grade), NMR grade deuterium oxide (D_2O) and other solvents were obtained from Sigma-Aldrich. Phosphate buffer [potassium hydrogen phosphate (K_2HPO_4, dried, $\geq 98\%$) and potassium dihydrogen phosphate (KH_2PO_4, $\geq 98\%$)] were purchased from Alfa Aesar. Phosphate-buffered saline (PBS, 1X, pH 7.4, without calcium and magnesium, Corning®), lactate dehydrogenase (LDH) cytotoxicity assay kit (Pierce) and fetal bovine serum (FBS, Hyclone) were obtained from Fisher Scientific. All chemicals were used directly without further purification. Deionized water (DI) with a resistance of 18 MΩ·cm was purified with Cascada LS MK2, Pall. Mesenchymal progenitor cells (C3*H*/10T1/2, Clone 8, CCL226) were obtained from the American Type Culture Collection (ATCC).

2.3.2. Comb macromer synthesis

Methacrylated (MA) comb macromers were synthesized under a nitrogen (N_2) atmosphere with a Teflon-covered stir bar to agitate the mixture. Product structures (including degree of polymerization, *n*) were determined via end group analysis with ^1H NMR spectroscopy on an Inova 500 MHz spectrometer operating in the FT mode with D_2O as the standard **(Figure 2.8** and **2.9)**.

2.3.2.1. Synthesis of "negatively charged" combs - PAMPS-MA (n = 5, 10 and 20)

First, oligomers with amine end groups were made from telomerization of AMPS using APS and AET redox couple as initiator and chain transfer agent, respectively.[149] Briefly, an aqueous AMPS monomer solution (1M) was neutralized with solid NaOH (pH = 7) and was bubbled with N_2 for 30 min at RT. APS and AET (with molar ratio of 1:2) were dissolved in DI separately and rapidly added into the solution. Next, the solution was heated to 60 ºC under positive N_2 pressure overnight and the pH intermittently was adjusted to 4-5 with phosphate buffer. The reaction was terminated by adjusting pH to ~12 with solid NaOH. The products were recovered via precipitation from ethanol and vacuum dried for 2 nights (RT, 30 in. Hg). The degree of polymerization (*n*) was controlled by the ratio of AMPS to AET (*n* = 5, 5:1; *n* = 10, 10:1; *n* = 20, 20:1). In the second step, amine-terminated macromers were methacrylated with methacrylate anhydride. A designated aqueous oligomer solution (0.1M) was neutralized with small amount of concentrated HCl (pH = 7) and was purged with N_2 for 10 min, following with dropwise addition of 1.3 equivalence of methacrylate anhydride at RT and maintain at 60 ºC overnight, under positive N_2 pressure. The final products were precipitated from ethanol and vacuum dried for 2 nights (RT, 30 in. Hg).

2.3.2.2. Synthesis of "positively charged" comb - PAPTAC-MA (n = 10)

The PAPTAC-MA was synthesized with a method analogous to that describe above. The degree of polymerization (*n*) was controlled by the ratio APTAC to chain transfer agent AET (*n* = 10, 10:1).

2.3.3. Hydrogel fabrication

Table 2.1 *DN-25%* (i.e. no combs) and *comb-DN-25%* hydrogel compositions and their VPTT values.

	1st network			2nd network		VPTT		
	monomer (1.11 M)			NIPAAm	NVP	T_o (°C)	T_m (°C)	ΔH (J/g)
	NIPAAm (mol %)	AMPS (mol %)	Comb (mol %)	(M)	(wt/vol %)			
DN-25%	85%	15.0%	-	2.5	9%	38.0 ± 0.6	41.9 ± 1.3	2.8 ± 0.4
PAMPS-c-5% (*n* = 10)	85%	14.25%	0.75%	2.5	8%	37.0 ± 0.7	40.1 ± 0.6	2.8 ± 0.4
PAMPS-c-15% (*n* = 10)	85%	12.75%	2.25%	2.5	5%	37.8 ± 0.3	42.5 ± 0.1	2.6 ± 0.2
PAMPS-c-25% (*n* = 10)	85%	11.25%	3.75%	2.5	5%	37.1 ± 0.5	41.4 ± 0.2	2.0 ± 0.3
PAMPS-c-50% (*n* = 5)	85%	7.5%	7.5%	2.5	5%	37.0 ± 0.6	41.4 ± 0.3	3.0 ± 0.1
PAMPS-c-15% (*n* = 20)	85%	12.75%	2.25%	2.5	5%	37.1 ± 0.4	41.9 ± 0.03	2.3 ± 0.3
PEG-c-25% (*n* = 10)	85%	11.25%	3.75%	2.5	8%	37.6 ± 1.7	42.3 ± 3.1	2.8 ± 0.5
PAPTAC-c-25% (*n* = 10)	85%	11.25%	3.75%	2.5	5%	37.1 ± 0.2	41.5 ± 0.3	2.5 ± 0.3

Comb-DN-25% hydrogels are denoted as *"comb oligomer-c-x% (n)"*, where *comb oligomer* = PAMPS [negatively charged], PEG [neutral] or PAPTAC [positively charged]; *x* = comb concentration percentage (i.e. mol% based on AMPS) and *n* = the comb length (i.e. degree of polymerization).

DN hydrogel sheets (~1.7 mm thickness) compositions were prepared as described in **Table 2.1**. As previously reported,[64, 65] fabrication was accomplished in a two-step UV-curing process wherein a single network (SN) hydrogel ("1st network") was soaked in the precursor solution of the 2nd network prior to curing, resulting in an interpenetrating, DN hydrogel. The aqueous SN precursor solutions comprised of 1.11 M monomer (consisting 85 mol% NIPAAm and 15 mol% of AMPS or a combination of AMPS and designated comb macromer), BIS crosslinker (3.3 mol% based on monomer concentration), and Irgacure 2959 photoinitiator (4.6 mol% based on monomer concentration). A designated 1st network precursor solution was injected to a rectangular mold consisting of a 1 mm thick silicone spacer separated between two glass slides (75 × 55 mm) and sealed with clips. The mold was submerged into an ice-water bath and exposed to UV light (UV-transilluminator, 6 mW/cm^2, λ_{peak} = 365 nm) for 30 min, rotating the mold after 15 min.

The resulting SN was removed from the mold, soaked in DI water for 1 day and submerged into the designated 2nd network precursor solution overnight (~5 ºC, refrigerator). The aqueous 2nd network precursor solutions were based on NIPAAm (2.5 M), NVP (5-9 % wt/vol, to adjust VPTT), BIS crosslinker (0.15 mol% based on NIPAAm concentration) and Irgacure 2959 photoinitiator (2 mol% based on NIPAAm concentration). After soaking, the hydrogel was then transferred to a similar mold (~1.25 mm thickness), submerged in an ice-water bath and cured with UV light for 30 min as described above. The resulting DN hydrogels were removed from the molds and soaked in DI for 3 days at RT with daily water changes prior to all characterizations.

A PEG-DA hydrogel control (PEG) was prepared as previously reported from 10 % (wt/vol) PEG-DA (M_n ~3.4k g/mol).[150] Briefly, the precursor solution (0.1 g PEG-DA, 10 μL of 30 wt% DMAP dissolved in NVP and 1 mL DI)[48, 151] was injected into a 1.7 mm (thickness) sandwich mold and cured with exposure to UV-light for 10 min, rotating the mold after 5 min. The resulting hydrogels were removed from the molds and soaked in DI for 3 days at RT with daily water changing prior to all characterizations.

2.3.4. Mesh size

Hydrogel mesh size was characterized by size-exclusion diffusion tests with FITC-dextrans.[124, 127] Hydrogel discs (13 mm × 1.7 mm, diameter × thickness, N = 3, from different hydrogel sheets) were harvested with biopsy punch. Each disc was soaked in 1 mL FITC-dextran solution (0.01 mg per mL DI water) for 24 hr in a sealed vial and then transferred into another vial containing 1 mL of DI. After 24 hr, the fluorescent intensity of the supernatant, was tested using microplate reader (Tecan, infinite M200 PRO,

excitation wavelength (λ_{ex}) at 480 nm; emission wavelength (λ_{em}) from 510 to 600 nm). To quantify FITC-dextran diffusion, a calibration curve (fluorescent intensity vs. FITC-dextran concentration, *R-squared value* > 0.99) was used to convert the fluorescent intensity to calculated concentration. A calculated concentration of ≤ 0.00005 mg/mL was considered negligible FITC-dextran diffusion as this corresponded to the average value of DI. FITC-dextrans of varying molecular weights (4k, 10k, 20k and 40k g/mol) corresponded to different hydrodynamic diameters (D_h ~3 nm, 4 nm, 7 nm and 10 nm, respectively)[152, 153]. A zwitterionic TRITC-dextran (4.4k g/mol, D_h ~3 nm) was also used in a size-exclusion diffusion test for comparison against the negatively charged FITC-dextran (4k g/mol, D_h ~3 nm).

2.3.5. Glucose diffusion coefficient

Hydrogel slabs were cut into square specimens (15 mm × 1.7 mm, length × thickness, N = 3, from different hydrogel sheets) with a single edge razor blade and used for glucose diffusion tests performed at RT and 37 ºC. A specimen was placed in a side-by-side diffusion chamber (PermeGear) with the receiver and donor chamber containing 7 mL each of DI water and glucose solution (10 mg/mL), respectively. Each chamber was mounted onto a stir plate and solutions were stirred with a Teflon-coated stir bar (100 rpm) to maintain constant solution concentrations. Solution temperature maintained at RT or 37 ºC with a water jacket/pump system. At 10 min intervals over a period of 3 hr, 50 μL of solution was collected from each chamber via pipette and the glucose concentration was measured (YSI 2700 Select Biochemistry Analyzer).

As previously reported,[65, 154, 155] the glucose diffusion coefficient though hydrogel membrane can be calculated using **Equation 1**, which was deducted from Fick's Laws. Here, Q is the quantity of glucose transferred, t is the time of the diffusion, L is the thickness of the specimen (1.7 mm), C_o is the initial glucose concentration (10 mg/mL) and A is the area of the hydrogel exposing for diffusion (1.767 cm^2). For the resulting plots of "Q" versus "t", the slope was calculated from the linear portion that followed the lag time (i.e. from ~30 min to ~140 min).

$$Q = \frac{ADC_0}{L} \times (t - \frac{L^2}{6D}) \quad (1)$$

2.3.6. Volume phase transition temperature (VPTT)

Hydrogel VPTT was determined using differential scanning calorimetry (DSC, TA Instruments Q100). A swollen hydrogel specimen (~10 mg) (N = 3, from different hydrogels sheets) was blotted with a Kim Wipe and then sealed in a hermetic pan. After cooling to 0 ºC, the temperature was increased to 60 ºC and immediately returned to 0 ºC at a rate of 3 ºC/min for 2 cycles. The VPTT was from the resulting endothermic phase transition peak based on the onset temperature (T_o) and the peak temperature (T_{max}). Furthermore, integration of the peak was used to determine enthalpy differentiation (ΔH). All the results reported were from the 2nd heating cycle to remove thermal history.

2.3.7. Equilibrium water content

Hydrogel discs (13 mm × 1.7 mm, diameter × thickness, N = 5) were harvested from a single sheet with biopsy punch. Each disc was placed in a sealed vial with 20 mL of DI water (RT, for 24 hr). Upon removal, the specimen was blotted with a Kim Wipe to

obtain its swollen weight (W_s) and subsequently vacuum dried overnight (60 °C, 30 in. Hg) for dry weight (W_d). Water content (W_c) was defined per **Equation 2**:

$$W_c = \frac{W_s - W_d}{W_s} \quad (2)$$

2.3.8. Mechanical properties

Compression tests were performed with an Instron 5944 at RT. Hydrogel discs (6 mm × 1.7 mm, diameter × thickness, N = 5, from different hydrogel sheets) were harvested with biopsy punch. The disc was blotted with a Kim Wipe and subjected to a 0.5 N pre-load force. A compressive force was applied at a constant strain rate (1 mm/min) until fracture (force drop > 0.5 N). The compressive modulus (E) was calculated from the linear potion of the strain-stress curve (from 0 to 10% strain). The compressive strength (σ_f) was determined as the stress at fracture.

2.3.9. Cytocompatibility

Cytocompatibility was assessed after 24 hr culture by measuring the secretion of lactate dehydrogenase (LDH) with a commercial assay kit (Pierce TM). Briefly, hydrogel discs (6 mm × 1.7 mm, diameter × thickness, N = 5, from different hydrogel sheets) were harvested with a biopsy punch and were sterilized by soaking in 70% (v/v) ethanol (45 min × 2) and recovered in sterilized PBS (30 min × 3). The samples were equilibrated in sterilized PBS for 24 hr (RT) prior to cell seeding. 10T1/2 cells were cultured in DMEM (without phenol red) supplemented with 10% FBS and 1% antibiotics solution (penicillin/streptomycin) and were seeded to each sample at a concentration of ~6000 cells/cm. After 24 hr, the supernatant for each sample was collected, reacted with the LDH

kit, and the absorbance was measured with plate-reader (Tecan, infinite M200 PRO) following a 25 min of development.

2.3.10. Statistical Analysis

All data is reported as means ± standard deviations (error bar). Mean values were compared in GraphPad Prism with 1-way or 2-way ANOVA and statistical significance assumed with a *p*-value < 0.05.

2.4. Results and discussion

2.4.1. Design and fabrication of comb hydrogels

Previously, we reported a thermoresponsive, electrostatic DN hydrogel membrane (*DN-25%*) consisting of a tightly crosslinked, negatively charged P(NIPAAM-*co*-AMPS) 1st network and loosely crosslinked P(NIPAAm-*co*-NVP) 2nd network.[64, 65, 74] Towards its implementation as a membrane for a subcutaneously implanted glucose biosensor, the desired mesh size is between approximately 1 and 3 nm, thereby retaining a small-size sensing assay molecule (e.g. APTS-MT, D_h ~ 3 nm) but allowing glucose diffusion (D_h ~ 0.8 nm). Thus, *comb-DN-25%* hydrogels were readily prepared herein by introducing methacrylated or acrylated comb oligomers during the formation of the 1st network (**Figure 2.1**). Expected to produce electrostatic repulsion between the combs and the primary network, negatively charged PAMPS-MA combs were introduced at varying concentrations (up to 50 mol% based on AMPS) and degrees of polymerization (n = 5, 10, 20). A series of *comb-DN-25%* hydrogels were also prepared with combs (n = 10, *concentration* = 25 mol%) that varied in terms of charge: PAMPS-MA (negatively charged), PEG-A (neutral) and PATAC-MA (positively charged). *Comb-DN-25%*

hydrogels are denoted as *"comb oligomer-c-x% (n)"*, where *comb oligomer* = PAMPS, PEG or PAPTAC; *x* = comb concentration percentage (i.e. mol% based on AMPS) and *n* = the oligomer length (i.e. degree of polymerization). For retention of the desired self-cleaning in response to body temperature fluctuations (i.e. cyclical deswelling/reswelling), the VPTT was desired to be maintained near that of the *DN-25%*. Thus, depending on the composition of the *comb-DN-25%* hydrogel, varying amounts of NVP (5-9 wt%) were copolymerized with NIPAAm during formation of the 2nd network (**Table 2.1**). Additionally, a *PEG* hydrogel (PEG-DA, 10 % wt/vol, 3.4 k g/mol) was prepared as a widely studied, non-thermoresponsive single network (SN) hydrogel control.

2.4.2. Hydrogel diffusivity

For conventional SN hydrogels, the mesh size (ξ) is simply defined as the average length in between crosslink and can be estimated by average polymer molecular weight between crosslinks (M_c).[114, 115, 118] This estimation is not possible for DN hydrogels due to the asymmetrically crosslinked and interpenetrating nature of the constituent networks. Herein, mesh sizes of *comb-DN-25%* hydrogels and controls were experimentally measured using FITC-dextran permeability studies. FITC-dextrans (molecular weight ~4k, 10k, 20k and 40k g/mol), corresponding to different hydrodynamic diameters (D_h ~3 nm, 4 nm, 7 nm and 10 nm, respectively), were utilized. A hydrogel specimen was allowed to sequentially soak in a designated FITC-dextran solution (0.01 mg/mL), transferred to fresh DI and the amount of FITC-dextran released via diffusion was analyzed. Thus, a hydrogel with mesh size larger than D_h of a particular FITC dextran would permit its diffusion in and out of the hydrogel. Based on a solution's fluorescence intensity, the

concentration of the FITC-dextran diffused from a hydrogel was calculated from a calibration curve (i.e. concentration vs. fluorescent intensity). Diffusion was considered negligible if the calculated concentration was ≤ 0.00005 mg/mL (i.e. that of DI water).

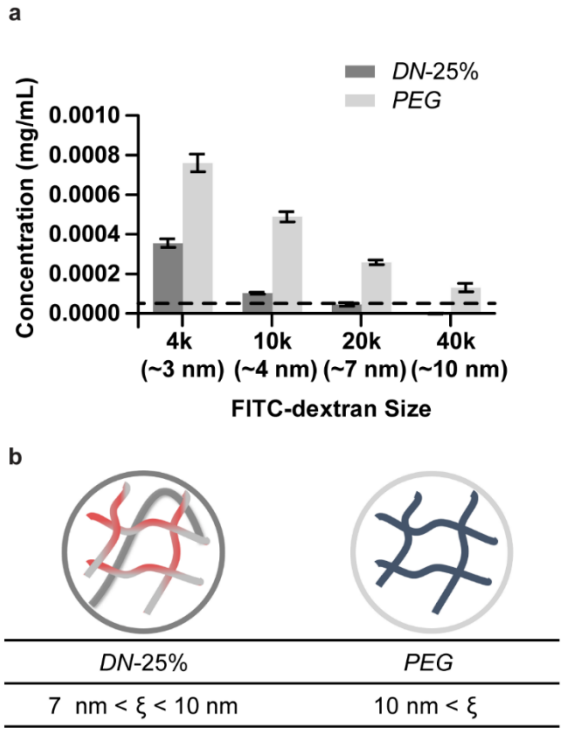

Figure 2.2 (a) Size exclusion study of *DN-25%* and *PEG* hydrogels. (b) Calculated mesh sizes (ξ) of these compositions. [*Note: The dash line represents a negligible concentration of FITC-dextran (≤ 0.00005 mg/mL).*]

First, the mesh size of the *DN-25%* (i.e. no combs) was determined as well as that of the *PEG* hydrogel **(Figure 2.2)**. For *DN-25%,* FITC-dextrans 4k and 10k were shown to have diffused but not FITC-dextrans 20k or 40k. Thus, its mesh size was estimated between 7 and 10 nm. As reported previously,[52] the *DN-25%* failed to encapsulate the sensing assay component (APTS-MT, D_h ~3 nm), which agrees with the experimentally determined mesh size. In the case of the *PEG* hydrogel, given the diffusion of FITC-

dextran 40k g/mol, its mesh size was estimated to be greater (> 10 nm). This agrees with a reported mesh size value 17.2 ± 1.0 nm.[124]

Towards tailoring and reducing the mesh size of DN-25%, a series of comb-DN-25% hydrogels were initially prepared with negatively charged PAMPS-MA of different lengths (n = 5, 10, 25) and concentrations **(Figure 2.3)**. For a given comb length, an increased concentration led to relatively decreased mesh sizes. For instance, with the shortest PAMPS-MA combs, the mesh size was reduced from 7 nm < ξ < 10 nm [PAMPS-c-5% (n = 5)] to ξ < 3 nm [PAMPS-c-50% (n = 5)] **(Figure 2.3a, e)**. At the intermediate comb length, the mesh sizes ranged from

7 nm < ξ < 10 nm [PAMPS-c-5% (n = 10)] to ξ < 3 nm [PAMPS-c-25% (n = 10)] **(Figure 2.3b, e)**. Finally, for the longest comb length, mesh size also decreased from 4 nm < ξ < 10 nm [PAMPS-c-5% (n = 20)] to ξ < 3 nm [PAMPS-c-15% (n = 20)] **(Figure 2.3c, e)**. Thus, several compositions prepared with PAMPS-MA combs were able to achieve the targeted mesh size value (ξ < 3 nm) **(Figure 2.3d)**, but the comb concentration required to do so decreased with increased comb length. It was also observed that longest PAMPS-MA combs (n = 20) were more difficult to dissolve into the aqueous precursor solutions. Thus, PAMPS-c-25% (n = 10) emerged as the best candidate of this series for achieving ξ < 3 nm.

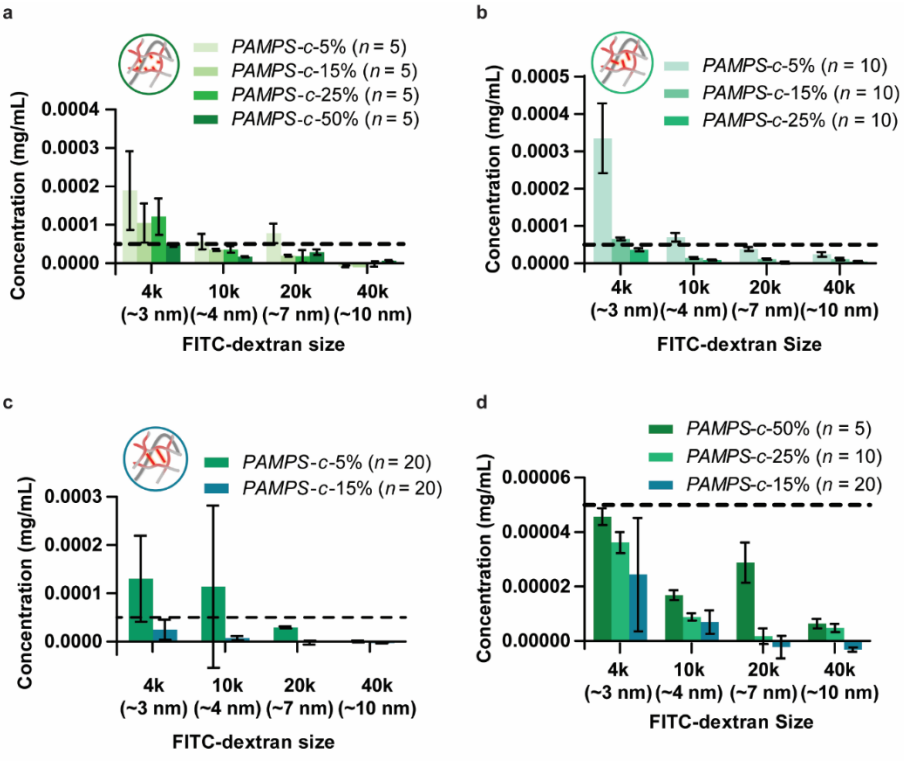

e

PAMPS-c-5% (*n* = 5) 7 nm < ξ < 10 nm	*PAMPS-c*-15% (*n* = 5) 3 nm < ξ < 4 nm	*PAMPS-c*-25% (*n* = 5) 3 nm < ξ < 4 nm	*PAMPS-c*-50% (*n* = 5) ξ < 3 nm
PAMPS-c-5% (*n* = 10) 7 nm < ξ < 10 nm	*PAMPS-c*-15% (*n* = 10) 4 nm < ξ < 7 nm	*PAMPS-c*-25% (*n* = 10) ξ < 3 nm	
PAMPS-c-5% (*n* = 20) 4 nm < ξ < 7 nm	*PAMPS-c*-15% (*n* = 20) ξ < 3 nm		

Figure 2.3 Size exclusion study of *comb-DN-25%* prepared with PAMPS-MA combs (negatively charged) (a) of the same length (n = 5) at different concentration (5, 15, 25 and 50%); (b) of the same lengths (n = 10) at different concentration (5, 15 and 25%); (c) of the same lengths (n = 20) at different concentration (5 and 15%); (d) of different lengths (n = 5, 10 and 20) at different concentration (15, 25 and 50%, respectively); (e) Calculated mesh sizes (ξ) of these compositions. [*Note: The dash line represents a negligible concentration of FITC-dextran (≤ 0.00005 mg/mL).*]

To examine the influence of combs charge, analogous *comb-DN*-25% hydrogels were prepared with the same concentration of neutral PEG-A and positively charged PAPTAC-MA combs (**Figure 2.4**). Versus the *DN*-25% [7 nm < ξ < 10 nm], the mesh size was reduced for *PEG-c*-25% (n = 10) [4 nm < ξ < 7 nm] but was similar for *PAPTAC-*

c-25% (*n* =10) [7 nm < ξ < 10 nm]. Thus, neither reduced the mesh size to that of *PAMPS*-*c*-25% (*n* = 10) [ξ < 3 nm]. We hypothesized that electrostatic repulsion between negatively charged PAMPS combs and the negatively charged 1st network limited comb flexibility and so better blocked diffusion. Neutral PEG combs, lacking repulsive forces to the 1st network, resulted in greater comb flexibility, leading to a relatively diminished reduction in mesh size. For positively charged PAPTAC combs, the lack of a reduction in mesh size was attributed to the electrostatic attraction of the combs to the 1st network, producing a lack of steric blocking. We also sought to understand the potential contribution of the slight negative charge of FITC-dextran to the ability of these *comb*-*DN*-25% hydrogels to restrict diffusion. Thus, diffusion tests were conducted with zwitterionic (i.e. net neutral charge) TRITC-dextran (4.4k g/mol) and compared to that with FITC-dextran (4.4k g/mol) (**Figure 2.9**). As observed for FITC-dextran diffusion, TRITC-dextran diffusion was most limited by *PAMPS*-*c*-25% (*n* = 10) versus *PEG*-*c*-25% (*n* = 10) and *PAPTAC*-*c*-25% (*n* =10). Thus, *PAMPS*-*c*-25% (*n* = 10) effectively blocks diffusion of small sized molecules irrespective of charge.

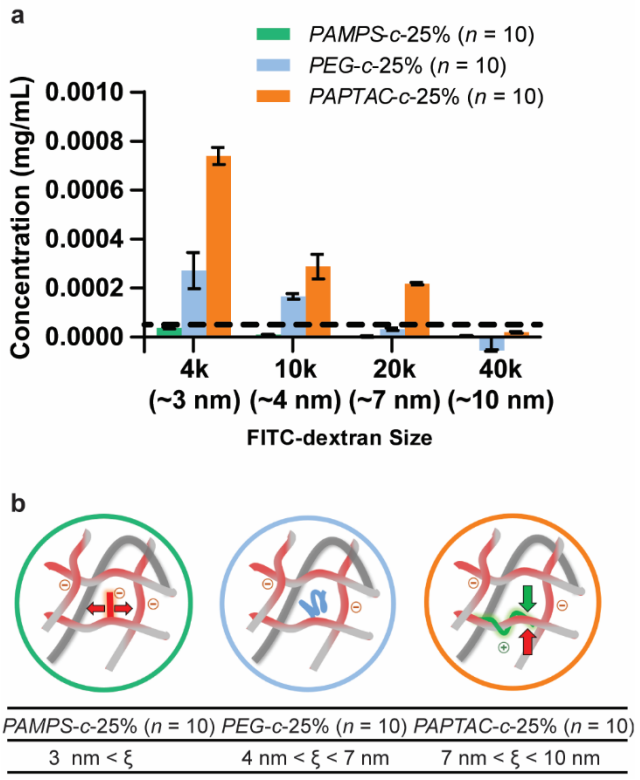

Figure 2.4 (a) Size exclusion study of *comb-DN-25%* hydrogels prepared combs of the same length (*n = 10*) and concentration (25%), including PAMPS-MA (negatively charged), PEG-A (neutral charge) and PAPTAC-MA (positively charged). (b) Calculated mesh sizes (ξ) of these compositions. [*Note: The dash line represents a negligible concentration of a FITC-dextran (≤ 0.00005 mg/mL).*]

While *PAMPS-c*-25% (*n* = 10) obtained a targeted reduced mesh size (ξ <3 nm), it is desirable that diffusion of an ultra-small molecule (e.g. glucose; D_h ~ 0.8 nm) be sustained (i.e. 1 nm < ξ < 3 nm). In this way, towards developing an implanted glucose biosensor, such a membrane could retain small sized optical assay molecules while permitting glucose diffusion to the assay. Thus, glucose diffusion experiments were conducted to compare *PAMPS-c*-25% (*n* = 10) to *DN*-25% and *PEG* hydrogels **(Figure 2.5)**. Due to the thermosensitivity of the former two hydrogels (VPTT T_o's ~37 °C; **Table 2.1**), diffusion tests were conducted at both 22 and 37 °C (i.e. in their swollen state and

onset of deswollen states, respectively). For the *PEG* hydrogel, the glucose diffusion coefficient (D_{eff}) values were ~2.48 × 10^{-6} cm^2 s^{-1} (at 22 °C) and ~3.51 × 10^{-6} cm^2 s^{-1} (at 37 °C). The slight increase at the hire temperature was attributed to a greater Brownian motion. At 22 °C, the D_{eff} values of both the *DN*-25% and the *PAMPS-c*-25% (n = 10) were very similar to each other (~1.9 × 10^{-6} cm^2 s^{-1}). At 37 °C, their D_{eff} values also increased somewhat despite the onset of deswelling. These results, when combined with the FITC-dextran diffusion studies, indicate that *PAMPS-c*-25% (n = 10) has a mesh size between 1 and 3 nm. Moreover, desirable for the potential application as an implanted biosensor membrane, this comb hydrogel exhibited D_{eff} values within the range of D_{eff} of glucose through subcutaneous tissue or fibrous capsule (~2 × 10^{-6} cm^2 s^{-1}).[156]

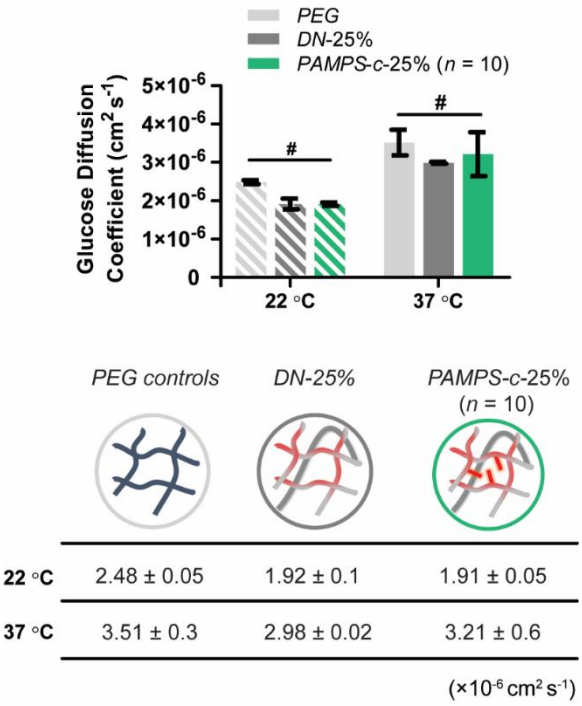

Figure 2.5 Measured glucose diffusion coefficient (D_{eff}) values of *PEG*, *DN*-25% and *PAMPS-c*-25% (n = 10) hydrogels. $^{\#}p > 0.05$.

2.4.3. Water content, mechanical properties and non-cytotoxicity

As previously noted, a reduction in mesh size achieved with typical approaches (e.g. increased crosslinking density or concentration) leads to concomitant reduction in hydration and brittleness. Thus, the hydration and compressive mechanical properties of a *PAMPS-c*-25% (n = 10), *PEG-c*-25% (n = 10) and *PAPTAC-c*-25% (n = 10) hydrogels were evaluated **(Figure 2.6)**. Their mesh sizes were reduced to varying extents versus the *DN-25%* or *PEG* hydrogel controls **(Figures 2.2, 2.4)**. Despite this, the hydration values of all comb hydrogels were statistically similar to the *DN-25%*. As previously observed,[65] the *DN-25%* achieved a higher compressive modulus and strength versus the *PEG* hydrogel, attributed to the former's electrostatic repulsive forces as well as asymmetrically crosslinked networks. Compressive moduli values increased in the order: *PAPTAC-c*-25% (n = 10) << *PEG-c*-25% (n = 10) < *DN-25%* ~ *PAMPS-c*-25% (n = 10). The modulus of *PAPTAC-c*-25% (n = 10) was notably lower than the *PEG* hydrogel. The compressive strengths of all *comb-DN-25%* hydrogels were lower than *DN-25%*, particularly *PAPTAC-c*-25% (n = 10) which was weaker than even the *PEG* hydrogel. This may stem from the increased electrostatic interactions that disrupt the dissipation of stress by the asymmetric DN, the mechanism by which ultra-high strength is thought to be imparted.[157] The superior modulus and moderate strength of *PAMPS-c*-25% (n = 10), versus other *comb-DN-25%* hydrogels, is attributed to the enhanced electrostatic repulsive forces between the negatively charged combs and negatively charged DN. Neutral PEG combs did not contribute to such repulsive forces, resulting in the diminished modulus of *PEG-c*-25% (n = 10). For *PAPTAC-c*-25% (n = 10), electrostatic attractive forces imparted by positively

charged combs diminished modulus substantially. Based on its superior mechanical properties and desirable mesh size [ξ < 3 nm], the non-cytotoxicity of *PAMPS-c*-25% (*n* = 10) was confirmed with an LDH **(Figure 2.11)**.

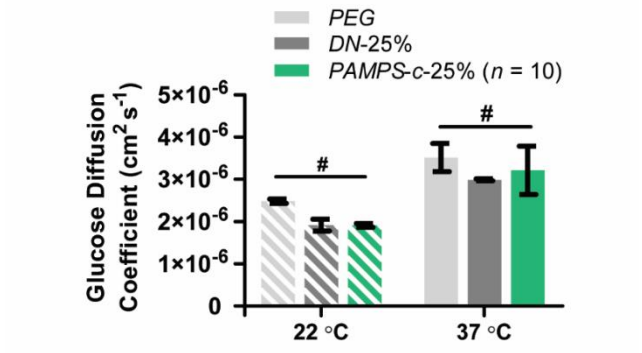

	PEG controls	DN-25%	PAMPS-c-25% (*n* = 10)
22 °C	2.48 ± 0.05	1.92 ± 0.1	1.91 ± 0.05
37 °C	3.51 ± 0.3	2.98 ± 0.02	3.21 ± 0.6

(×10⁻⁶ cm² s⁻¹)

Figure 2.6 Measured glucose diffusion coefficient (D_{eff}) values of *PEG, DN*-25% and *PAMPS-c*-25% (*n* = 10) hydrogels. $^{\#}p > 0.05$.

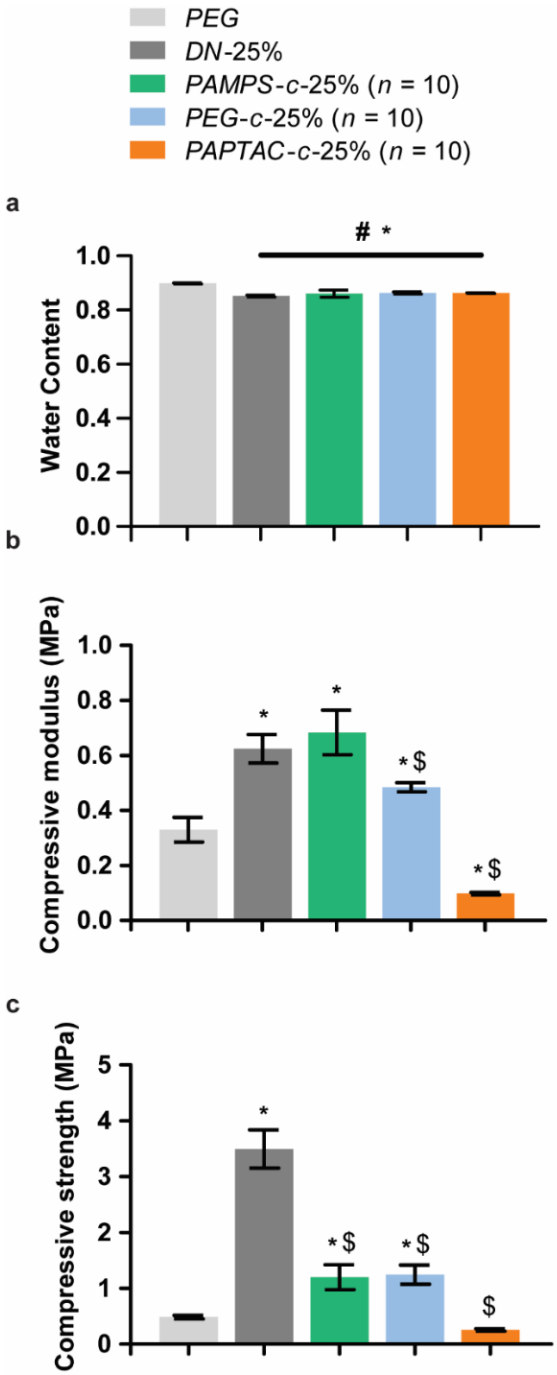

Figure 2.7 For *PEG*, *DN-25%*, *PAMPS-c*-25% (n = 10), *PEG-c*-25% (n = 10) and *PAPTAC-c*-25% (n = 10), values for: (a) water content, (b) compressive modulus, and (c) compressive strength .$^{\#}p > 0.05$; $^{*}p < 0.05$ vs. PEG; $^{\$}p < 0.05$ vs. *DN-25%*.

2.5. Conclusion

The use of a comb architecture to tailor and reduce the mesh size (ξ) of a thermoresponsive, electrostatic double network (DN) hydrogel was evaluated. *DN-25%* (7 nm < ξ < 10 nm) consisted of a tightly crosslinked, negatively charged P(NIPAAM-*co*-AMPS) 1st network and loosely crosslinked P(NIPAAm-*co*-NVP) 2nd network. *Comb-DN-25%* hydrogels were prepared by introducing methacrylated or acrylated combs of different charge [PAMPS-MA (negatively charged), PEG-A (neutral) and PATAC-MA (positively charged)], concentration and length (*n*) during formation of the negatively charged 1st network. In this way, the combs were expected to sterically block the mesh "window" and reduce the mesh size, to varying extents. By tailoring the amount of NVP incorporated with NIPAAm in the 2nd network, the VPTT was maintained in the desired range, near that of *DN-25%*. When prepared with negatively charged PAMPS-MA combs, an increase in comb concentration led to a decreased mesh size. All comb lengths (*n* = 5, 10, 20) achieved the targeted mesh size (ξ < 3 nm), but a longer comb did so at a reduced relative concentration. However, *PAMPS-c-25%* (*n* = 10) did so without any observed comb insolubility in the precursor solution. Analogous *comb-DN*-25% hydrogels were prepared with the same concentration of neutral PEG-A and positively charged PAPTAC-MA. However, their mesh sizes were not effectively reduced versus that of *DN-25%*, particularly for the latter: *PEG-c*-25% (*n* = 10) [4 nm < ξ < 10 nm] and *PAPTAC-c*-25% (*n* = 10) [7 nm < ξ < 10 nm]. Thus, negatively charged combs were the most effective in reducing mesh size, attributed to electrostatic repulsive forces with the DN's 1st network. Due to a lack of interaction and attractive forces to the 1st network, respectively, neutral and particularly positively charged combs were less effective. Moreover, *PAMPS-c-25%*

(n = 10) was shown to allow diffusion of glucose, indicating its mesh size to be ~1 < ξ < 3 nm. Despite the reduction in mesh size, these *comb-DN-25%* hydrogels favorably exhibited similar hydration versus *DN-25%*. Moreover, *PAMPS-c-25%* (n = 10) exhibited a greater compressive modulus versus the ultra-strong *DN-25%*, as well as moderate strength and cytocompatibility. Based on its thermosensitivity, mesh size and mechanical properties, this hydrogel is an excellent candidate for an implanted glucose biosensor membrane based on its anticipated ability to house small size glucose-response assay components and to undergo "self-cleaning" due to cyclical deswelling/reswelling.

2.6. Supplement

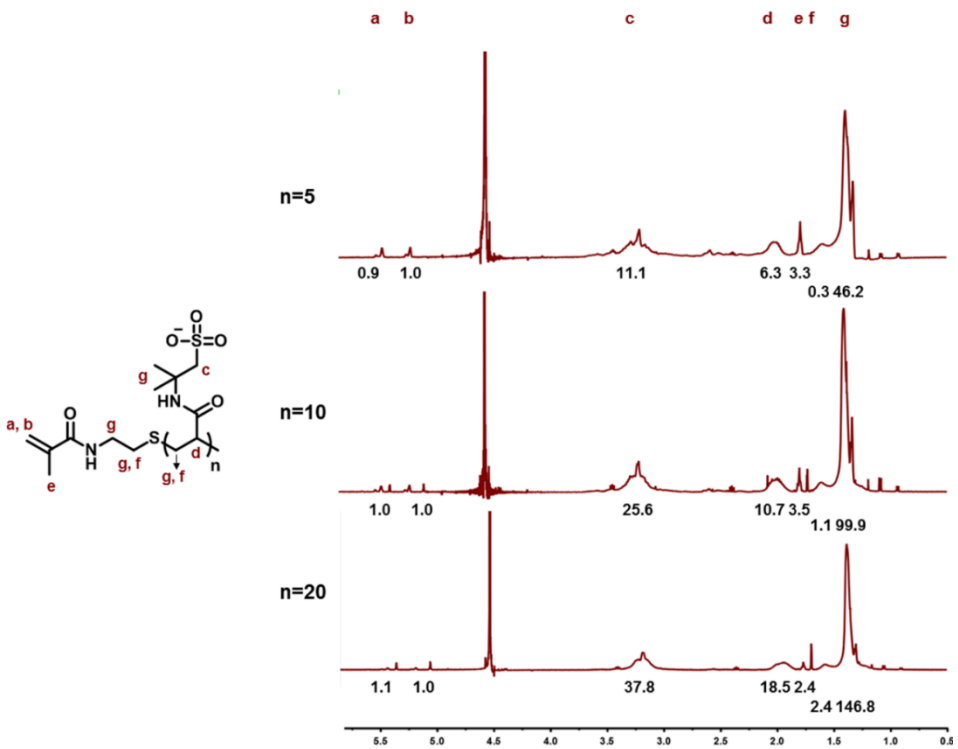

Figure 2.8 ^{1}H NMR spectra of PAMPS-MA macromers (n = 5, 10 and 20). Peaks labelled (a-g) correspond to protons noted on structure. The peak integration values are noted beneath each spectra.

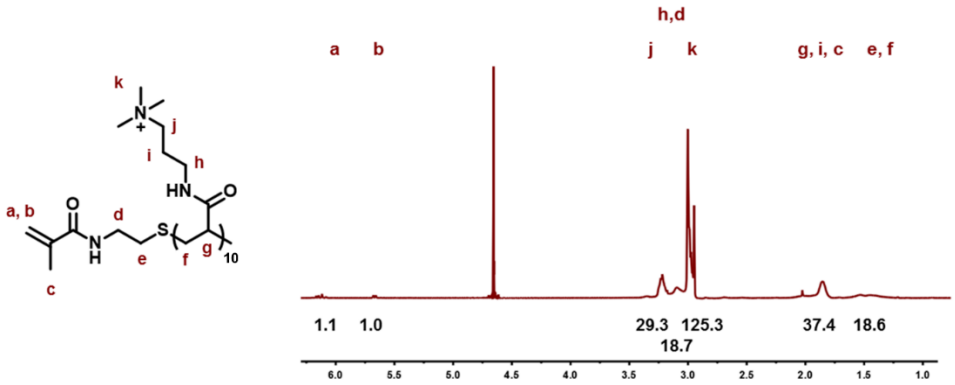

Figure 2.9 ^{1}H NMR spectrum of the PAPTAC-MA (n = 10). Peaks labelled (a-k) correspond to protons noted on structure. The peak integration values are noted beneath the spectrum.

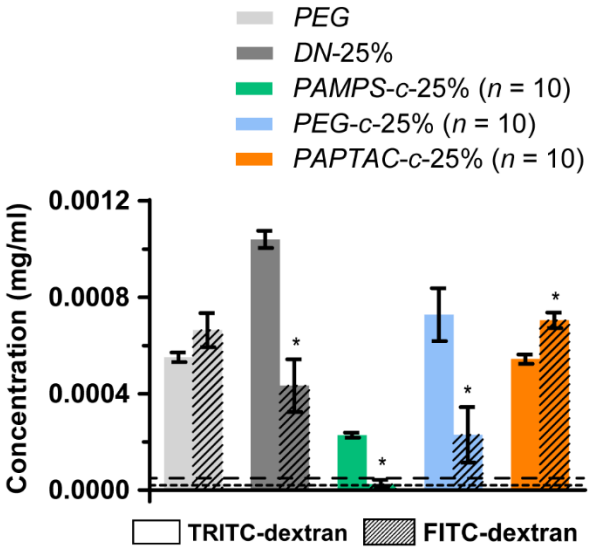

Figure 2.10 Size exclusion diffusion using neutral TRITC-dextran and negatively charged FITC-dextran of the *PEG* hydrogel, *DN-25%* and *comb-DN-25%* hydrogels prepared combs of the same length (*n = 10*) and concentration, including PAMPS-MA (negatively charged), PEG-A (neutral charge) and PAPTAC-MA (positively charged). $^{*}p < 0.05$ vs. TRITC-dextran. [*Note: The dash line (- - -) represents a negligible concentration of a FITC-dextran (≤ 0.00005 mg/mL). The dash line (---) represents a negligible concentration of a TRITC-dextran (≤ 0.00002 mg/mL).*]

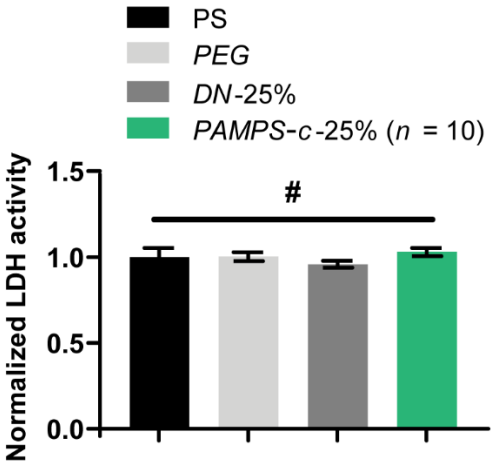

Figure 2.11 Cytocompatibility evaluated with LDH assay (PS culture dish control, *PEG*, *DN*-25% and *PAMPS-c*-25% (n = 10). $^{\#}p > 0.05$

Table 2.2 Water content of *PEG*, *DN*-25%, *PAMPS-c*-25% (n = 10), *PEG-c*-25% (n = 10) and *PAPTAC-c*-25% (n = 10) (Data corresponds to that reported in Figure 2.7a.)

	Water Content (%)
PEG	89.8 ± 0.2
DN-25%	85.2 ± 0.3
PAMPS-c-25% (n = 10)	86 ± 1.3
PEG-c-25% (n = 10)	86.2 ± 0.1
PAPTAC-c-25% (n = 10)	86.2 ± 0.4

Table 2.3 Compressive modulus of PEG, DN-25%, PAMPS-c-25% (n = 10), PEG-c-25% (n = 10) and PAPTAC-c-25% (n = 10) (Data corresponds to that reported in Figure 2.7b.)

	Compressive Modulus (MPa)
PEG	0.33 ± 0.05
DN-25%	0.62 ± 0.05
PAMPS-c-25% (n = 10)	0.68 ± 0.08
PEG-c-25% (n = 10)	0.58 ± 0.02
PAPTAC-c-25% (n = 10)	0.098 ± 0.01

Table 2.4 Compressive strength of *PEG*, *DN*-25%, *PAMPS-c*-25% (*n* = 10), *PEG-c*-25% (*n* = 10) and *PAPTAC-c*-25% (*n* = 10) (Data corresponds to that reported in Figure 2.7c.)

	Compressive Strength (MPa)
PEG	0.49 ± 0.03
DN-25%	3.5 ± 0.34
PAMPS-c-25% (n = 10)	1.2 ± 0.22
PEG-c-25% (n = 10)	1.25 ± 0.17
PAPTAC-c-25% (n = 10)	0.26 ± 0.02

3. A GLUCOSE BIOSENSOR BASED ON PHOSPHORESCENCE LIFETIME SENSING AND A SELF-CLEANING MEMBRANE

3.1. Overview

The adoption of existing continuous glucose monitors (CGMs) is limited by user burden. Herein, we present a design for a glucose biosensor with the potential for subcutaneous implantation, without the need for a transcutaneous probe or affixed transmitter. The design is based on the combination of an enzyme-driven phosphorescence lifetime-based glucose sensing assay and a thermoresponsive, self-cleaning membrane to reduce biofouling. The metalloporphyrin, Pd meso-tetra(sulfophenyl)-tetrabenzo-porphyrin ($[PdPh_4(SO_3Na)_4TBP]_3$, HULK) as well as glucose oxidase (GOx) were successfully incorporated into the UV-cured double network (DN) membranes by leveraging electrostatic interactions and covalent conjugation, respectively. The oxygen-sensitive metalloporphyrin was incorporated at different levels within the DN membrane. These HULK-containing membranes retained the desired thermosensitivity, as well as glucose diffusivity and primary optical properties of the metalloporphyrin. After subsequently modifying the membranes with GOx, glucose-sensing experiments revealed that membranes prepared with the lowest GOx level exhibited the expected increase in phosphorescent lifetime for glucose concentrations up to 200 mg/dL. For membranes prepared with relative higher GOx, oxygen-limited behavior was considered the source of diminished sensitivity at higher glucose levels. This proof-of-concept study demonstrates

the promising potential of a new biosensor design integrating a specific optical biosensing chemistry into a novel thermoresponsive hydrogel membrane.

3.2. Introduction

Diabetes affects over 422 million people worldwide and over 30 million people in just the USA.[2, 158] Central to minimizing both short- and long-term complications of this chronic condition is the judicious monitoring of blood sugars and subsequent appropriate actions to correct hypo- and hyperglycemia.[1, 2] The widely utilized finger-prick test affords only intermittent glucose measurements, presenting a major barrier to diabetes management.[159, 160] Continuous glucose monitors (CGMs) provide real-time monitoring of glucose levels both day and night.[22, 159, 161-163] Since introduction in the late 1990s, use of CGMs has been primarily limited to use for Type I diabetes and adoption has remained relatively low due to their "user-burden".[22, 23, 164]

Diabetes affects over 422 million people worldwide and over 30 million people in just the USA.[2, 158] Central to minimizing both short- and long-term complications of this chronic condition is the judicious monitoring of blood sugars and subsequent appropriate actions to correct hypo- and hyperglycemia.[1, 2] The widely utilized finger-prick test affords only intermittent glucose measurements, presenting a major barrier to diabetes management.[159, 160] Continuous glucose monitors (CGMs) provide real-time monitoring of glucose levels both day and night.[22, 159, 161-163] Since introduction in the late 1990s, use of CGMs has been primarily limited to use for Type I diabetes and adoption has remained relatively low due to their "user-burden".[22, 23, 164]

Current CGMs on-the-market (Abbott FreeStyle® Libre 2, Dexcom G6, and Medtronic MiniMed™) are designed with transcutaneous electrochemical sensor probes to measure glucose in the interstitial fluid (ISF). The probe is linked to a transmitter that is adhered to the skin on the upper arm or abdomen, and delivers the data to a customized reader or a smart phone. Although transcutaneous CGMs have evolved with improved user experiences (e.g., reduced irritation and infections)[22], the obtrusive "skin-attached" transmitter design and frequency of probe replacement (~7-14 days) has led to underwhelming adoption.[22, 23, 164] A subcutaneously implanted CGM is anticipated to provide superior user comfort.

The fully-implantable Senseonics Eversense® device was more recently introduced, wherein the subcutaneous cylindrical implant is comprised of hydrogel sensors, optical diodes, and electronics, all placed within a poly(methyl methacrylate) (PMMA) case.[29] An anti-inflammatory drug release "collar" containing dexamethasone acetate is incorporated into the PMMA construct, aimed at reducing foreign body response (FBR) and consequently extending the sensor lifetime to up to 3 months.[29, 30] However, its somewhat large size (d ~3.5 mm × l ~ 18.3 mm) requires surgical placement and limits the options for implantation site to the upper arm, rather than the wrist.[29, 31, 165] Additionally, a power module and data transmitter must be affixed to the skin over the site of this implant. The optics and electronics within the non-reusable PMMA constructs add failure modes and likewise increase the replacement cost.[31, 165] Moreover, a voluntary recall was issued following a manufacturing issue that led to inadequate hydration of the sensor, reducing sensor lifetime to < 3 weeks.[33] Given the limitations of current devices,

a CGM that would permit subcutaneous implantation in the wrist without the need for skin-attached transmitter is expected to improve adoption. To do so, the method of glucose detection as well as the approach to enhance implant biocompatibility for an extended lifetime are essential.

Wrist-wearable devices with activity tracking capabilities have become popular technology products.[166-168] A glucose biosensor that could be implanted subcutaneously at the wrist for wearable detection would represent a convenient, reduced user-burden CGM design.[23, 164] Specifically, detection of a subcutaneous optical glucose sensor could be accomplished via an LED and photodiode pair on a smart watch. Optical glucose sensors based on fluorescence intensity measurements have been widely studied, such as with Förster resonance energy transfer (FRET) assays,[52, 169] or phenylboronic acid assays.[170, 171] However, the fluorescence intensity values, and thus apparent glucose levels, may be significantly affected by factors influencing the fluorophores, the excitation efficiency, or measured light intensity. For example, decreased fluorescence intensity is observed with repeated optical interrogation due to assay photo-bleaching,[31, 95, 172] and the skin thickness or skin tone has been shown to affect the fluorescence intensity by attenuating the excitation signals.[173-175] As an alternative, we have utilized oxygen-sensitive metalloporphyrins for optical biosensing based on phosphorescence lifetime measurements.[95, 172, 176-180] The phosphorescence lifetime of the metalloporphyrin is controlled by oxygen collision quenching, such that increased oxygen levels lead to a decreased lifetime, which is proportional to intensity changes but is independent of the assay concentration, excitation source intensity, or other environmental factors.[176, 181, 182]

Moreover, metalloporphyrins exhibit long phosphorescence lifetimes of 10-100's microseconds; these are measurable with low-cost electronics and most importantly they are distinct from the autofluorescence lifetime ranges of tissues of a few nanoseconds.[95, 172] Herein, a commercially available metalloporphyrin, Pd meso-tetra(sulfophenyl)-tetra-benzoporphyrin ($[PdPh_4(SO_3Na)_4TBP]_3$), was chosen to construct a glucose biosensor. We coined this metalloporphyrin as "HULK" based on its distinct green color. In combination with glucose oxidase (GOx), the phosphorescence lifetime response of HULK to oxygen can be related to glucose concentration according to Equation 1, from which it may be seen that the enzyme drives the reaction in which oxygen is consumed with the introduction of glucose.

$$\beta\text{-D-Glucose} + O_2 + H_2O \xrightarrow{GOx} D\text{-}Glucono\text{-}1,5\text{-}Lactone + H_2O_2 \quad (1)$$

To build a glucose biosensor for subcutaneous implantation at the wrist and detection with wearable devices, the carrier or "housing" of the HULK possesses equal importance. The FBR is considered a primary obstacle to the longevity of implanted biosensors.[27, 183] Hydrogels have been widely studied as implantable materials,[102, 184] largely based on their relative biocompatibility due to significant hydration that gives rise to passive resistance to biofouling. In contrast, we previously reported a thermoresponsive double network hydrogel (DN) membrane with robust mechanical properties and an exceptional ability to limit the FBR via cyclical "self-cleaning".[48, 65] Based on thermoresponsive *N*-isopropylacrylamide (NIPAAm) and anionic 2-acrylamido-2-methylpropane sulfonic acid (AMPS), the membrane was comprised of a tightly crosslinked 1st network of [P(NIPAAm-*co*-AMPS)] (75:25 wt% ratio) and a loosely

crosslinked 2nd network of NIPAAm copolymerized with *N*-vinylpyrrolidone (NVP). The NVP content can be tailored to precisely tune the volume phase transition temperature (VPTT) such that the membranes cycles between fully swollen and slightly deswollen states with ~1 ºC fluctuations, known to occur in in subcutaneous tissue of the human wrist (~35-36 ºC)[185, 186] and in commonly utilized rat models (~37-38 ºC)[187, 188]. To evaluate self-cleaning in a rat subcutaneous model, we tailored the VPTT to exhibit a T_{onset} ~36.5 °C and a T_{max} of ~41 °C.[48] Such an implant-sized cylindrical membrane (~2.5 x 5 mm) exists largely in the relatively swollen state, but slightly deswells (~20-25 μm) at intermittent higher body temperatures. This dynamic, active process affords "self-cleaning" by driving the release of adhered cells as well as deterring initial cellular adherence. In the rat model, after 90 days, these implant-size membranes exhibited remarkable biocompatibility marked by a rapid healing response, and minimal fibrous capsule.[48]

Herein, this self-cleaning membrane inspired a design to permit effective encapsulation of the phosphorescence lifetime-based glucose sensing assay, HULK and GOx **(Figure 3.1 and 3.2)**. The membrane's 1st network was prepared from NIPAAm and cationic (3-acrylamidopropyl)trimethylammonium chloride (APTAC) at a 75:25 mol%. The 2nd network was formed from loosely crosslinked NIPAAm copolymerized with acrylamide (AAm). The VPTT was precisely adjusted for a future rat subcutaneous model based on the AAm level. The anionic HULK was incorporated during UV-cure of the 1st network so that electrostatic interactions with the cationic membrane would promote its retention. The GOx enzyme was covalently bonded to the DN membranes by leveraging

the 2nd network's AAm segments' primary amides, and also a glutaraldehyde linker's dialdehydes. DN membranes were first prepared with three HULK concentrations and characterized in terms of key material properties, such as phosphorescence intensity, VPTT, glucose diffusivity, and mechanical properties. Next, GOx was incorporated into the HULK-containing membranes at different concentrations, and the phosphorescent properties related to local glucose levels were characterized.

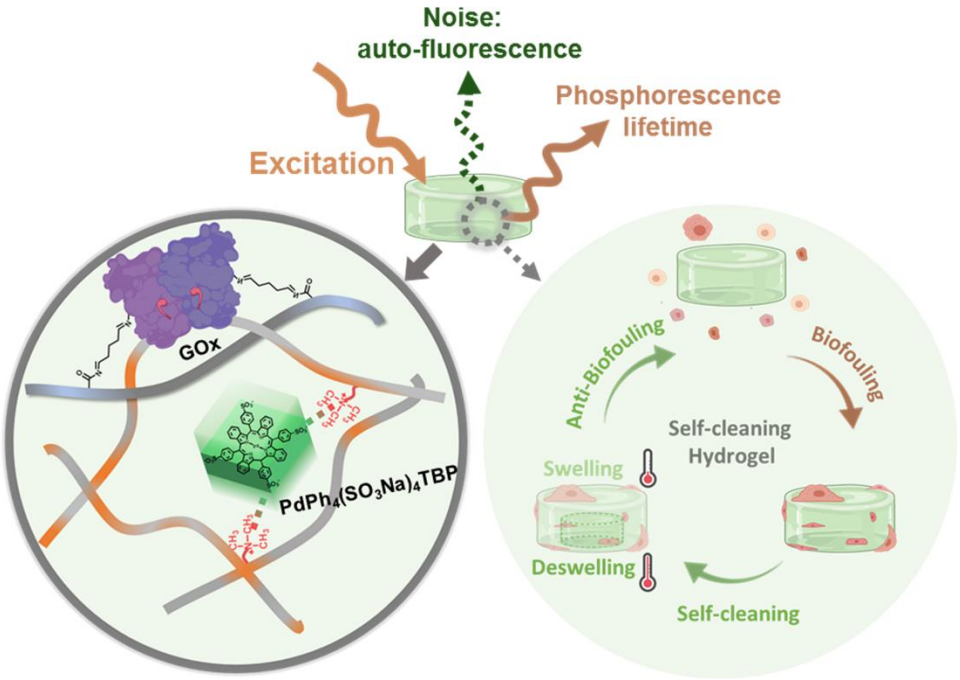

Figure 3.1 Towards a subcutaneous implanted CGM, glucose biosensors were constructed with a metalloporphyrin [$PdPh_4(SO_3Na)_4TBP$] (i.e., "HULK") and glucose oxidase (GOx) embedded in a self-cleaning membrane disc. The phosphorescence lifetime response of HULK to oxygen can be correlated to glucose concentrations. The cyclical deswelling/reswelling of the thermoresponsive membrane due to body temperature fluctuations reduces biofouling and, hence, the foreign body reaction (FBR) for an extended the biosensor lifetime.

3.3. Experimental

3.3.1. Materials

(3-Acrylamidopropyl)trimethylammonium chloride solution (APTAC, 75% wt.% in H_2O), *N*-isopropylacrylamide (NIPAAm, 97%), *N*,*N*'-methylenebisacrylamide (BIS, 99%), 2-hydroxy-4'-(2-hydroxyethoxy)-2-methylpropiophenone (Irgacure 2959, 98%), acrylamide (AAm, ≥ 99%), sodium acetate (NaAc, ≥ 99%), tris(hydroxymethyl)aminomethane (TRIS, ≥ 95%), D-(+)-glucose (≥ 99.5%), glucose oxidase (GOx) from *Aspergillus niger* (100,000-250,000 units/g solid, without added oxygen), and glutaraldehyde solution (grade II, 25 wt% in H2O) were obtained from Sigma-Aldrich. Peroxidase (horseradish, 85 units/mg dry weight) and *o*-dianisidine dihydrochloride (99%) were purchased from Alfa Aesar. Pd (II) meso-tetra(sulfophenyl)tetra benzoporphyrin sodium salt ($[PdPh_4(SO_3Na)_4TBP]_3$, > 95%; "HULK") was obtained from Frontier Scientific (Logan, UT, USA). The HULK was dissolved in DMSO (10 mM), aliquoted into 500 µL, and stored in a refrigerator (~5 °C). Dimethyl sulfoxide (DMSO, ≥ 99.9%) were obtained from VWR. All chemicals were used directly without further purification. Deionized water (DI) with a resistance of 18 MΩ·cm was purified with Pall Cascada LS MK2.

3.3.2. Fabrication of DN membranes containing $[PdPh_4(SO_3Na)_4TBP]_3$ (i.e., "HULK")

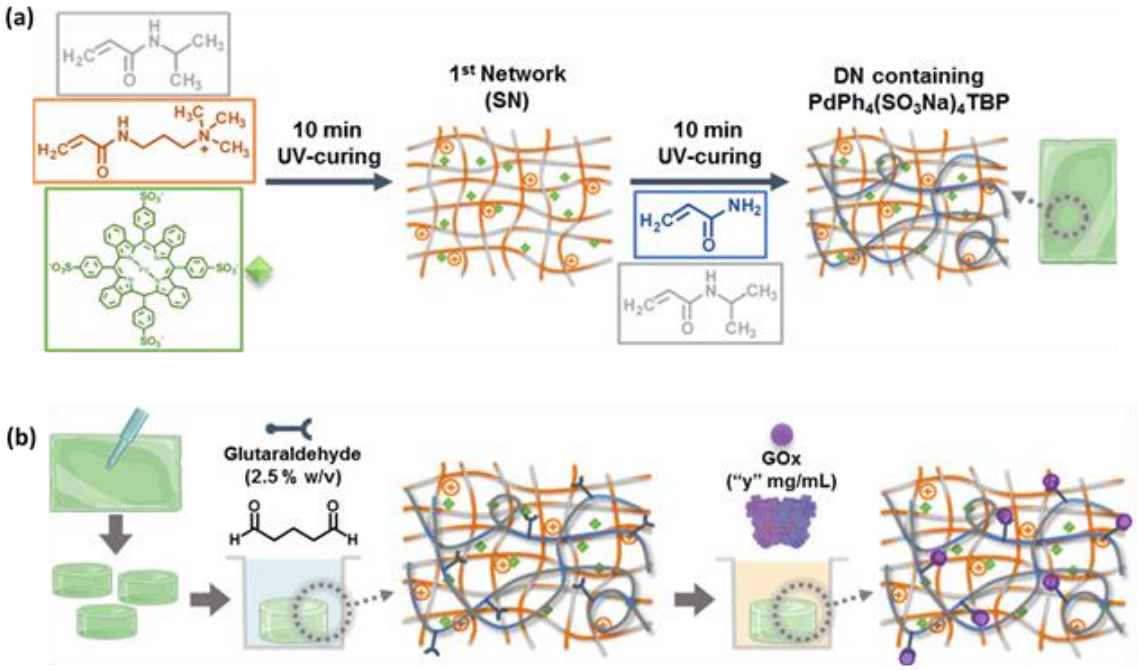

Figure 3.2 (a) Fabrication of double network (DN) membranes containing "HULK" [i.e., $PdPh_4(SO_3Na)_4$] using a two-step UV-cure process. (b) Subsequent incorporation of GOx enzyme into HULK-containing DN membranes with a glutaraldehyde linker.

DN membranes containing varying concentrations of HULK were fabricated with a 2-step UV-curing process **(Figure 3.2a)**. Briefly, a single network (SN) precursor solution was prepared, comprised of 1 M monomer (75 mol% NIPAAm and 25 mol% of APTAC), HULK (0, 0.1, 0.3, or 0.5 mM), BIS crosslinker (2.5 mol% based on monomer concentration), and Irgacure 2959 photoinitiator (0.5 mol% based on monomer concentration). The solution was degassed with nitrogen (N_2) sparging for 5 min, and then immediately injected into a rectangular mold assembled by clipping a silicone spacer (0.7 mm) between two glass slides (75 × 55 mm). While submerged in an ice-water bath, the mold was subjected to UV light (UV-transilluminator, 6 mW/cm2, λ_{peak} = 365 nm) for 5 min on each side. The resulting SN membrane was removed from the mold, soaked in DI water for 1 day, and subsequently submerged into a 2nd precursor solution overnight (~5

ºC, in refrigerator). This solution was prepared with NIPAAm (2 M), AAm (5 wt% in addition to NIPAAm), BIS crosslinker (0.1 mol% based on NIPAAm concentration), and Irgacure 2959 photoinitiator (2 mol% based on NIPAAm concentration). After soaking, the membrane was then transferred to another rectangular glass mold having 1 mm thick polycarbonate spacers. The mold was likewise submerged in an ice-water bath, and UV-cured for 5 min per side. The resulting HULK-containing DN membrane "slabs" were removed from the molds and equilibrated in DI for 3 days at room temperature (RT) with daily water changes prior to all subsequent characterizations. These membranes are denoted as "*DN-x*" where "*x*" is the concentration of HULK in the 1st network precursor solution (0, 0.1, 0.3, and 0.5 mM). Analogous SN membranes are likewise denoted as "SN-*x*".

Table 3.1 Compositions, VPTTs, and water contents of *DN-x* membranes prepared with different concentrations of HULK.

	1st network			2nd network		DN		
	Monomer (1 M)		HULK (concentration in 1st network precursor solution)	Monomer		VPTT		Water content
	NIPAAm	APTAC		NIPAAm	AAm	T_o	T_{max}	
DN-0	75%	25%	0 mM	2 M	5%	36.7 ± 0.1	38.5 ± 0.1	93.8 ± 0.4%
DN-0.1	75%	25%	0.1 mM	2 M	5%	36.6 ± 0.6	38.4 ± 0.2	92.7 ± 0.6%
DN-0.3	75%	25%	0.3 mM	2 M	5%	36.5 ± 0.3	38.4 ± 0.2	93.3 ± 0.7%
DN-0.5	75%	25%	0.5 mM	2 M	5%	36.5 ± 0.4	38.5 ± 0.3	93.8 ± 0.3%

DN hydrogels are denoted as "*DN-x*", where *x* = HULK concentration (i.e., 0, 0.1, 0.3, or 0.5 mM) in the 1st network precursor solution. Corresponding 1st networks are denoted as "*SN-x*". The 1st network contained 2.5 mol% of crosslinker (BIS) based on monomer concentration, and 0.5 mol% of photoinitiator (Irgacure 2959) based on monomer concentration. The 2nd network consisted of 5 wt% of AAm in addition to 2M NIPAAm, 0.1 mol% of BIS based on NIPAAm, and 2 mol% of Irgacure 2959 based on NIPAAm**.**

3.3.3. HULK absorbance profile and leaching study

The incorporation of HULK into *DN-x* membranes was confirmed by absorbance measurements as follows. Discs (d ~ 6 mm × t ~1.2 mm, $N = 3$) were harvested via biopsy punch from *SN-x* and *DN-x* membranes. The discs were blotted with Kimwipes and placed in a 96-wellplate without the addition of any buffer. Absorbance of each disc (at 460 and 640 nm) was characterized with a microplate reader (Tecan, Infinite M200 PRO). Absorbance profiles of a 0.1 mM HULK aqueous solution (to confirm maintenance of HULK absorbance peak) and of the "supernatant" produced from soaking a single DN slab in DI water (~25 mL) for 3 days without changing water (to confirm a lack of HULK leaching) were also characterized. The absorbance profiles of these solutions were compared to representative DNs containing HULK, specifically *DN-0.3*. For each of the above solutions, 100 µL was added into a 96-wellplate and absorbance scan from 350 to 900 nm was performed with the microplate reader.

3.3.4. HULK concentration

According to Beer-Lambert law,[189] the actual concentration of HULK in a *DN-x* membrane is expected to follow a linear relationship with the membrane's absorbance. Therefore, calibration curves plotting absorbance (at 460 and 640 nm) versus a series of membranes that had fully absorbed a HULK aqueous solution of a designated concentration were prepared. *DN-0* discs (d ~ 6 mm × t ~1.2 mm, $N = 12$) were harvested from 5 different slabs using biopsy punches and each disc was placed into a well of a 48-wellplate. To each well was added 1 mL of a HULK aqueous solution (0.005, 0.01, 0.015, or 0.02 mM; $N = 3$ for each concentration). The absorbance of the supernatant (at 460 and 640 nm) from each well was recorded with the microplate reader until none could be

detected (~48 hr). At this point, the HULK (at a specified mM concentration) was considered fully adsorbed by the disc. The absorbance of these discs (at 460 and 640 nm) were then recorded with the microplate reader, and used to construct the calibration curves. The HULK concentrations for the calibration curves was recorded to account for disc volume (~34 µL), thereby equaling 0, 0.3, 0.44, and 0.6 mM.

3.3.5. Sol content

Discs (d ~13 mm × t ~ 0.7 mm, N = 5) were harvested via biopsy punch from *SN-x* or *DN-x* slabs immediately after UV-curing. The discs were vacuum dried overnight (RT, 30 in. Hg) to obtain the dry weight ('prior to water equilibration') (W_{d0}) of each. These discs were then equilibrated in DI for 24 hr, vacuum dried overnight (RT, 30 in. Hg), and the dry weight ('after water equilibration') (W_{d1}) of each recorded. The sol content was defined per Equation 2:

$$\text{Sol content} = \frac{W_{d0} - W_{d1}}{W_{d0}} \times 100\% \quad (2)$$

3.3.6. Volume phase transition temperature (VPTT)

The VPTTs of *DN-x* membranes were characterized using differential scanning calorimetry (DSC, TA Instruments Q100). A piece of a swollen DN membrane (~10 mg) (N = 3, each from a different hydrogel slab) was blotted with a Kimwipe and then sealed in a hermetic pan. After cooling to 0 ºC, the temperature was ramped to 60 ºC and returned to 0 ºC at a rate of 3 ºC/min for 2 cycles. The VPTT was reported with onset temperature of the endothermic phase transition (T_o) and the peak temperature (T_{max}) of the transition. All the results were reported from the 2nd heating cycle to remove any thermal history.

3.3.7. Swelling and deswelling kinetics

DN-x discs (d ~13 mm × t ~1.2 mm; *N* = 5, each from a different DN slab) were harvested with a biopsy punch. Each disc was equilibrated in DI water at 36 ºC overnight. Afterward, the discs were sequentially submerged in a 38 ºC water bath for 10 min, transferred to a water bath at 36 ºC for 10 min, and moved to 38 ºC water bath for 10 min. During this process, the weight changes of the discs was monitored every 5 min. At each time point (0, 5, 10, 15, 20, 25, and 30 min), discs were removed from water bath, and blotted with Kimwipes in order to obtain their weight.

3.3.8. Equilibrium water content

Hydrogel discs (d ~13 mm × t ~1.2 mm, *N* = 5) were harvested from a single *DN-x* slab with a biopsy punch. Each disc was equilibrated in 20 mL of DI in a sealed via at RT for 24 hr. Upon removal, the discs were blotted with Kimwipes and weighed on a digital scale (swollen weight, W_s). The swollen discs were subsequently vacuum dried overnight (RT, 30 in. Hg) in order to obtain the dry weight (W_d). The water content (W_c) was defined per Equation 3:

$$W_c = \frac{W_s - W_d}{W_s} \times 100\% \quad (3)$$

3.3.9. Glucose diffusion coefficient

DN-x slabs were cut into square shapes (d ~15 mm × t ~1.2 mm, *N* = 3, from different DN slabs) with a single edge razor blade. Each sample was placed and gently clamped in between two side-by-side diffusion chambers (PermeGear). DI water (7 mL) and glucose solution (10 mg/mL) were added into the receiver and donor chambers, respectively. Each chamber was stirred with a Teflon-coated stir bar at 100 rpm to maintain a homogenous solution within. The solution temperature was maintained at RT

(22 ºC) or 37 ℃ with the water heating jacket system. At 10 min intervals over a period of 1.5 hr, 50 μL of solution was collected from each chamber. Afterward, the glucose concentrations of the collected samples were measured with a benchtop glucose analyzer (YSI 2700 Select Biochemistry Analyzer).

As reported in previous studies,[53, 65] Fick's laws were used to derive mathematical calculations for diffusion coefficient (D_{eff}) of glucose passing through a hydrogel membrane. The following Equation 4 was used for a side-by-side diffusion model. [Q: quantity of glucose transferred, t: time interval of the diffusion, L: thickness of the sample (~1.2 mm), C_o: the initial glucose concentration (10 mg/mL) and A: the area of the samples exposing for diffusion (1.767 cm^2)]

$$Q = \frac{ADC_0}{L} \times (t - \frac{L^2}{6D_{eff}}) \quad (4)$$

3.3.10. Mechanical properties

Compression tests were performed with an Instron 5944 at RT. *DN-x* discs (d ~6 mm × t ~1.2 mm, N = 5, from different hydrogel slabs) were harvested with biopsy punches and were blotted with Kimwipes prior to tests. Each disc was placed at the center of the bottom platen and was subjected to a 0.5 N pre-load force, following with compression at a constant strain rate (1 mm/min) until fracture (force drop > 0.5 N). The compressive modulus was calculated from the linear portion of the strain-stress curve (from 0 to 10% strain). The compressive strength and the compressive strain were determined at fracture point.

3.3.11. Incorporation of GOx

After equilibrating in DI for 3 days, *DN-x* discs were harvested from the slabs with biopsy punches (d ~8 mm). Each of the discs were immersed in 1 mL glutaraldehyde solution (2.5 wt/v) for 1.5 hr, following with washes using DI for 30 min (10 min × 3 times). Afterward, each disc was immersed in 1 mL of GOx aqueous solution (0.05, 0.1, and 0.5 mg/mL in DI water) overnight (~5 ºC, in refrigerator) **(Figure 3.2b)**. The resulting GOx-modified DN membranes were then equilibrated in 5 mM NaAc solution (pH ~5) for 3 days (~5 ºC, in refrigerator) with daily water changes prior to all characterizations. These membranes are denoted as "*DN-x-Gy*" where "*x*" is the concentration of HULK in the 1st network precursor solution (0, 0.1, 0.3, and 0.5 mM), and "*Gy*" denotes the GOx concentration in solution (0.05, 0.1, and 0.5 mg/mL) used in the fabrication. VPTT, equilibrium content, and compressive mechanical properties were performed according to protocols described above for *DN-x* membranes.

3.3.12. GOx enzyme activity test

One-unit activity of GOx incorporated into DN membranes was defined as the amount of GOx that is capable to catalyze 1 μmol glucose and produce hydrogen peroxide (H_2O_2) at 37 ºC, pH ~5.[190-192] Based on the GOx enzymatic assay,[193] horseradish peroxidase (POD), and *o*-dianisidine dihydrochloride (*o*-DDH) were used to characterize the activity within the membranes.[192, 194-196] *DN-x-Gy* discs (d ~ 6 mm × t ~1.2 mm, N = 3) were harvested with biopsy punches, and were placed in a 96-wellplate. The discs were equilibrated at 37 ºC for 10 min, followed by the addition of 145 μL assay consisting of 0.17 mM *o*-DDH, 1.72% (w/v) glucose, and 5 μL 60 unit/mL POD (pH ~5, at 37 ºC). The absorbance at 500 nm was monitored every 15 s for 5 min. As the light penetrated through

two phases (liquid assay and the hydrogel), the Beer-Lambert law was applied to derive Equation 6 for calculating the GOx activity ($\frac{\Delta Ab_{500nm}}{min}_{test}$: rate of absorbance change for testing samples; $\frac{\Delta Ab_{500nm}}{min}_{blank}$: rate of absorbance change for blank cells; ε: molar attenuation coefficient of oxidized *o*-DDH at 500 nm, which equals 7.5 $mM^{-1} \bullet cm^{-1}$; ℓ: light pathlength, which was measured to be ~0.5 cm; V_{assay}: volume of the assay, which was 150 µL; and V_{disc}: volume of the disc, which was calculated to be ~34 µL.)

$$\frac{Units}{mL} of\ enzyme = \left(\frac{\frac{\Delta Ab_{500nm}}{min}_{test} - \frac{\Delta Ab_{500nm}}{min}_{blank}}{\varepsilon * l} \right) * \frac{V_{assay}}{V_{disc}} \quad (6)$$

3.3.13. Glucose sensing based on phosphorescence intensity

DN-x-Gy discs (d ~6 mm × t ~1.2 mm; N = 3) were placed into wells of a 96-wellplate and incubated at 37 ºC for 10 min. Next, 100 µL glucose solution (0, 50, 100, 200, or 300 mg/dL) was added and the discs equilibrated for precisely 5 min (at 37 ºC). Next, to determine phosphorescence intensity, fluorescence intensity was recorded with a lag-time of 25 µs (excitation wavelength: 640 nm). A given disc was sequentially equilibrated with glucose solutions of increasing concentration, washing 3X with 5 mM NaAc solution.

3.3.14. Glucose sensing based on phosphorescence lifetime

After cutting the edges with biopsy punches (d ~ 6 mm × t ~1.2 mm; N = 3), the *DN-x-Gy* discs were placed in a custom-designed flow-through system[95, 178, 180] to evaluate the phosphorescent lifetime changes at different glucose concentrations (0, 50, 100, 200 and 300 mg/dL). Glucose solutions were pumped through at a rate of 5 mL/min, while the oxygen concentration was not specifically controlled (ambient condition, ~8 mg/L oxygen

dissolved in solution at RT and 0.21 atm oxygen[197]). The discs were incubated at 37 ºC for 60 min with 0 mg/dL solution flow-through and were subjected to 1 min glucose solution flows at each concentration. A 10 min washing in between different glucose concentration was performed with 0 mg/dL solution. During this process, each disc was excited with a 630 nm light-emitting diode, and was monitored with a custom time domain phosphorescence lifetime measurement system.[95, 180]

3.3.15. Statistical analysis

All data are reported as means ± standard deviations (error bar). Mean values were compared in GraphPad Prism with 1-way or 2-way ANOVA and statistical significance assumed with a *p*-value ≤ 0.05.

3.4. Results and discussion

DN membranes containing different levels of HULK were successfully fabricated with the 2-step UV-curing process **(Figure 3.1a and Figure 3.3a)**. These membranes are denoted as "*DN-x*" where "*x*" is the concentration of HULK in the 1st network precursor solution (0, 0.1, 0.3, and 0.5 mM). Likewise, the 1st cured single networks are denoted as "*SN-x*". The absorbance profiles of HULK of the *DN-0.3* and of the aqueous solution (0.1 mM) were qualitatively similar, suggesting HULK had no substantial physical-chemical interactions that altered its optical properties after incorporation into the *DN-x* membranes **(Figure 3.3b)**. The "equilibrium supernatant", in which a *DN-0.3* slab was equilibrated for 3 days, showed no absorbance near 460 nm or 640 nm, indicating an absence of HULK leaching. This successful retention is attributed to the electrostatic attraction between the cationic APTAC segments of the DN membranes and the anionic HULK. There was

generally no significant difference between absorbance of a *SN-x* membrane and the corresponding *DN-x* membrane **(Figure 3.3c; Table 3.2)**, indicating that the HULK introduced during the formation of a SN membrane was well-preserved after the subsequent UV cure to form the DN membrane. While a certain concentration of HULK was added to the 1st network precursor solution, the actual amount of HULK within *DN-x* membrane **(Figure 3.3d; Table 3.3)** was determined using the designated calibration curves **(Figure 3.9)**. These results reveal that ~26-30% of the HULK in the 1st network precursor solution concentration was present in the final *DN-x* membrane. This apparent reduction in concentration is attributed primarily to the increased volume of swollen DN membranes, but there is also some loss due to photo-bleaching of the phosphor during UV curing of the 2nd network.

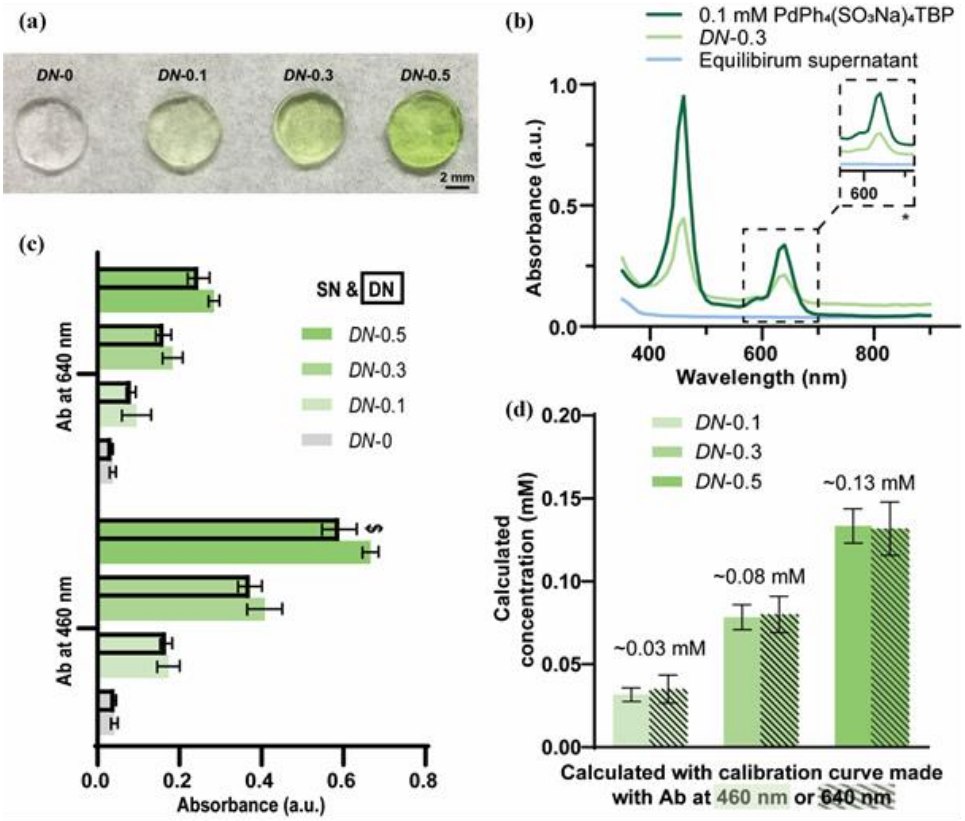

Figure 3.3 (a) Photo image of *DN-0*, *DN-0.1*, *DN-0.3*, and *DN-0.5* discs (i.e., increasing amounts of HULK). (b) Absorbance spectra [350-900 nm] of 0.1 mM HULK (i.e., $[PdPh_4(SO_3Na)_4TBP]_3$) aqueous solution, *DN*-0.3, and the supernatant of a *DN-0.3* slab following equilibration for 3 days. (c) Absorbance of *SN-x* and *DN-x* at 460 and 640 nm (\$: $p \leq 0.05$, significantly different versus corresponding *SN-x*). (d) Calculated concentration of HULK in *DN-x* membranes.

The aforementioned successful retention of HULK absorbance is attributed to a carefully selected UV cure schedule. To reduce the potential for photo-bleaching of the HULK, the cure time for both the 1st and 2nd networks were shortened to 10 min (versus 30 min of prior reports to form similar DN membranes[48, 65]) and precursor solutions were also sparged with N_2. Compared to when cured for 30 min, the *DN-0* cured for 10 min expectedly showed an increased sol content, higher hydration, and also reduced modulus (E) and compressive strength (CS) **(Figure 3.10a-c, Tables 3.4-3.6)**. Still, the E (~0.44

MPa) and CS (~0.37 MPa) of the *DN-0* prepared with the shorter cure time is similar to conventional hydrogels, such as those prepared from poly(ethylene glycol) diacrylate (PEG-DA; M_n = 3.4 kDa, 10% w/v; E = ~0.33 MPa; CS = ~0.48 MPa).[53] Even a slight increase in cure time from 10 min to 14 min showed evidence of photo-bleaching **(Figure 3.10d)**. Thus, the utilized 10 min UV cure protocol is judicious for incorporation of HULK within the *DN-x* membranes.

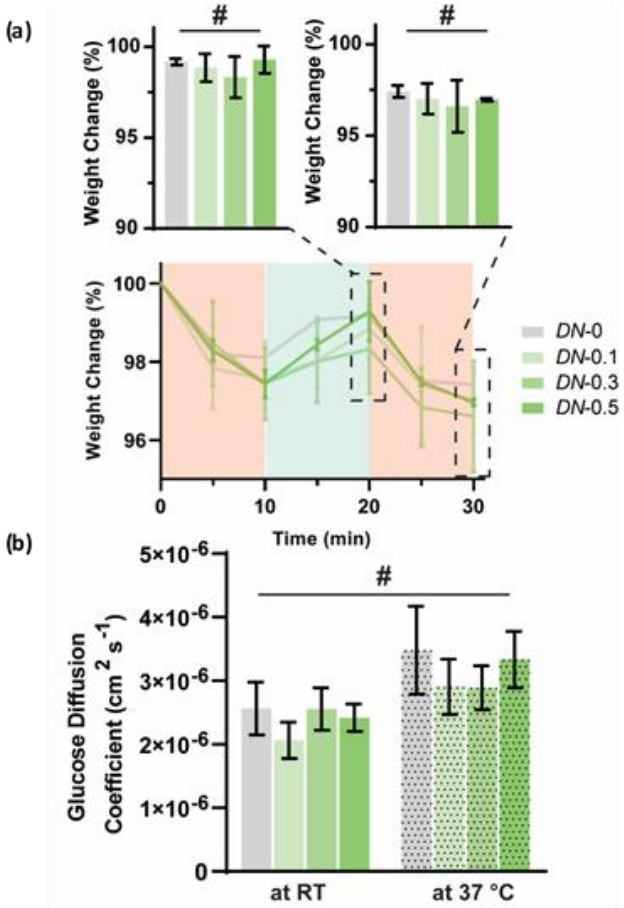

Figure 3.4 (a) Deswelling/swelling kinetics, in which the weight changes of the *DN-x* were recorded when the DN membranes were subjected to temperature changes between 36 °C and 38 ºC while submerged in water. The results at 20 min and 30 min were isolated and plotted into bar graphs. (b) Glucose diffusion coefficient (D_{eff}) values of *DN-x* at RT and 37 °C. (#: $p > 0.05$, no significant difference)

In order to achieve self-cleaning *in vivo*, the VPTTs of the DN membranes must be precisely adjusted to consider subcutaneous temperature fluctuations.[48, 65] As described earlier, for a rat subcutaneous model, a VPTT with a T_o ~36.5 ºC and a T_{max} ~38.5 ºC would afford cycling between swollen and slightly deswollen states, avoiding excessive deswelling that could compromise glucose diffusion and impart brittleness. Since the VPTT of PNIPAAm hydrogels (~33-35 ºC) is known to increase with the incorporation of hydrophilic comonomers,[198] the addition of 5 wt% of AAm to the 2nd network precursor solution produced the targeted VPTT for all *DN-x* membranes **(Table 3.1)**. Gravimetric cyclic deswelling/reswelling studies were also conducted **(Figure 3.4a; Table 3.7)**. Since the 1st cycle of deswelling (0-10 min) and reswelling (10-20 min) may be influenced by thermal history, specimen weights were considered for the 2nd cycle, at the start of reswelling (at 20 min) and at the end of subsequent deswelling (at 30 min). An average of 1.9 ± 0.5 % weight decreased was observed upon deswelling. The lack of significant differences in % weight changes among *DN-x* membranes indicates that HULK concentration does not impact thermosensitivity.

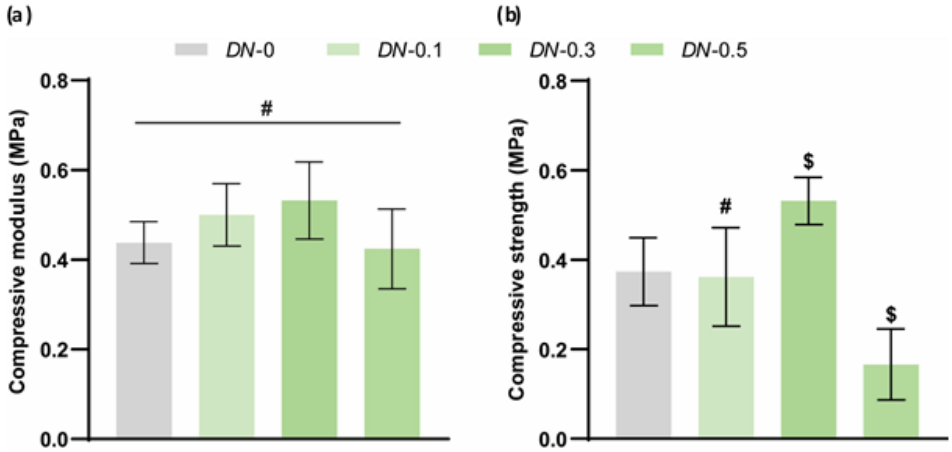

Figure 3.5 (a) Compressive modulus (E), and (b) strength (CS) of the *DN-x* membranes. ($: $p \leq 0.05$, significantly different versus *DN-0*. #: $p > 0.05$, no significant difference)

All the *DN-x* membranes exhibited similarly high water contents (~93%) **(Table 3.1)**. This was expected to contribute to good diffusivity of glucose. The D_{eff} of each *DN-x* membrane was measured at both RT and 37 ºC, representing a fully swollen state and an onset of deswelling state, respectively. No significant difference of D_{eff} values [~2.8 ± 0.6 × 10^{-6} cm^2 s^{-1}] were observed among all *DN-x* membranes at either temperature **(Figure 3.4b; Table 3.8)**. While a higher temperature can induce greater glucose Brownian motion for accelerated diffusion, the lack of a relative increase in D_{eff} values of *DN-x* membranes at 37 ºC may stem from slight membrane deswelling. A similar D_{eff} value (at 37 ºC) was observed for a non-thermoresponsive PEG-DA membrane.[53] The D_{eff} of *DN-x* membranes was notably higher than that of subcutaneous tissue (~2 ×10^{-6} cm^2 s^{-1}).[156] Thus, when used to prepare a glucose biosensor, the glucose diffusion lag time would be limited by the subcutaneous tissue, not the membrane.

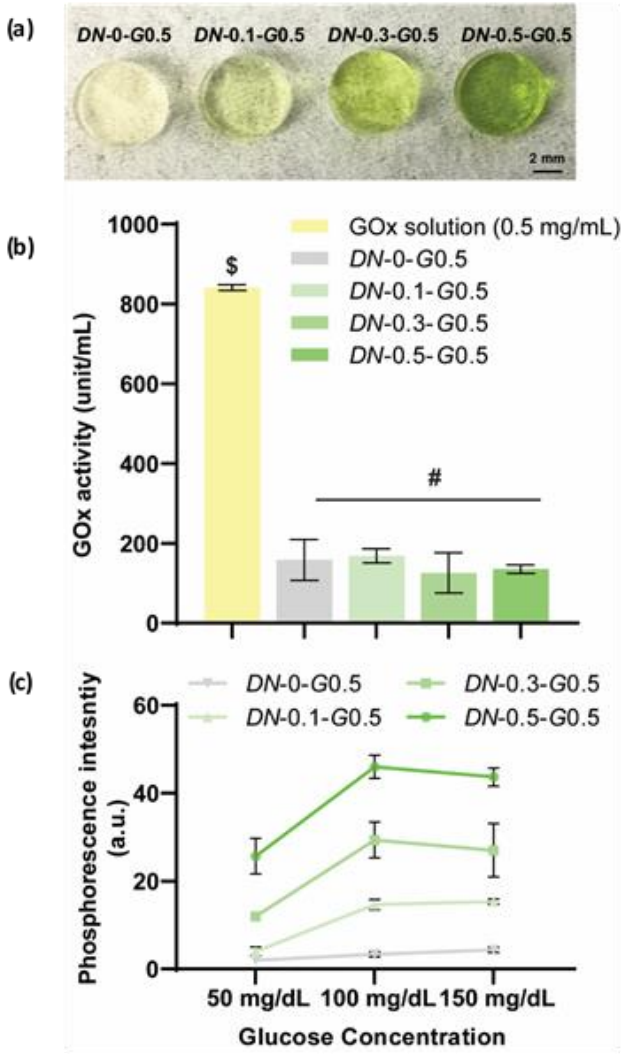

Figure 3.6 (a) Photo image of *DN-x-G0.5* hydrogel discs (x = 0, 0.1, 0.3, and 0.5). (b) GOx concentration based on its enzyme activity (unit/mL) for aqueous GOx fabrication solution (0.5 mg/mL) and *DN-x-G0.5* (x = 0, 0.1, 0.3, and 0.5). (c) Preliminary glucose sensing test based on the phosphorescence intensity of *DN-x-G0.5* (x = 0, 0.1, 0.3, and 0.5). ($: $p \leq 0.05$, significantly different; #: $p > 0.05$, no significant difference)

The *E* and *CS* of *DN-x* membranes were also determined **(Figure 3.5; Table 3.9)**. Due to their similarly high hydration, this was not a contributing factor to any differences in mechanical properties. The incorporation of HULK into membranes, irrespective of concentration, did not influence *E* values significantly. *DN-0.3* showed a statistically

greater *CS* versus *DN-0*, possibly due to the electrostatic attraction between the HULK and the membrane network. *DN-0.5* showed a decreased *CS*, which is attributed to the observed aggregation of HULK in precursor solutions at this higher concentration **(Figure 3.11)**, as previously noted by others.[199-202]

Following confirmation of the successful incorporation of HULK into *DN-x* membranes, the GOx enzyme was subsequently added as a necessary component for glucose detection. Glutaraldehyde was used to covalently link the primary amine on GOx to the primary amide of PAAm segments in the DN's 2nd network. GOx incorporation was performed on *DN-x* (*x* = 0, 0.1, 0.3 and 0.5) membranes (discs, d ~ 8 mm) by sequential absorption of glutaraldehyde and GOx **(Figure 3.2b, Figure 3.6a)**. These resulting membranes are denoted as "*DN-x-Gy*" where "*x*" is the concentration of HULK in the 1st network precursor solution (0, 0.1, 0.3, and 0.5 mM), and "*Gy*" denotes the GOx concentration in solution (0.05, 0.1, and 0.5 mg/mL) used in the fabrication. The inclusion of GOx did not produce significant changes in VPTT values nor in mechanical properties, while a very slight decrease in water content to ~90% was observed **(Figure 3.12; Tables 3.10-3.11)**. The effective GOx concentration and accessibility within membranes were assessed by measuring GOx activity, specifically for membranes prepared with a 0.5 mg/mL GOx solution (i.e., *DN-x-G0.5*) **(Figure 3.6b; Table 3.12)**. All *DN-x-G0.5* membranes (x = 0, 0.1, 0.3, and 0.5) exhibited similar GOx activity. The expected reduction versus the GOx solution is attributed to incomplete absorption from the aqueous solution.

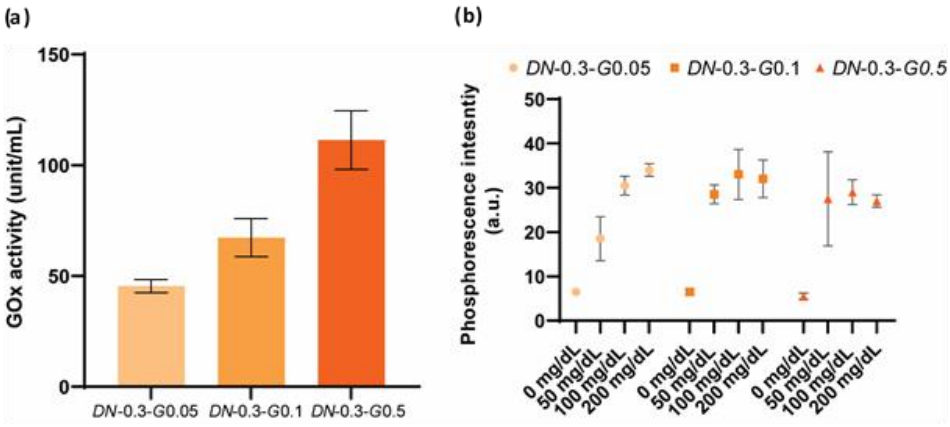

Figure 3.7 For *DN-0.3-Gy* membranes (y = 0.05, 0.1, and 0.5): (a) GOx activity, and (b) glucose sensing based on phosphorescence intensity. ($: $p \leq 0.05$, significantly different)

With this series of membranes, initial glucose sensing tests based on HULK phosphorescence intensity were conducted using a microplate reader. After incubating in glucose solution (50, 100, or 150 mg/dL) for 5 min, phosphorescence intensity of *DN-x-G0.05* membranes were recorded with a reading lag time of 25 μs **(Figure 3.6c)**. As expected for membranes prepared with the same GOx levels, an increased phosphorescence intensity was observed for all membranes when the glucose level was raised from 50 to 100 mg/dL. However, similar readings were exhibited at 100 and 150 mg/dL. This result may be explained in terms of oxygen depletion within the membranes. As noted previously, the expected increase in phosphorescence intensity (or lifetime) response of HULK with increased glucose levels is related to the reduction of oxygen that is consumed during glucose oxidation **(Equation 1)**. Thus, the lack of a further increase in phosphorescent intensity for a 150 mg/dL glucose concentration indicates that either the oxygen was consumed within the membranes or the enzyme was overwhelmed.

Hypothesizing that the depletion of oxygen limited glucose sensitivity at higher concentrations, the GOx was subsequently incorporated at lower levels in DN membranes

to reduce the oxidation rate. Based on its superior mechanical properties, a series of membranes was prepared based on *DN-0.3* with increasing GOx concentration: *DN-0.3-G0.05* < *DN-0.3-G0.1* < *DN-0.3-G0.5*. The GOx levels within these membranes were quantified in terms of activity, and showed the expected increase **(Figure 3.7a; Table 3.13)**. *DN-0.3-G0.05*, having the lowest GOx levels, exhibited an increase in phosphorescent intensity across the entire glucose concentration range (0 – 200 mg/dL) **(Figure 3.7b)**. In contrast, the increase in phosphorescent intensity of *DN-0.3-G0.1* and *DN-0.3-G0.5* plateaued at glucose concentrations of 50 mg/dL. These results support our hypothesis that a lower GOx concentration in HULK-containing membranes avoids oxygen depletion by reducing the rate of oxygen consumption.

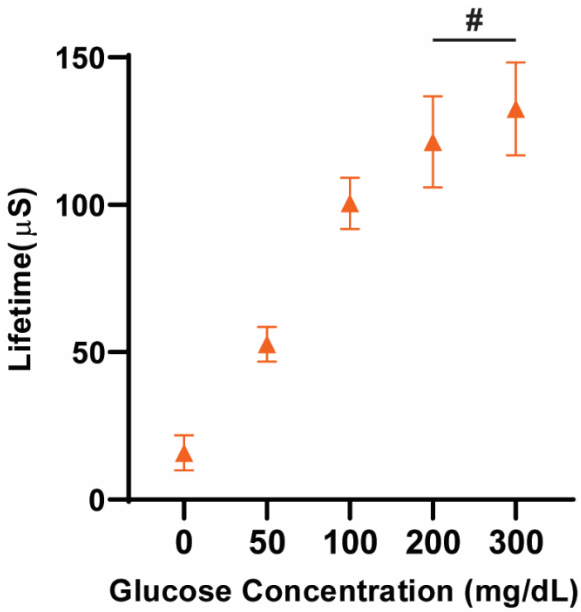

Figure 3.8 Glucose sensing test based on the phosphorescence lifetime of *DN*-0.3-*G*0.05. (#: $p > 0.05$, no significant difference)

Based on the above results, *DN-0.3-G0.05* was selected for additional phosphorescence lifetime analysis towards advancing to use as an implanted sensor.

Glucose response tests were performed using a custom designed flow-through system and reader-heads.[95, 180] As glucose concentrations increased to 50 mg/dL and then to 100 mg/dL, this membrane exhibited substantial increases (~37% and ~36%, respectively) in phosphorescence lifetime **(Figure 3.8; Table 3.14)**. At higher glucose concentration (100 – 300 mg/dL), the phosphorescent lifetime continued to increase, but to a reduced extent (~26%). Moreover, at 200 and 300 mg/dL concentrations, the lifetimes were statistically similar. This nonlinear response behavior is consistent with many other examples of these enzymatic optical systems developed using various hydrogel matrices.[178, 203-205] Although the reduction in GOx improved glucose sensitivity at higher glucose concentrations, oxygen depletion may still be a factor. While beyond the scope of this work, it is noted that the response sensitivity, linearity, and range may be adjusted using different approaches to decrease the reaction rate by slowing glucose delivery to the enzyme.[178, 203] However, it is noteworthy that detection of low glucose levels are clinically most critical, as it is the hypoglycemic episodes that present acute risk to the patient. The sensors demonstrated here have exquisite sensitivity at low glucose levels, with a 2-2.5X increase in lifetime over 50 mg/dL steps.

3.5. Conclusion

Towards the development of a subcutaneously implanted glucose biosensor, the metalloporphyrin $PdPh_4(SO_3Na)_4TBP]_3$ (i.e., "HULK") and glucose oxidase (GOx) were incorporated into a self-cleaning membrane. Glucose levels can thus be related to the oxygen-sensitive phosphorescence lifetime of HULK. A thermoresponsive DN membrane design, previously shown to limit the FBR reaction via body temperature fluctuation-

driven cyclical swelling/deswelling, was strategically tailored to enable incorporation of HULK and GOx. Introduced at varying concentrations (0, 0.1, 0.3, and 0.5 mM HULK) during the UV cure of the 1st network, the resulting DN membranes stably immobilized HULK via electrostatic interactions and maintained the metalloporphyrin's absorbance profile. The DN membranes demonstrated the targeted thermosensitivity and glucose diffusion kinetics despite presence of HULK. Compressive moduli (E) were also similar for all HULK-containing DN membranes, while compressive strength (CS) was greatest for an intermediate HULK concentration (i.e., *DN-0.3*) and reduced for a high HULK concentration (i.e., *DN-0.5*). To immobilize GOx within the HULK-containing DN membranes, glutaraldehyde was used as a covalent linker. During initial glucose sensing testing of membranes formed with a high GOx concentration (i.e. *DN-x-Gy0.5*), the phosphorescent intensity plateaued at glucose levels >50 mg/dL, indicating oxygen-limited behavior; membranes formed with lower GOx levels were found to reduce the rate of oxygen consumption, and the membrane with the lowest GOx levels (i.e., *DN-0.3-G0.05*) exhibited an increase in phosphorescent intensity from 0 to 200 mg/dL. Methods to reduce the rate of oxygen consumption (e.g., improve oxygen permeability) may further improve the range of glucose response, but the current system has exceptional sensitivity to low glucose levels that are critical in detecting hypoglycemia. Overall, these membranes represent a promising candidate for subcutaneous glucose biosensors. Based on these promising results, future work will include assessment of this biosensor design *in vivo*.

3.6. Supplement

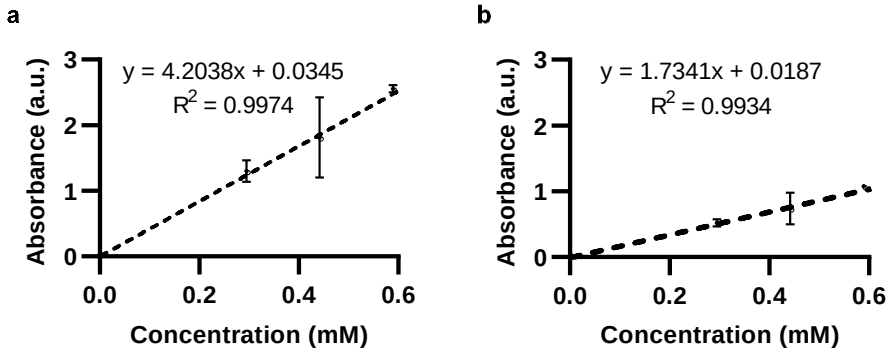

Figure 3.9 Calibration curves for absorbance at (a) 460 nm and (b) 640 nm versus the concentration of HULK absorbed into *DN-0* membranes. From these calibration curves, the actual concentration of HULK within *DN-x* membranes was calculated (Figure 3.3 d).

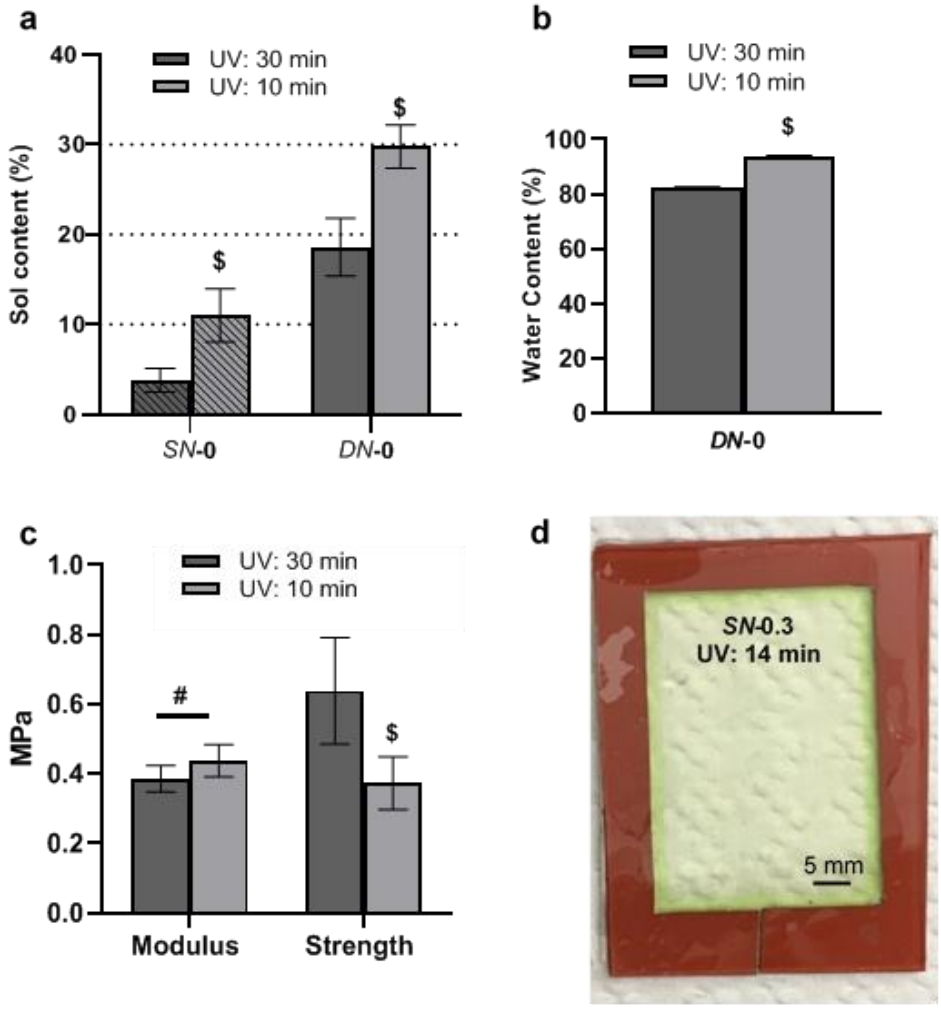

Figure 3.10 (a) Sol content of *SN-0* and *DN-0* membranes fabricated with 30 min or 10 min UV-cure. (b) Water content of *DN-0* membranes cured for 30 min and 10 min. (c)

Compressive strength of *DN-0* cured for 30 min and 10 min. (d) Photo image of *SN-0.3* membrane cured for 14 min. (\$: $p \leqslant 0.05$, significantly different versus 'UV: 30 min'; #: $p > 0.05$, no significant difference)

Figure 3.11 Photo image of an empty vial previously used to contain the precursor solution of *SN-0.5*. Visible aggregation was observed on the bottom of the glass vial, attributed to the high HULK concentration.

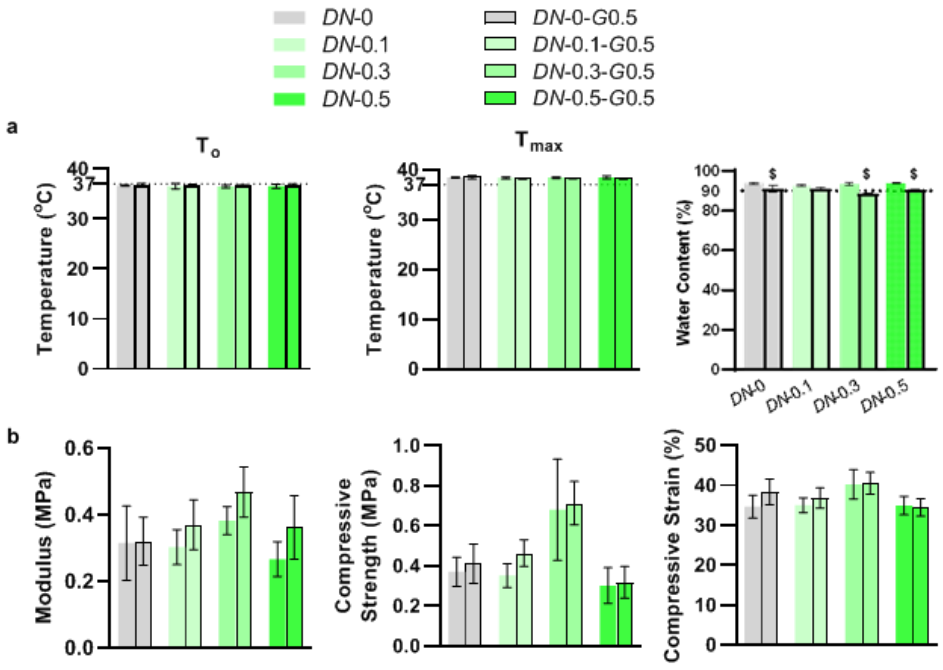

Figure 3.12 (a) VPTT (T_o and T_{max}), and water content of *DN-x* and *DN*-x-*G*0.5 (x = 0, 0.1, 0.3, and 0.5). (b) Compressive mechanical properties of DN-x and *DN-x-G*0.5 (x = 0, 0.1, 0.3, and 0.5). There were no significant changes between *DN*-x and the corresponding

DN-x-*G*0.5 (i.e., same value of *x*). (\$: $p \leqslant 0.05$, significantly different versus corresponding *DN-x*). Data also shown in Tables S4a and S4b.

Table 3.2 Absorbance of *SN-x* and *DN-x* membranes at 460 nm & 640 nm. (Data corresponds to that reported in Figure 3.3c.)

	460 nm (a.u.)	**640 nm (a.u.)**
DN-0	0.042 ± 0.003	0.035 ± 0.003
DN-0.1	0.168 ± 0.015	0.082 ± 0.011
DN-0.3	0.372 ± 0.029	0.161 ± 0.019
DN-0.5	0.59 ± 0.043	0.247 ± 0.027
SN-0	0.041 ± 0.008	0.037 ± 0.008
SN-0.1	0.173 ± 0.028	0.095 ± 0.036
SN-0.3	0.408 ± 0.043	0.183 ± 0.025
SN-0.5	0.666 ± 0.02	0.284 ± 0.013

Table 3.3 Calculated concentration of actual amount of HULK in *DN-x* membranes. (Data corresponds to that reported in Figure 3.3d.)

	Calculated Conc. with Ab at 460 nm (mM)	**Calculated Conc. with Ab at 640 nm (mM)**
DN-0.1	0.032 ± 0.004	0.035 ± 0.008
DN-0.3	0.078 ± 0.008	0.08 ± 0.011
DN-0.5	0.133 ± 0.01	0.132 ± 0.016

Table 3.4 Sol content (%) of *SN-0* and *DN*-0 membranes fabricated with 10 min or 30 min UV-cure. (Data corresponds to that reported in Figure 3.10a.)

	***SN*-0 (%)**	***DN*-0 (%)**
10 min UV-curing	3.8 ± 1.3	11 ± 2.9
30 min UV-curing	18.6 ± 3.2	29.8 ± 2.4

Table 3.5 Water content (%) of *DN-0* membranes fabricated with 10 min or 30 min UV-cure. (Data corresponds to that reported in Figure 3.10b.)

	***DN*-0 (%)**
10 min UV-curing	93.8 ± 0.4
30 min UV-curing	82.3 ± 0.4

Table 3.6 Compressive modulus (E) and strength (CS) and of *DN-0* membrane fabricated with 10 min or 30 min UV-cure. (Data corresponds to that reported in Figure 3.10c.)

	E (MPa)	**CS (MPa)**
10 min UV-cure	0.44 ± 0.05	0.37 ± 0.08
30 min UV-cure	0.39 ± 0.04	0.64 ± 0.15

Table 3.7 Deswelling/swelling kinetics at 20 min and 30 min of *DN-x* membranes. (Data corresponds to that reported in Figure 3.4a.)

	Weight Change at 20 min (%)	**Weight Change at 30 min (%)**
DN-0	99.3 ± 0.75	97.0 ± 0.09
DN-0.1	98.3 ± 1.1	96.6 ± 1.4
DN-0.3	98.8 ± 0.77	97.0 ± 0.83
DN-0.5	99.2 ± 0.17	97.4 ± 0.32

Table 3.8 Glucose diffusion coefficient (D_{eff}) values of *DN-x* membranes at RT and 37 °C. (Data corresponds to that reported in Figure 3.4b.)

	D_{eff} at RT ($\times 10^{-6} cm^2 s^{-1}$)	**D_{eff} at 37 °C ($\times 10^{-6} cm^2 s^{-1}$)**
DN-0	2.56 ± 0.41	3.48 ± 0.69
DN-0.1	2.01 ± 0.29	2.9 ± 0.44
DN-0.3	2.56 ± 0.33	2.90 ± 0.35
DN-0.5	2.42 ± 0.22	3.33 ± 0.44

Table 3.9 Mechanical properties of *DN-x* membranes. (Data corresponds to that reported in Figure 3.5.)

	Compressive Modulus (MPa)	**Compressive Strength (MPa)**	**Compressive Strain (%)**
DN-0	0.44 ± 0.05	0.37 ± 0.08	37.3 ± 3.8
DN-0.1	0.5 ± 0.07	0.36 ± 0.11	32.9 ± 4.9
DN-0.3	0.53 ± 0.09	0.53 ± 0.05	38.2 ± 1.8
DN-0.5	0.42 ± 0.09	0.17 ± 0.08	24.5 ± 8.2

Table 3.10 VPTT and water content of DN membranes before (*DN-x*, x = 0.1, 0.3 & 0.5) and after incorporation of GOx (*DN-x-G0.5*, x = 0.1, 0.3, & 0.5). (Data corresponds to that reported in Figure 3.12a.)

	T_o (° C)	**T_{max} (° C)**	**Water Content (%)**
DN-0	36.7 ± 0.1	38.5 ± 0.1	93.8 ± 0.4
DN-0.1	36.6 ± 0.6	38.4 ± 0.2	92.7 ± 0.6
DN-0.3	36.5 ± 0.3	38.4 ± 0.2	93.3 ± 0.7
DN-0.5	36.5 ± 0.4	38.5 ± 0.3	93.8 ± 0.3
DN-0-G0.5	36.8 ± 0.3	38.5 ± 0.4	91.1 ± 1.8
DN-0.1-G0.5	36.8 ± 0.1	38.2 ± 0.1	91.0 ± 0.8
DN-0.3-G0.5	36.7 ± 0.1	38.2 ± 0.1	88.6 ± 0.3
DN-0.5-G0.5	36.8 ± 0.2	38.2 ± 0.1	90.7 ± 0.2

Table 3.11 Mechanical properties of DN membranes before (*DN-x*, x = 0.1, 0.3 & 0.5) and after incorporation of GOx (*DN-x-G0.5*, x = 0.1, 0.3, & 0.5). (Data corresponds to that reported in Figure 3.12b.)

	E (MPa)	**CS (MPa)**	**ε (%)**
DN-0	0.31 ± 0.11	0.37 ± 0.07	34.6 ± 2.9
DN-0.1	0.30 ± 0.05	0.35 ± 0.06	35.0 ± 1.9
DN-0.3	0.38 ± 0.04	0.68 ± 0.25	40.2 ± 3.7
DN-0.5	0.27 ± 0.05	0.30 ± 0.09	34.9 ± 2.3
DN-0-G0.5	0.32 ± 0.07	0.41 ± 0.10	38.3 ± 3.2
DN-0.1-G0.5	0.37 ± 0.08	0.46 ± 0.07	36.8 ± 2.5
DN-0.3-G0.5	0.47 ± 0.08	0.71 ± 0.11	40.5 ± 2.7
DN-0.5-G0.5	0.36 ± 0.10	0.32 ± 0.08	34.4 ± 2.2

Table 3.12 GOx concentration based on its enzyme activity (unit/mL) for aqueous GOx fabrication solution (0.5 mg/mL) and *DN-x-G0.5*. (Data corresponds to that reported in Figure 3.6b.)

	GOx Activity (unit/mL)
GOx solution	841.2 ± 6.8
DN-0-G0.05	158.4 ± 51.4
DN-0.1-G0.5	168.5 ± 17.6
DN-0.3-G0.5	125.7 ± 50.6
DN-0.5-G0.5	135.5 ± 10.8

Table 3.13 GOx concentration based on its enzyme activity (unit/mL) for *DN-0.3-Gy*. (Data corresponds to that reported in Figure 3.7a.)

	GOx Activity (unit/mL)
DN-0.3-G0.05	45.4 ± 2.9
DN-0.3-G0.1	67.3 ± 8.6
DN-0.3-G0.5	111.3 ± 13.2

Table 3.14 Glucose sensing based on phosphorescence lifetime of *DN-0.3-G0.05*. (Data corresponds to that reported in Figure 3.8.)

Glucose Concentration (mg/dL)	**Phosphorescence lifetime (µs)**
0	15.9 ± 5.9
50	52.7 ± 5.9
100	100.5 ± 8.6
200	121.4 ± 11.5
300	132.6 ± 15.8

4. A SELF-CLEANING SILICONE CONTAINING DOUBLE NETWORK HYDROGEL MEMBRANE TO ENHANCE GLUCOSE SENSING

4.1. Overview

Hydrogels as one of the most utilized materials in biomedical engineering possess wide-range adjustable properties. Their properties can be easily controlled with network structures and polymer chemistries. For example, silicones were added to hydrogels for contact lens applications, for the increased oxygen permeability. In our previous work, a hydrogel glucose sensor was fabricated based on a biocompatible "self-cleaning" hydrogel membrane and phosphorescence sensing assay. In this study, micro-domains of silicone contents were crosslinked into the hydrogel glucose sensor. The oxygen permeability of the silicone containing hydrogels was evaluated toward their glucose sensitivity. The silicone phase solution, containing silicone monomer 3-(methacryloyloxy)propyltris(trimethylsiloxy)silane, crosslinker methacryloxypropyl terminated polydimethylsiloxane and photoinitiator 2-hydroxy-2-methylpropiophenone, was dispersed into the aqueous phase precursor solution with a ultrasonicator processor. The emulsion was cured as first network, and a second network based on poly(*N*-isopropylacrylamide-*co*-acrylamide) was cured as follow. With the addition of silicones, the hydrogels exhibited increased toughness. However, we observed that the diffusion properties of the hydrogels were also influence by macro-structure of the hydrogel. *SiHy*-0.25, with 0.25 M silicones in the first network, showed significant increased glucose and

oxygen permeability due to phase separation. This composition also showed the best glucose sensitivity, especially toward the higher glucose ranges (~300 mg/dL).

4.2. Introduction

With the prevalence and rapid growth of diabetes,[1-3] continuous glucose monitors (CGMs) that allow 24 hour tracking of glucose levels in real-time have been emerged for improved blood sugar management in order to minimize the short- and long-term complications.[23, 162, 206-209] On-the-market CGMs (Medtronic Guardian™, Dexcom G6, and Abbott FreeStyle® Libre 2) employ a transcutaneous electrochemical sensor design for monitoring glucose levels in the interstitial fluid (ISF). The transcutaneous probe is linked to a transmitter that is adhered to the skin on the upper arm or abdomen, and delivers the data to a customized reader or a smart phone. While improvements have been made (e.g., ease of insertion, and reduced less irritation and infections),[22] transcutaneous sensors still require frequent replacements (~7-14 days) due to biofouling, leading to inconvenience, reoccurring costs, and the potential for subcutaneous fibroses.[15, 23, 26, 164] Anticipated to improve user comfort and convenience, Senseonics developed a CGM (Eversense®) based on a fully subcutaneous implant (d ~3.5 mm × l ~ 18.3 mm) that contained an optical hydrogel sensor, optics, and electronics in a poly(methyl methacrylate) (PMMA) cylinder case.[29, 30] With a silicone collar releasing dexamethasone acetate targeting the inflammatory response, this implant was FDA approved for 90-day use, and potential for 180-day utility.[13, 32] However, this CGM requires surgical implantation and removal (in the upper arm) and there was voluntary recall in 2019 due

to inadequate hydration of hydrogel sensors from manufacturing issue, which resulted in shortened lifetime to < 3 weeks.[33]

A glucose sensor that would be small enough to non-surgically implant in the wrist subcutaneous tissue (e.g., via trocar needle), interrogated without a skin-attached transmitter, and able to function for extended periods requires overcoming significant challenges. Optical glucose sensors offer advantages over electrochemical sensors as they could be interrogated exclusively via a LED and photodiode pair on a smart-watches, allowing for the exclusion of skin-attached transmitters. Numerous optical glucose sensing approaches have been has been studied,[7, 15, 210, 211] including with assays based on fluorescent intensity measurements (e.g., Förster resonance energy transfer (FRET) assays,[13, 20, 24, 27, 35, 212] phenylboronic fluorescence assays,[31, 171] and phosphorescence lifetime assays[178]). To advance the design of an optical glucose biosensor, the manner in which the assay is housed is paramount and must address numerous issues, including ease of biosensor fabrication, assay retention, glucose diffusion to assay, and minimizing surface biofouling and the foreign body reaction (FBR). This latter issue is considered a primary barrier to the long-term functionality of implanted glucose biosensors in general.[13, 20, 24, 27, 35, 212] Numerous material strategies have been explored to improve implant biocompatibility, including refining implant shape, size and stiffness,[40-42] anti-inflammatory drug elution,[43, 44] and surface modifications.[45-47] Owing to the tunability of diffusivity, permeability, and other key properties, hydrogels have emerged as particularly intriguing options for constructing glucose biosensors,[31, 49] as both surface coatings [47, 50, 51] as well as bulk matrices to embed assays.[31, 52]

Herein, we reported the proof-of-concept study of an optical glucose biosensor constructed from a phosphorescence lifetime assay and a customized thermosensitive matrix. The assay is based on a commercially available metalloporphyrin fluorophore, Pd meso-tetra(sulfophenyl)-tetrabenzoporphyrin ($[PdPh_4(SO_3Na)_4TBP]_3$), denoted as "HULK" for its bright green color,[93] in combination with glucose oxidase (GOx). HULK provides distinct benefits versus other glucose-sensitive assay based on fluorescent intensity values.[13, 20, 24, 27, 31, 35, 171, 212] For HULK, the phosphorescence lifetime is regulated by oxygen collision quenching, such that increased oxygen levels generally lead to a decreased lifetime, which is proportional to intensity changes but is independent of the assay concentration, excitation source intensity, or other environmental factors (such as skin thickness or pigmentation).[176, 181, 182] Specifically, the phosphorescence lifetime of HULK can be related to glucose levels as oxygen is consumed via glucose oxidation as catalyzed by GOx,[95, 176, 178-180] per Equation 1.

$$\beta\text{-D-Glucose} + O_2 + H_2O \xrightarrow{GOx} D\text{-}Glucono\text{-}1,5\text{-}Lactone + H_2O_2 \quad (1)$$

For the membrane housing, a first consideration for incorporation of the HULK/GOx assay is anticipation of biofouling upon implantation. In contrast to typical strategies employing passive resistance to biofouling,[35, 213, 214] we have previously reported a thermoresponsive, "self-cleaning" double network (DN) hydrogel membranes with excellent biocompatiblity.[48] Based on thermoresponsive *N*-isopropylacrylamide (NIPAAm) and anionic 2-acrylamido-2-methylpropane sulfonic acid (AMPS), the membrane was comprised of a tightly crosslinked 1st network of [P(NIPAAm-*co*-AMPS)] (75:25 wt% ratio), and a loosely crosslinked 2nd network of NIPAAm copolymerized with

N-vinylpyrrolidone (NVP) to precisely tune the volume phase transition temperature (VPTT). Thus, the membrane's VPTT can be tailored to produce cyclical deswelling/reswelling with temperature fluctuations occurring in subcutaneous tissues, both [52, 65] rat models (~37-38 ºC)[187, 188] and a human wrist (~35-36 ºC).[185, 186] Implant-sized cylindrical membranes (~2.5 x 5 mm) were shown to intermittently and slightly deswell (~20-25 μm) at these relatively higher temperatures. This active "self-cleaning" process was shown to diminish adhesion of cultured cells.[65, 215] Moreover, when implanted for 90 days the rat model, these implant-size membranes (VPTT: T_{onset} ~36.5 °C, T_{max} of ~41 °C) exhibited excellent biocompatibility with fast healing response and a remarkably thin fibrous capsule.[48]

For construction of a glucose biosensor, a customized thermosensitive membrane was required for effective incorporation of the HULK and GOx. In a more recent report, new self-cleaning DN hydrogel membrane was prepared from a NIPAAm and cationic (3-acrylamidopropyl) trimethylammonium chloride at 75:25 mol% [P(NIPAAjm-*co*-APTAC)] 1st network and loosely crosslinked NIPAAm and acrylamide [P(NIPAAm-*co*-AAm)] 2nd network. The VPTT was precisely tuned with AAm levels.[93] During formation of the cationic 1st network, the anionic HULK was incorporated to leverage electrostatic interactions for its retention. GOx was introduced along with glutaraldehyde during formation of the 2nd network, permitting covalent bonding of GOx with AAm segments' primary amides, and also with the dialdehydes of glutaraldehyde. The HULK and GOx were successfully immobilized in the membrane, and could achieve sensitivity for glucose levels in the lower physiological range (50 to 200 mg/dL). The loss of sensitivity at higher

glucose levels (i.e., 200-500 mg/dL) was attributed to a sub-optimal oxygen permeability of the membrane, leading to oxygen consumption within the membrane. For oxygen-sensitive HULK/GOx glucose sensing, membrane oxygen levels are critical **(Figure 4.1a)**. As the oxygen concentration directly influenced the phosphorescence signals, there are three possible scenarios that may occur in glucose concentration range of interest (50 - 500 mg/dL) **(Figure 4.2 b)**. Two scenarios would not yield differences in phosphorescence signal: (i) if membrane oxygen permeability is very low relative to oxygen consumption ("oxygen consumption dominant"), and (ii) if membrane oxygen permeability is very high relative to oxygen consumption ("oxygen diffusion dominant"). A third and ideal scenario occurs when membrane oxygen permeability affords desirable oxygen levels ("oxygen diffusion sufficient").

To afford the desired sensitivity of HULK/GOx to glucose levels across the physiological range, the oxygen permeability of the thermosensitive membrane must be enhanced. To achieve this, membranes were herein modified with silicone microdomains. Polydimethylsiloxane (PDMS) has been incorporated into hydrogels to improve gas permeability,[216, 217] related to its flexibility of chains comprised of siloxane bonds that yield free volumes for the transportation.[218, 219, 220, 221] Due to the insolubility of PDMS in aqueous solution, the manner of introduction is imperative to achieve good distribution. To modify the 1st network precursor solution, an ultrasonicate processor was used to disperse the silicone phase, consisting of 3-(methacryloyloxy)propyltris(trimethylsiloxy)-silane (TRIS), methacryloxypropyl terminated polydimethylsiloxane (crosslinker), and photoinitiator. The resulting emulsion was UV-cured, producing a 1st network

[P(NIPAAjm-*co*-APTAC)] with embedded silicone microparticles. The P(NIPAAm-*co*-AAm) 2nd network was subsequently formed. Membranes were first characterized in terms of key material properties, such as phosphorescence intensity, VPTT, glucose diffusivity, and mechanical properties. Next, HULK and GOx were incorporated into the silicone containing membranes at different concentrations, and the phosphorescent properties related to local glucose levels were characterized.

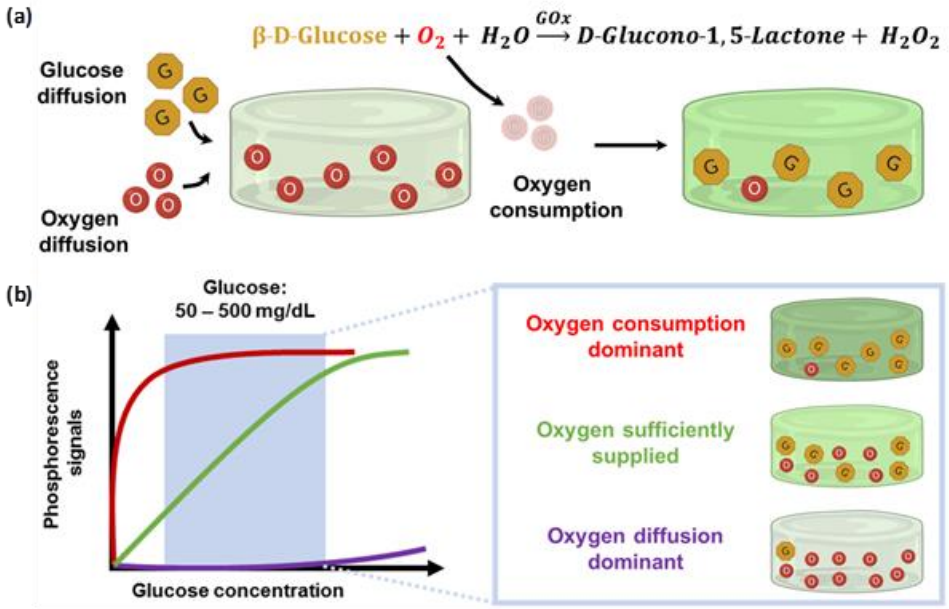

Figure 4.1 (a) An illustration of sensing mechanism of HULK/GOx, after the introduction of glucose, the oxygen in the membrane can be consumed via glucose oxidation, resulting in increased phosphorescence signals. The phosphorescence intensity was directly linked to the oxygen concentration in the membrane, which was determined by the oxygen consumption and oxygen diffusion. (b) An illustration of three possible sensing profile between the interested glucose concentration range (50 - 500 mg/dL). The three profiles were determined by the relationship between oxygen diffusion and oxygen consumption.

4.3. Experimental

4.3.1. Materials

3-(Methacryloyloxy)propyltris(trimethylsiloxy)silane (TRIS) was purchased from Alfa Aesar. Methacryloxypropyl terminated polydimethylsiloxane (4-6 cSt, DMS-R05)

was purchased from Gelest. (3-Acrylamidopropyl)trimethylammonium chloride solution (75% wt.% in water, APTAC), *N*-isopropylacrylamide (97%, NIPAAm), *N*,*N*'-methylenebisacrylamide (99%, BIS), 2-hydroxy-4'-(2-hydroxyethoxy)-2-methylpropiophenone (98%, Irgacure 2959), acrylamide (≥ 99%, AAm), 2-Hydroxy-2-methylpropiophenone (97%, Darocur® 1173), poly(vinyl alcohol) (87-90% hydrolyzed, Mw ~30-70 kg/mol, PVA), ethanol (HPLC grade), triton X-100, glucose oxidase (100k - 250k units/g solid, without added oxygen) and glutaraldehyde solution (Grade II, 25% in water) were obtained from Sigma-Aldrich. Mouse fibroblast cells (NIH/3T3) were obtained from the American Type Culture Collection (ATCC). Dulbecco's Modified Eagle's Medium (DMEM, HyClone, GE Sciences), phosphate-buffered saline (PBS, 1X, pH 7.4, without calcium and magnesium, Corning®) and trypsin-EDTA (0.5%, no phenol red, Gibco) were purchased from Fisher Scientific. Fetal bovine serum (Atlanta Biologicals, USA), and penicillin/streptomycin (100 U/100 µg/mL, Gibco), alamarBlue, phalloidin stain (Biotium) and Hoechst 33258 (Biotium) were obtained from Thermo Fisher. All chemicals were used directly without further purification. Deionized water (DI) with a resistance of 18 MΩ·cm was purified with Cascada LS MK2, Pall.

4.3.2. Fabrication of DNs

Similar to our previous works, the double network hydrogels (DNs) were fabricated via a 2-step UV-curing process **(Figure 4.2)**. Briefly, the 1st network precursor solution was injected into a "sandwich" mold assembled with one piece of silicone spacer (thickness: 0.7 mm or 0.2 mm) in between two pieces of glass slides (75 mm × 50 mm). It was immediately subjected to a UV lamp (UV-transilluminator, 6 mW/cm2, λ_{peak} = 365

nm) for 60 min (rotating the side facing down every 30 min). During the UV-curing, the mold was immersed in an ice bath preventing raised temperature due to curing. The resulting single network (SN) was removed from the mold, and equilibrated in 2nd network precursor solution in refrigerator. After 24 hr, the SN was placed in a sandwich mold assembled with one piece of polycarbonate spacer (thickness: 1 mm or 0.25 mm) in between two pieces of glass slides (75 mm × 50 mm). The mold was immersed in an ice bath while subjecting to UV-curing (60 min, rotating every 30 min). Before characterization or sequential sensor fabrication, the cured DN was immersed in 100% IPA for 2 days and DI for 2 days, with media changes every 12 hr.

The slabs prepared with 0.7 mm and 1 mm spacer for SN and DN were utilized to characterize the physical properties of the DNs. The slabs prepared with 0.2 mm and 0.25 mm spacer for SN and DN were used for later glucose sensor fabrication.

To prepare 1st network precursor containing silicone microdroplets, silicone monomer (TRIS) crosslinker (DMS-R05, 2.5 mol% based on TRIS concentration) and photoinitiator (Darocur 1173, 0.5 mol% based on TRIS concentration) were mixed together forming silicone phase. Meanwhile, monomer NIPAAm and APTAC, crosslinker (BIS, 2.5 mol% based on NIPAAm and APTAC concentration), and photoinitiator (Irg 2959, 0.5 mol% based on NIPAAm and APTAC concentration) were dissolved in 1 % (wt/vol) PVA aqeuous solution forming water phase. The silicone phase liquid was mixed with the water phase solution with ultrasonicator processor (Fisher Scientific, 120 Watt, 20 kHz), with 30% amplitude for 5 min **(Figure 4.2)**. The 2nd network solution was prepared as described in Table 1, 2 M NIPAAm, 5 wt% AAm (based on NIPAAm), 0.1

mol% of BIS (based on NIPAAm), and 2 mol% of Irgacure 2959 (based on NIPAAm) were dissolved in DI. The resulting compositions were denoted as *SiHy*-x (x = 0, 0.25 or 0.5), where x representing the concentrations (M) of TRIS in the 1st network.

Table 4.1 Compositions, VPTTs, and water contents of DN membranes prepared with different concentrations of silicones.

	1st network (1 M)			2nd network		DN		
	Aqueous Phase		Silicone Phase	Monomer		VPTT		Water content
	NIPAAm	APTAC	TRIS	NIPAAm	AAm	T_o	T_{max}	
SiHy-0	0.75 M	0.25 M	0 M	2 M	5%	36.4 ± 0.2	38.5 ± 0.1	87.7 ± 0.3%
SiHy-0.25	0.5 M	0.25 M	0.25 M	2 M	5%	36.4 ± 0.2	38.4 ± 0.3	88.6 ± 0.4%
SiHy-0.5	0.25 M	0.25 M	0.5 M	2 M	5%	36.5 ± 0.2	38.1 ± 0.3	88.9 ± 0.2%

DN hydrogels were denoted as "*SiHy-x*", where *x* = TRIS concentration (i.e., 0, 0.25 or 0.5 M) in the 1st network precursor solution. BIS (2.5 mol% based on monomer concentration in aqueous phase) and Irg (0.5 mol% based on monomer concentration in aqueous phase) were added in the aqueous phase as crosslinker (BIS) and photoinitiator. For the silicone phase, DMS-R05 (2.5 mol% based on TRIS concentration) and EGDA (0.5 mol% based on TRIS concentration) were added as crosslinker and photoinitiator. The 2nd network was consisted of 5 wt% of AAm in addition to 2M NIPAAm, 0.1 mol% of BIS based on NIPAAm, and 2 mol% of Irgacure 2959 based on NIPAAm.

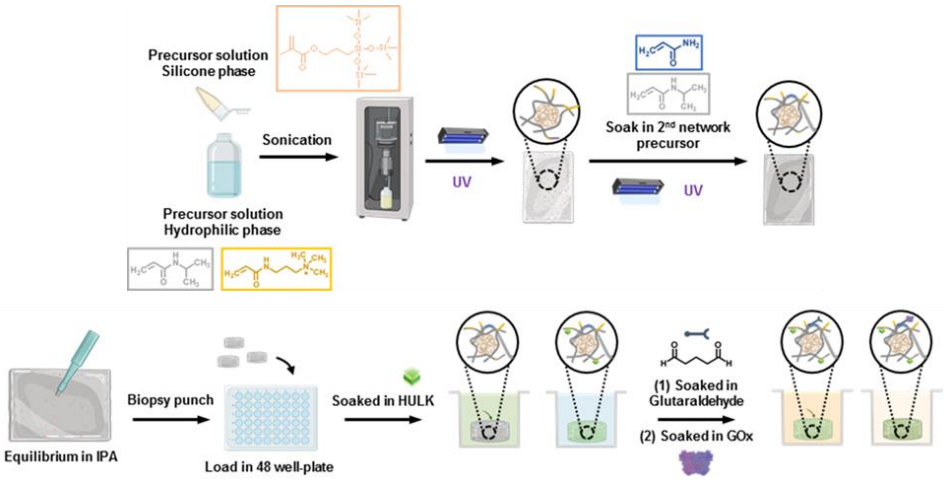

Figure 4.2 (a) a scheme showing the UV-curing fabrication for the DN hydrogels containing the silicone microdomains. (b) a scheme showing the incorporation of HULK and GOx post UV-curing.

4.3.3. Characterization of microdroplet size

The 1st network precursor solution (*SiHy*-0.25 or *SiHy*-0.5) was diluted 100× with 1 % (wt/vol) PVA solution. 0.5 μL of the diluted solution was vacuum dried (30 in. Hg) on an aluminum specimen mount at room temperature (RT). The dried samples were subjected to Au-Pt sputter coating (~ 7 nm) and imaged with a scanning electron microscope (SEM, Tecan Vega 3, accelerating voltage of 10 kV).

Image analysis software (Image J) was used to further analyze the size of the microdroplets. Measurements (N = 20) were taken along the two diagonal midlines of each SEM image (N = 5 for each composition).

4.3.4. Sol content

For cured SN and DN, disc samples were harvest from the different slabs (SN thickness = 0.7 mm, DN thickness = 1 mm) immediately after curing (N = 5, Ø = 8 mm) and were vacuum dried at RT (30 in. Hg) to obtain the original dry weight (W_{d0}). Each dis sample (SN or DN) was sequentially immersed in 20 mL of 100% IPA for 2 days and 20 mL of DI for 2 days, with media changing every 12 hr. The disc samples were vacuum dried again (RT, 30 in. Hg) to obtain the dry weight after equilibrium in solvents, obtaining the dry weight (W_{d1}). The Sol content for SNs and DNs were calculated using equation one.

$$\text{Sol content} = \frac{W_{d0} - W_{d1}}{W_{d0}} \times 100\% \quad (1)$$

4.3.5. Volume phase transition temperature (VPTT)

The VPTT of *SiHy*-x (x = 0, 0.25 or 0.5) was measured using differential scanning calorimetry (DSC, TA Instruments Q100). A small piece (~10 mg, N = 3) was harvested from a swollen DN slab (thickness = 1.2 mm) with razor blade, blotted with a Kimwipe

and then sealed in a hermetic pan. During the DSC measurements, the samples were cooled to 0 ºC, and were heated up to 60 ºC at a rate of 3 ºC/min for 2 cycles. The VPTT was reported as the temperature (T_o) at the beginning of the endothermic transition and the peak temperature (T_{max}) of the transition. All the results reported were from the 2nd cycle to remove any thermal history.

4.3.6. Equilibrium water content

Hydrogel discs (Ø ~8 mm × thickness ~1.2 mm, N = 5) were harvested from a swollen slab (*SiHy*-x, x = 0, 0.25 or 0.5) with a biopsy punch. Each disc was equilibrated in 20 mL DI for 24 hr (RT). Upon removal, the discs were blotted with Kimwipes and weighed on a digital scale (swollen weight, W_s). The swollen discs were subsequently vacuum dried overnight (RT, 30 in. Hg) to obtain the dry weight (W_d). The water content (W_c) was defined per Equation 2:

$$W_c = \frac{W_s - W_d}{W_s} \times 100\% \quad (2)$$

4.3.7. Attenuated total reflectance-Fourier transform infrared spectroscopy (ATR-FTIR)

Disc samples (N = 3, Ø = 8 mm) were punched from hydrogel slabs (*SiHy*-x, x = 0, 0.25 or 0.5) and were vacuum dried (30 in. Hg) under RT. ATR-FTIR (Bruker ALPHA-Platinum, n = 32) were used to confirm the peaks of Si-CH_3 (1280 – 1240 nm), Si-O-Si (1100 – 1000 nm) and Si-$(CH_3)_2$ (840 – 790 nm).

4.3.8. Morphology of the DNs

SEM (Tecan Vega 3, accelerating voltage of 10 kV) was used to observe the cross-section morphology of the DNs. A small hydrogel piece was harvested from a slab (*SiHy*-

x, x = 0. 0.25 or 0.5) with a razor blade, cutting off a thin layer on both top and bottom exposing the cross-section. The samples were vacuum dried (~30 in. Hg) under RT and were sputter coated with Au-Pt (~ 7 nm) prior to imaging.

4.3.9. Confocal laser scanning microscope (CLSM)

Representative discs samples (Ø ~8 mm × thickness ~1.2 mm, N = 1) were harvested with a biopsy punch and were stained with Nile Red solution for 24 hr. Nile red solution was made as previously reported, by dilute 75 µL of 20 mg/mL Nile red methanol solution with 128 mL of DI.[222] An Olympus FV1000 confocal microscope was used to image each sample (excitation: 488 nm and emission: 500–600 nm). Z-stacks images were acquired with a 0.53 µm/slice for 20 µm depth. Representative slices of the stacks were exported without pseudo-color.

4.3.10. Hydrophilicity

Surface hydrophilicity of the DNs was characterized via static water contact angle (θ_{static}), and was measured using CAM-200 goniometer (KSV instruments) equipped with an autodispenser, video camera and drop-shape analysis software (Attention Theta). A 5 µL DI droplet was placed on the surface of a DN slab (*SiHy*-x, x = 0, 0.25 or 0.5) (blotted with Kim Wipes) and the θ_{static} was monitored over 1 min. The θ_{static} (N = 5) at 0 min and 1 min were compared through all compositions.

The bulk hydrophilicity of DNs was evaluated with H-index. Disc samples (N = 10, Ø = 8 mm, thickness = 1.2 mm) were harvested from slabs (*SiHy*-x, x = 0, 0.25 or 0.5) and were vacuum dried (30 in. Hg, RT, overnight) for dry weight (W_d). Those discs were submerged in 20 mL of 70% IPA (N = 5) or 100% DI (N = 5) for 24 hr. The swollen

weight (W_s) of each disc was measured and the equilibrium swollen ratio ($Q = W_s/W_d$) was calculated for either swollen in 100% DI (Q_{DI}) or 70% IPA (Q_{IPA}). The H-index (H) was defined as Q_{IPA}/Q_{DI}).

4.3.11. Mechanical properties

Compression tests were performed with an Instron 5944 at RT. *SiHy*-x, x = 0, 0.25 or 0.5) discs (d ~6 mm × thickness ~1.2 mm, N = 5) were harvested with biopsy punches from a slab and were blotted with Kimwipes prior to tests. Each disc was placed at the center of the bottom platen and was subjected to a 0.5 N pre-load force, following with compression at a constant strain rate (1 mm/min) until fracture (force drop > 0.5 N). The compressive modulus was calculated from the linear portion of the strain-stress curve (from 0 to 10% strain). The compressive strength and the compressive strain were determined at fracture point.

4.3.12. Glucose diffusion coefficient

SiHy-x (x = 0, 0.25 or 0.5) slabs were cut into square shapes (d ~15 mm × t ~1.2 mm, N = 3, from different DN slabs) with a single edge razor blade. Each sample was placed and gently clamped in between two side-by-side diffusion chambers (PermeGear). DI water (7 mL) and glucose solution (7 mL, 10 mg/mL) were added into the receiver and donor chambers, respectively. Each chamber was stirred with a Teflon-coated stir bar at 100 rpm to maintain a homogenous solution within. The solution temperature was maintained at RT (22 ºC) or 37 ℃ with the water heating jacket system. At 10 min intervals over a period of 1.5 hr, 50 μL of solution was collected from each chamber.

Afterward, glucose concentration of individual collected solution was measured with YSI (YSI 2700 Select Biochemistry Analyzer).

As reported in previous studies,[53, 65] Fick's laws were used to deduct mathematical calculations for diffusion coefficient (D_{eff}) of glucose passing through a hydrogel membrane. The following Equation 4 was used for a side-by-side diffusion model. [Q: quantity of glucose transferred, t: time interval of the diffusion, L: thickness of the sample (~1.2 mm), C_o: the initial glucose concentration (10 mg/mL) and A: the area of the samples exposing for diffusion (1.767 cm^2)]

$$Q = \frac{ADC_0}{L} \times (t - \frac{L^2}{6D_{eff}}) \quad (3)$$

4.3.13. Fabrications of DNs containing HULK

As illustrated in Scheme 3, Disc samples were harvested from hydrogel slabs (thickness: 0.5 mm) using a 6 mm biopsy punch. Each of the disc was immersed in 300 μL of 0.1 mM HULK solution (in IPA) for 48 hr at 35 °C. After soaking, each disc was washed with DI (1 mL, 3 × 10 min) and equilibrated in DI overnight for lateral fabrication.

As the relationship between absorbance and concentration of Hulk in DNs is expected to follow Beer-Lambert law, in order to determine the Hulk concentration in the disc, a linear calibration curves (absorbance at 460 or 640 nm vs. concentration) were plotted using a series of DNs with determined Hulk concentrations **(Figure 4.13)**. The absorbance of the samples were characterized with microplate reader (Tecan, Infinite M200 PRO). Disc samples (Ø = 6 mm, thickness = 0.5 mm, N = 15) were harvested from *SiHy*-x (x = 0, 0.1 or 0.25) slabs (thickness = 0.5 mm) with a biopsy punch. Each sample was soaked in 300 μL HULK solution at 35 °C (in IPA, 0.0018 mM, 0.0037 mM, 0.018

mM, 0.037 mM and 0.07 mM, N = 3 for each concentration). After 48 hr, the discs were washed with IPA (1 mL, 3 × 10 min) and equilibrated in IPA overnight. Considering the transparency of the DNs, all absorbance readings were taken when the DNs were equilibrated with IPA and each sample was immersed in 100 μL in IPA during characterization.

The Hulk concentration in each disc was calculated with moles of loaded Hulk (moles of Hulk in original supernatant subtracts moles of residual Hulk in the final supernatant) divided by the volume of the disc (~11 μL). To determine the residual Hulk concentration in the final supernatant, a calibration curve was made plotting the absorbance of Hulk IPA solution and their concentrations (0.01 mM, 0.05 mM, 0.1 mM and 0.2 mM) (**Figure 4.14**).

4.3.14. Fabrications of hydrogel glucose sensors

The last step to finish a glucose sensor was incorporating the GOx. The disc samples, equilibrated in DI, were sequentially soaked in 2.5 % (w/v) of glutaraldehyde aqueous solution (300 μL) for 1.5 hr and Gox aqueous solution overnight. In between these two soakings, each disc was washed with DI (1 mL, 3 × 10 min) and equilibrated in DI for 1 hr. The finished hydrogel sensors, containing HULK and Gox, were stored in 5 mM NaAc solution (pH ~5) in refrigerator before all following characterizations.

The Gox activity was determined using a colorimetric activity assay kit. The disc samples were placed in a 96 well-plate and were equilibrated in 5 mM NaAc solution at 37 °C prior to testing. After 10 min, the NaAc solution was removed, followed by the addition of 150 μL activity assay solution (pH ~5, at 37 ºC), which was comprised of 145

μL of 0.17 mM *o*-DDH and 1.72% (w/v) glucose (dissolved in 50 mM NaAc solution), and 5 μL 60 unit/mL POD aqueous solution. Immediately after the addition, the absorbance at 500 nm was recorded every 15 s for 5 min. The GOx enzyme activity was calculated with equation 3 ($\frac{\Delta Ab_{500nm}}{min}_{test}$: absorbance changes within one minute for testing samples; $\frac{\Delta Ab_{500nm}}{min}_{blank}$: absorbance changes within one minute for blank cells; ε: molar attenuation coefficient of oxidized *o*-DDH at 500 nm, which equals 7.5 mM^{-1}•cm^{-1}; l: light pathlength, which was measured to be ~0.5 cm; V_{assay}: volume of the assay, which was 150 μL; and V_{disc}: volume of the disc, which was calculated to be ~11 μL).

$$\frac{Units}{mL} of\ enzyme = \left(\frac{\frac{\Delta Ab_{500nm}}{min}_{test} - \frac{\Delta Ab_{500nm}}{min}_{blank}}{\varepsilon * l} \right) * \frac{V_{assay}}{V_{disc}} \quad (3)$$

4.3.15. Oxygen permeability

Hydrogel glucose sensors (*SiHy*-x, x = 0, 0.25 and 0.5. Ø = 6 mm, thickness = 0.5 mm, N = 3 for each composition) were fabricated containing ~0.3 mM HULK and ~100 unit/mL GOx. For each composition, three samples were immersed in 15 mL NaAc solution (5 mM) within a 20 mL scintillation vial and were degassed by bubbling with N_2 for 1 hr. The scintillation vials were than sealed with parafilm and equilibrated at 37 °C. Each sample was quickly placed in a cell of a 96-wellplate, containing 80 μL DI which was equilibrated in open container to air overnight. The phosphorescence intensity (fluorescence intensity at excitation: 460 nm, emission: 800 nm and lagtime: 25 μs) changes of the sample were recorded over 1 min. As the phosphorescence intensity changing rate is directly related to oxygen permeability, the slope of phosphorescence intensity vs time was calculated and used as indicator for oxygen permeability.

4.3.16. Glucose sensitivity

Hydrogel glucose sensors (*SiHy*-x, x = 0, 0.25 and 0.5. Ø = 6 mm, thickness = 0.5 mm, N = 3 for each composition) were fabricated containing ~0.3 mM HULK and ~100 unit/mL GOx. For each composition, three samples were equilibrated in 15 mL NaAc solution (5 mM) at 37 °C. Each sample was placed into one cell of a 96-wellplate and 50 µL glucose solution (0, 50, 100, 150, 200, or 300 mg/dL) was added and the discs equilibrated for precisely 5 min (at 37 ºC). The phosphorescence intensity (fluorescence intensity at excitation: 460 nm, emission: 800 nm and lagtime: 25 µs) were recorded over 5 min equilibration. The normalized phosphorescence intensity (intensity at 0 min equilibrating in NaAc solution / intensity at 5 min equilibrating in given glucose solution) was calculated for each glucose concentration to value the sensitivity. A given sample was sequentially equilibrated with glucose solutions of increasing concentration, washing 3X with 5 mM NaAc solution for 5 min in between.

4.3.17. Cytocompatibility

Hydrogel discs (6 mm × 0.5 mm, diameter × thickness, N = 3, from different hydrogel sheets) were harvested with a biopsy punch, and were loaded with 0.3 mM Hulk. They were sterilized by soaking in 70% (v/v) ethanol (30 min × 3) and recovered in sterilized PBS (30 min × 3). After sterilization, ~100 unit/mL GOx was bonded to the hydrogel discs. Mouse fibroblast cells (NIH/3T3) (ATCC) were cultured under normal media conditions consisting of Dulbecco's Modified Eagle's Medium (DMEM) with 10 % fetal bovine serum and 1% penicillin/streptomycin (100 U/100 µg/mL). After every 2-3 days, culture media was exchanged for fresh media. Cells were passaged with 0.5%

trypsin-EDTA upon reaching confluency of ~70% and seeded at ~2500 cells/cm^2. For indirect cellular viability assay, NIH/3T3 cells were cultured in a 24 well plate at 10,000 cells per wells. The hydrogels of each composition were placed with a transwell insert, which were then placed within the 24 well plate, with cells without transwell inserts acting as control (n=3). After 24 hrs cellular viability was determined using alamarBlue™ according to manufactured protocol. For cellular morphology studies, NIH/3T3 cells were seeded directly on to hydrogels of different compositions for 24 hrs, with cells cultured in a 96 well plate acting as control. For actin staining, cells were, fixed with 2.5% glutaraldehyde and permeabilized with 0.1% TritonX-100. Phalloidin stain was then added according to manufacturer's protocol and samples were incubated for 20 minutes at 37 °C. The stain was removed, washed with 1X PBS three times. Cells were then treated with Hoechst 33258 according to manufacturer's protocol and incubated for 5 minutes at room temperature. Samples were then washed with 1X PBS three times followed by imaging using a fluorescent inverted microscope (ZEISS Axio Vert.A1).

4.4. Results and discussion

For common silicone containing hydrogels, the hydrophilic monomers used were able to mixed with the silicone monomers. The mixed monomer liquid was then cured via UV and the products were equilibrated in DI to allow swelling. However, the critical NIPAAm monomers, to achieve self-cleaning, was not able to dissolve in any silicone monomers. Although, all the components chosen in IPA, the precursor solution was not able to be UV cured with the setup in our lab.

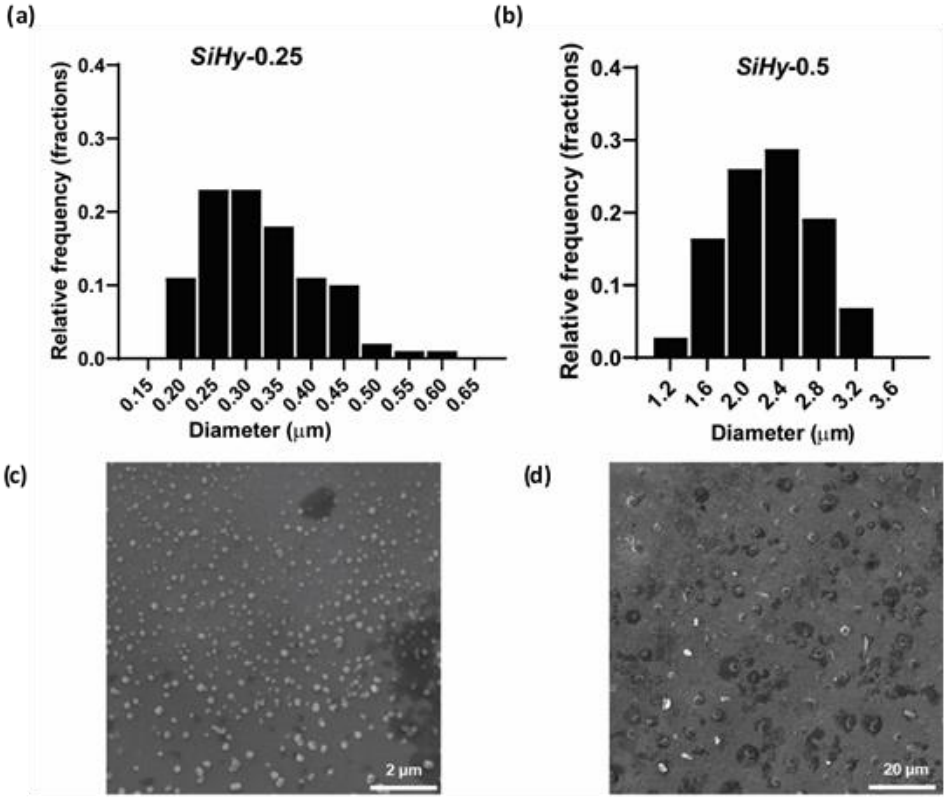

Figure 4.3 (a) Distribution of microdroplet in the 1st network precursor emulsion of *SiHy*-0.25 diameter (μm) measured by image J. (b) Distribution of microdroplet in the 1st network precursor emulsion of *SiHy*-0.5 diameter (μm) measured by image J. (c) Representative SEM image of *SiHy*-0.25 microdroplet in the 1st network precursor emulsion (scale bar: 2 μm). (d) Representative SEM image of *SiHy*-0.5 microdroplet in the 1st network precursor emulsion (scale bar: 20 μm).

In order to successfully incorporate silicones into the hydrogel system, the silicone phase precursor was dispersed in the aqueous phase precursor with a ultrasonicating processor **(Figure 4.2)**. After ultrasonicating, the silicones were dispersed in the 1st network precursor as micro-droplets **(Figure 4.3)**, generating the opaque emulsion precursors **(Figure 4.11)**. With increased silicone concentration, the average diameter of microdroplets in *SiHy*-0.5 precursor (0.32 ± 0.08 μm) was increased comparing to it in *SiHy*-0.25 precursor (2.24 ± 0.5 μm).

The emulsions were stabilized by the addition of 1% PVA. Although no visible phase separation observed within 30 days **(Figure 4.11)**, precursor emulsions were made and used freshly (within 1 hr) for each fabrication. Also due to the opaqueness, aiming for designed degree of curing, the length of the UV-curing for both 1st network and 2nd network was increased to 60 min comparing to our previous works. After extended UV-curing, DNs were equilibrated in 100% IPA and DI in sequence, extracting unreacted monomers, prior to all characterizations. As shown in Figure 4.4a, silicone containing hydrogels (*SiHy*-x, x = 0, 0.25 or 0.5)) were successfully fabricated as described. When equilibrated in DI, the resulted DNs went from clear (*SiHy*-0), translucent (*SiHy*-0.25) to opaque (*SiHy*-0.5) with increasing silicone concentration. This was possibly due to the collapsing silicone chains when they are interacting with a bad solvent (DI), while the hydrophilic sections of the polymers [P(NIPAAm-*co*-APTAC) and P(NIPAAm-*co*-AAm)], at the same time, were extended when interacting DI, a good solvent. As contrast, the resulted DNs were clear equilibrated 100% IPA, a good solvent for both hydrophilic polymer chains and the silicone contents.

To examine the curing degree, SNs and DNs were all sequentially equilibrated in IPA and DI to extract unreacted monomers, and the sol content of each hydrogel was characterized **(Figure 4.4b; Table 4.2)**. Comparing SNs or DNs among *SiHy*-x (x = 0, 0.25 or 0.5), there was no significant difference between three compositions, indicating a similar extend of curing, independent of silicone contents, between SNs or DNs. Moreover, the silicone peaks were confirmed using ATR-FTIR, further demonstrating the success incorporation of silicones **(Figure 4.4c)**. Comparing to *SiHy*-0, peaks of Si-$(CH_3)_2$

(~840 nm), Si-O-Si (~1050 nm) and Si-(CH_3) (~1250 nm) were observed in curves of *SiHy*-0.25 and *SiHy*-0.5.

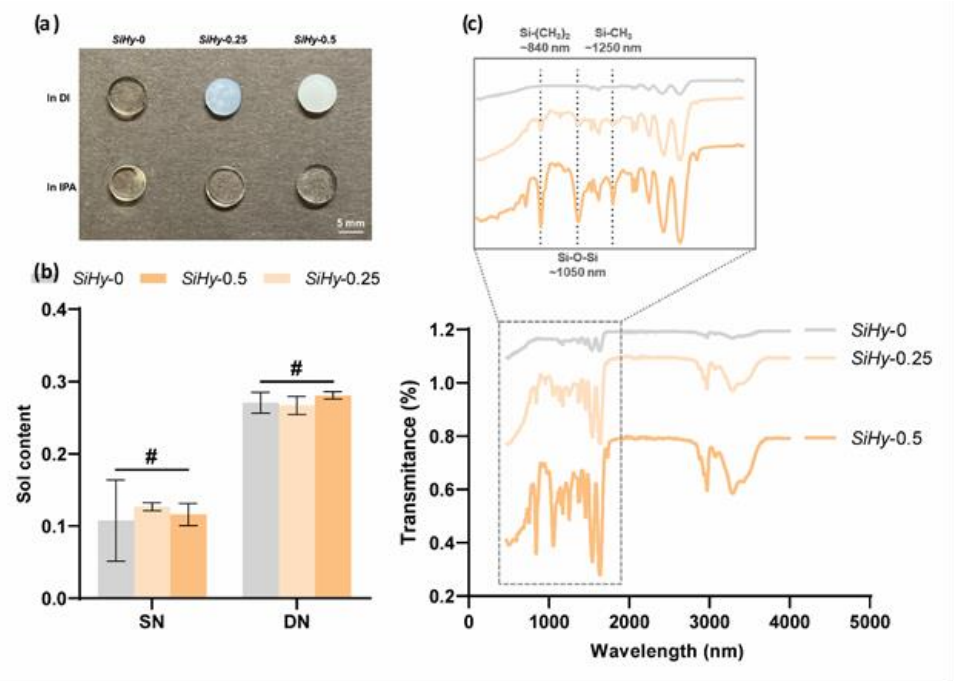

Figure 4.4 (a) Representative photo image of *SiHy*-x (x = 0, 0.25 or 0.5) disc samples immersed in DI or IPA. (b) Sol content of both SNs and DNs for all compositions (*SiHy*-0, *SiHy*-0.25, and *SiHy*-0.5). (c) Representative ATR-FTIR curves of *SiHy*-x (x = 0, 0.25 and 0.5), peaks of Si-CH3 (~1250 nm), Si-O-Si (~1050 nm) and Si(CH3)2 (~ 840 nm) were labeled. (#: $p > 0.05$, no significant difference)

After staining the hydrophobic silicone contents with Nile red, the distribution of the silicones was observed via CLSM **(Figure 4.5)**. Comparing to *SiHy*-x showing no stained component, the micro-domains of stained silicones were thoroughly in the *SiHy*-0.25 and *SiHy*-0.5. Similar to the 1st network precursors, the micro-domains in *SiHy*-0.5 were larger than it in *SiHy*-0.25. More aggregation of the silicones was also observed in *SiHy*-0.5.

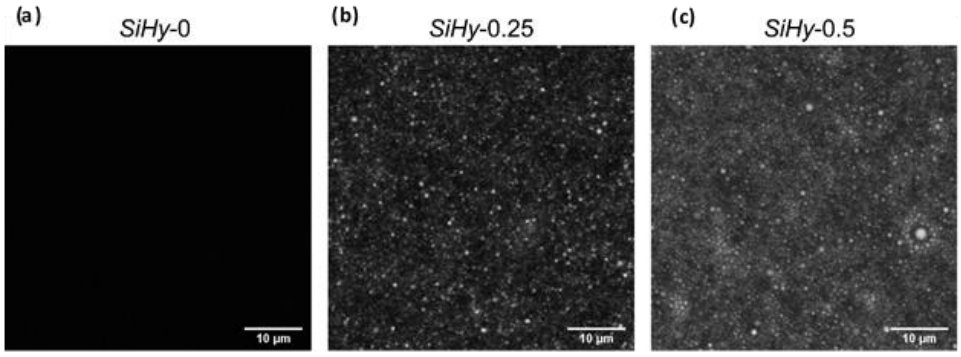

Figure 4.5 Representative CLSM image of (a) *SiHy*-0, (b) *SiHy*-0.25 and (c) *SiHy*-0.5. (Scale bar: 10 µm)

SEM and EDS were used to characterize the DN cross-sections **(Figure 4.6 and Figure 4.12)**. Silicone elements were detected from *SiHy*-0.25 and *SiHy*-0.5 compositions, comparing to blank *SiHy*-0 controls. Interestingly, at this lower silicone concentration, a rough morphology was observed on the cross-section of *SiHy*-0.25, indicating phase separation behaviors. This phase separation could be driven by the hydrophobic sections of [P(NIPAAm-*co*-APTAC) and P(NIPAAm-*co*-AAm)] tending to interact with the silicone micro-domains, while their hydrophilic sections were prone to avoid the micro-domains. With increasing silicone concentration, *SiHy*-0.5 presented a smoother cross-section similar to *SiHy*-0.

The influence of the silicones toward DN hydrogel properties were characterized using *SiHy*-x (x = 0, 0.25 or 0.5, thickness = ~1.2 mm) before the addition of sensing assay. As reported in our previous papers[53, 93], to achieve proper "self-cleaning", the VPTTs of the DNs were tailored to be close to the implant site temperature. **(Table 4.1)**. During self-cleaning process, the DNs deswell / swell upon temperature fluctuations above or below the VPTT, which dynamically prevent the biofouling. Here, considering the future studies on rat model (~37-38 °C), 5 wt% of AAm was added into the 2nd networks

of all the DNs, resulting a VPTT of T_o ~36.5 °C and T_{max} ~38.5 °C. There was no significant difference between *SiHy*-x (x = 0, 0.25 or 0.5), indicating that the silicones did not significantly affect the VPTT. The *SiHy*-x (x = 0, 0.25 or 0.5) exhibited similar water content **(Table 4.1)** as well. Yet, decreased surface hydrophilicity were observed when silicone contents increased **(Figure 4.7a; Table 4.3)**. As the droplet just contacted with the slab (0 min), a contact angle > 90 ° were observed for *SiHy*-0 (~94 °), *SiHy*-0.25 (~101 °) and *SiHy*-0.5 (~108 °). After contacting for 1 min, the surface of the slab restructured and the contact angle of all composition decreased < 90 ° (*SiHy*-0: ~61 °, *SiHy*-0.25: ~78 ° and *SiHy*-0.5 ~85 °), indicating that each of the composition was able to present a hydrophilic surface in aqueous environment. As expected, the bulk hydrophilicity also decreased with increasing silicones, which was confirmed with the H-index **(Figure 4.7b; Table 4.4)**. The H-index was defined using the ratio between swelling degrees in a more hydrophobic solvent (70% IPA) and a more hydrophilic solvent (DI). As *SiHy*-x (x = 0, 0.25 or 0.5) exhibited similar water content, or swelling degree in DI, the increased H-index indicated that the DNs swelled better in more hydrophobic 70% IPA with increased silicones. The decreased hydrophilicity, due to the incorporation of silicones, could lead to decreased diffusivity in aqueous environment. However, there was no significant influence of silicones toward glucose diffusion **(Figure 4.7c; Table 4.5)**. *SiHy*-0.5 showed similar glucose diffusion coefficient to *SiHy*-0 at both RT or 37 °C. An increased glucose diffusion coefficient was observed of *SiHy*-0.25 at both testing temperatures, which was possibly due to phase separation observed in SEM. Notably, *SiHy*-x (x = 0, 0.25 or 0.5) showed higher glucose diffusion coefficient comparing with the subcutaneous tissue

(~2 $\times 10^{-6}$ cm^2 s^{-1}), and were expected to allow efficient glucose diffusion as glucose biosensors.

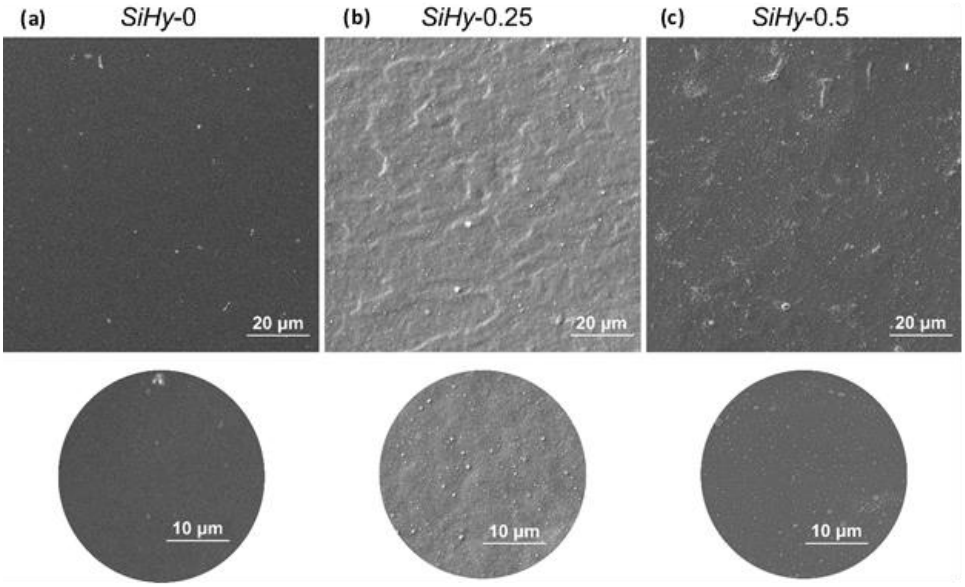

Figure 4.6 (a) Representative SEM image of *SiHy*-0 cross-section (scale bar: up – 20 µm, down – 10 µm). (b) Representative SEM image of *SiHy*-0.25 cross-section (scale bar: up – 20 µm, down – 10 µm). (c) Representative SEM image of *SiHy*-0.5 cross-section (scale bar: up – 20 µm, down – 10 µm).

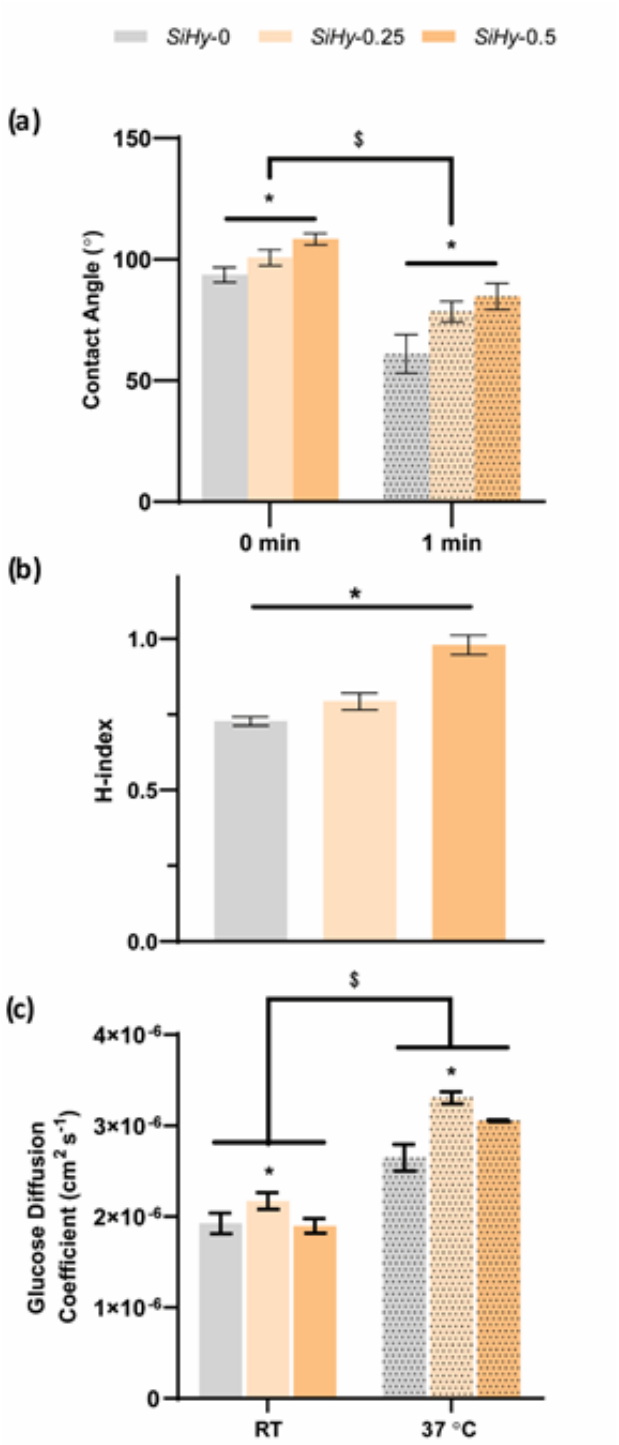

Figure 4.7 Physical properties of *SiHy*-x (x = 0, 0.25 or 0.5) (a) Contact angel. (b) H-index. (c) Glucose diffusion coefficient. (*: $p < 0.05$, significantly different from each other sample at the same condition; $: $p < 0.05$, *SiHy*-x (x = 0, 0.25 or 0.5) is significantly different from its own at different condition.)

As shown in Figure 4.8 **(Table 4.6)**, the mechanical properties were influenced by the silicone micro-domains. With the addition of the soft and flexible silicones microdomains, the hydrogels became more ductile and softer, showing increased compressive strain and decreased compressive modulus decreased. The strength of the *SiHy*-0.25 decreased comparing to *SiHy*-0, due to the soft silicone microdomains. However, the SiHy-0.5 showed increased compressive strength due to increased ductility. As results, *SiHy*-0.5 showed similar toughness comparing to *SiHy*-0, while *SiHy*-0.25 exhibited much higher toughness.

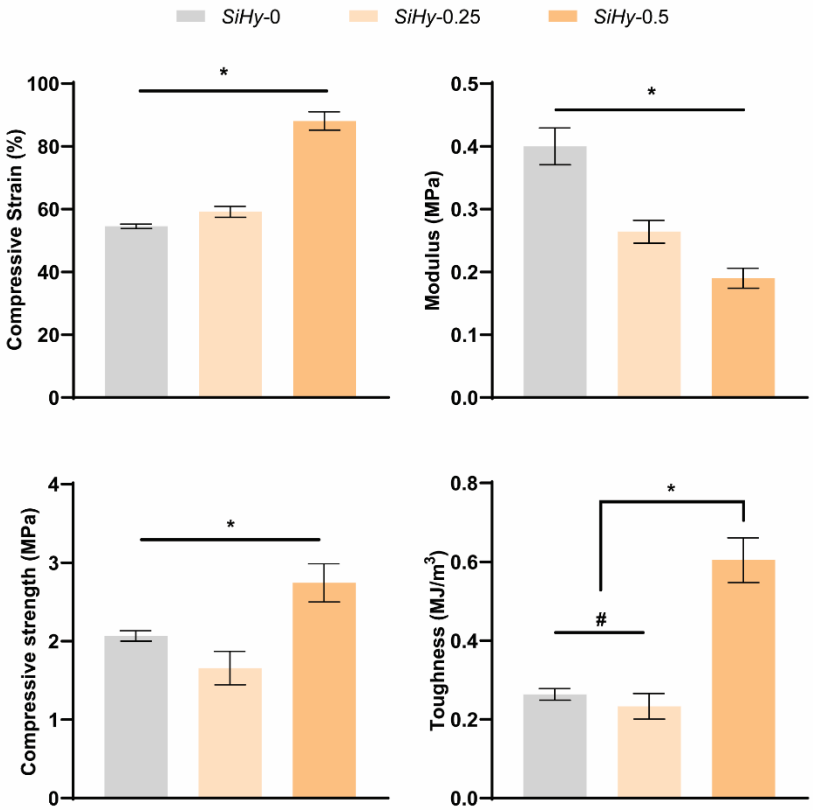

Figure 4.8 Mechanical properties of *SiHy*-x (x = 0, 0.25 or 0.5) (a) Compressive strain (ε). (b) Compressive modulus (*E*). (c) Compressive strength (*CS*). (d) Toughness. (*: $p < 0.05$, significantly different from each other)

After characterized the influence of silicone to the physical properties, *SiHy*-x (x = 0, 0.25 or 0.5, thickness = 0.5 mm) were incorporated with sensing assay as described. Much thinner samples allowed homogenous loading of HULK. The loading HULK concentration was characterized to be ~0.3 mM and the GOx concentration was ~100 unit/mL **(Figure 4.9a and b)**.

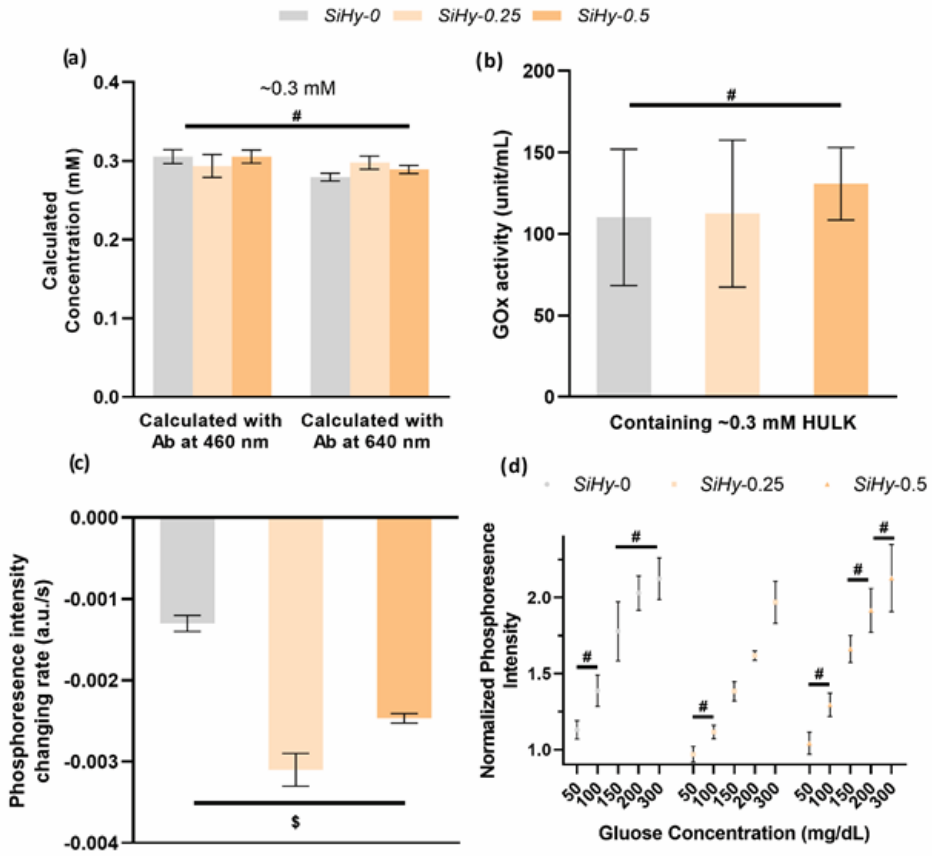

Figure 4.9 (a) Calculated concentration of HULK loaded in the hydrogel discs (Ø = 6 mm, thickness = 0.5 mm, *SiHy*-0, 0.25 or 0.5). (b) GOx activity of the hydrogel discs (Ø = 6 mm, thickness = 0.5 mm, *SiHy*-0, 0.25 or 0.5, loaded with ~0.3 mM HULK). (c) Phosphorescence intensity changing rate within the first minute when the hydrogel discs were first exposing to oxygen (Ø = 6 mm, thickness = 0.5 mm, *SiHy*-0, 0.25 or 0.5, loaded with ~0.3 mM HULK and ~100 unit/mL GOx). (#: $p > 0.05$, not significantly different from each other) ($: $p < 0.05$, significantly different from each other)

The oxygen permeability was indirectly accessed by measuring the phosphorescence intensity changes within the first minute as the sensor exposed to aqueous environment containing satirized oxygen **(Figure 4.9c)**. Comparing to *SiHy*-0, *SiHy*-0.25 and *SiHy*-0.5 both showed faster changing rate, indicating better oxygen permeability. As expected, the silicone micro-domians did result in better oxygen permeability. Moreover, *SiHy*-0.25 showed the fastest changing rate and highest oxygen

permeability, exceeding the *SiHy*-0.5. This was similar to the trend of glucose diffusion coefficient, which was possibly due to the phase separation observed with SEM. The preliminary glucose sensing was characterized with phosphorescence intensity changes when the sensor exposed to different glucose solution (0, 50, 100, 150, 200 and 300 mg/dL) **(Figure 4.9d)**. As expected, the *SiHy*-0.25 showed the best sensing range from 100 - 300 mg/dL, while the other two compositions lost sensitivity at higher concentration (> 150 mg/dL). All the compositions showed lack of sensitivity at lower concentration (50 - 100 mg/dL), which was not observed in previous studies. Comparing the difference between the previous sensor and the sensor fabricated in this work, this lack of sensitivity at lower concentration, even for non-silicone composition *SiHy*-0, was possibly due to the thickness of the sensor.

The cytocompatibility was evaluated by indirect cellular viability assay (Fig. 8e). Cells cultured in the environment containing *SiHy*-x (x = 0, 0.25 or 0.5) sensors showed good viabilities. The cells were also seeded to the sensors. Although the surface hydrophilicity changed with the addition of silicones, cells were not able to grow on the sensor hydrogels **(Figure 4.10a-c).**

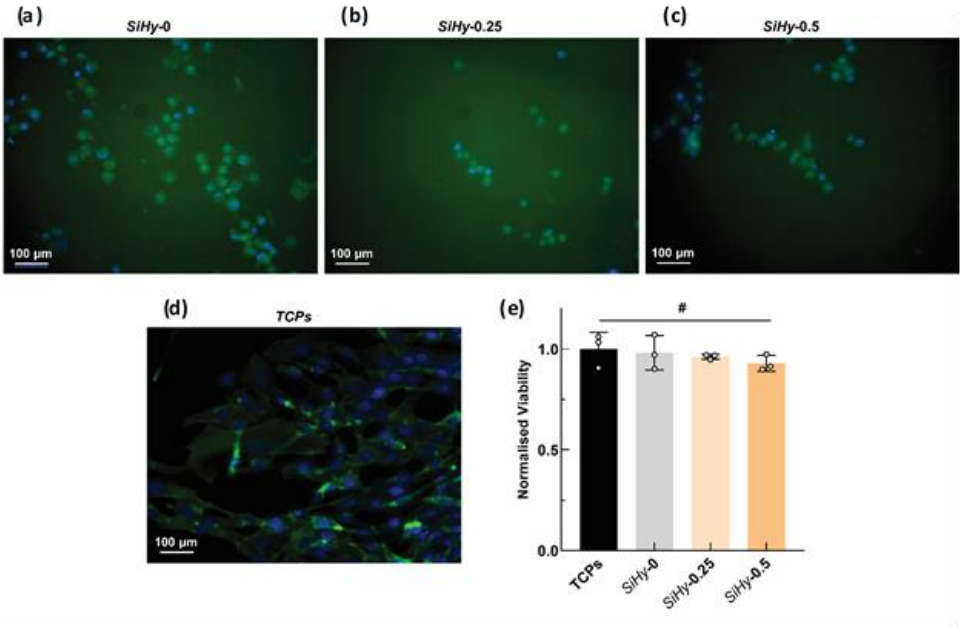

Figure 4.10 (a-d) Fluorescence imaging of cells seeded on *SiHy*-0. 0.25 or 0.5 and tissue culture plates (TCPs) after 24 hr. (e) Normalized cell viability of *SiHy*-0. 0.25 or 0.5 and tissue culture plates (TCPs). (#: $p > 0.05$, not significantly different from each other)

4.5. Conclusion

In this paper, we introduced a novel method to incorporate silicones in a self-cleaning double network hydrogel. Micro-domains of silicones were cured within the P[NIPAAm-*co*-APTAC] 1st network, followed with an additional curing of a P[NIPAAm-*co*-AAm] 2nd network. The introduction of the hydrophobic silicones resulted in an increased surface and bulk hydrophobicity of *SiHy*-x (x = 0, 0.25 or 0.5). The silicones also generated different swelling profiles within the hydrogels in different solvent (i.e. DI or IPA), which in otherwise influence the opacity of the hydrogels equilibrating in different solvents. As expected, Silicones, owing to the flexible and soft chains, also retained the hydrogels more ductile and soft mechanical properties, as well as better oxygen permeability. Additional to the silicones, the micro-domain structure also influenced the physical properties of the hydrogels significantly. From SEM imaging, it was observed that the *SiHy*-0.25 exhibited

significant phase separation, other than the silicone micro-domain. This was possibly due to the different interaction tendency of hydrophobic and hydrophilic sections of P[NIPAAm-*co*-APTAC] and P[NIPAAm-*co*-AAm] with the silicone micro-domains. As result, the diffusivity (glucose or oxygen) of *SiHy*-0.25 was significantly increased. This composition also showed widest sensing range (100 - 300 mg/dL). In this paper, the sensitivity was only preliminary characterized phosphorescence intensity. Future study would be conducted with *SiHy*-0.25, with the investigation with better GOx loading (narrow concentration range), thickness of the sensor and phosphorescence lifetime sensing.

4.6. Supplement

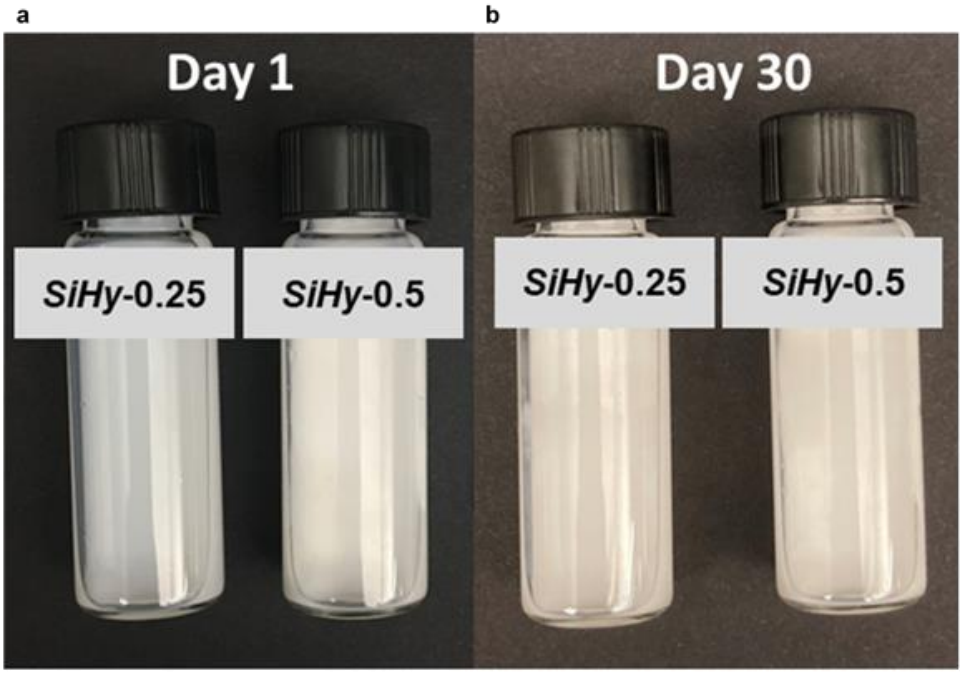

Figure 4.11 (a) Photo image of 1st network precursor emulsion for *SiHy*-0.25 and *SiHy*-0.5 took on first day. (b) Photo image of 1st network precursor emulsion for *SiHy*-0.25 and *SiHy*-0.5 took after sitting for 30 days.

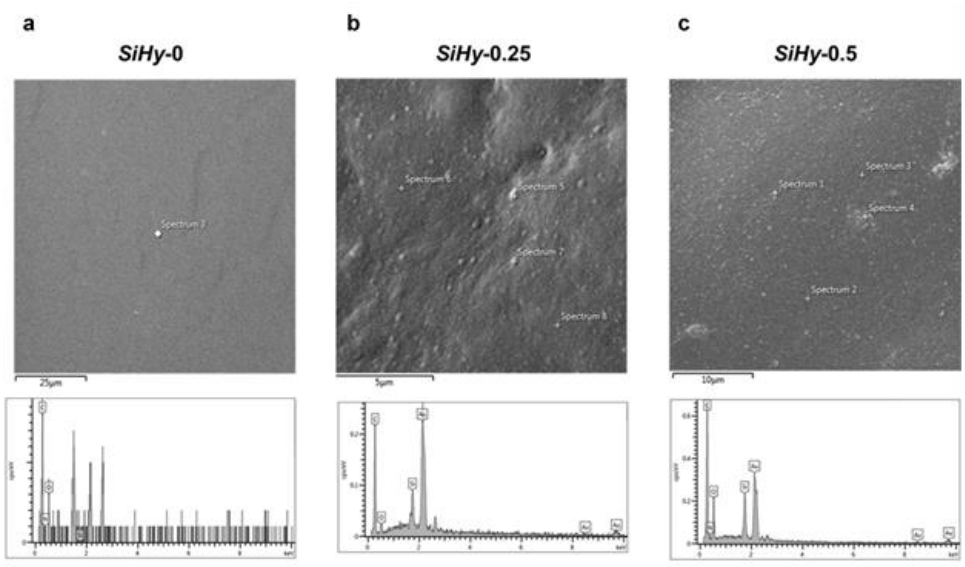

d

	C	O	N	Si
SiHy-0	58 ± 12 %	24 ± 11 %	21 ± 10 %	0.07 ± 0.1 %
SiHy-0.25	64 ± 7 %	25 ± 5 %	5 ± 1 %	6 ± 1 %
SiHy-0.5	67 ± 9 %	23 ± 7 %	3 ± 3 %	6 ± 2%

Figure 4.12 (a) Representative SEM and EDS images of *SiHy*-0. (b) Representative SEM and EDS images of *SiHy*-0.25. (c) Representative SEM and EDS images of *SiHy*-0.5. (d) Average elements percentages of *SiHy*-x (x = 0, 0.25 or 0.5) characterized with SEM-EDS.

SEM, (Tecan Vega 3) with oxford energy-dispersive x-ray spectroscopy (EDS) detector was used to analysis the elements on *SiHy*-x (x = 0, 0.25 or 0.5) cross-sections. 5 random points were selected for the EDS scanning and the average elements concentration at those points were calculated.

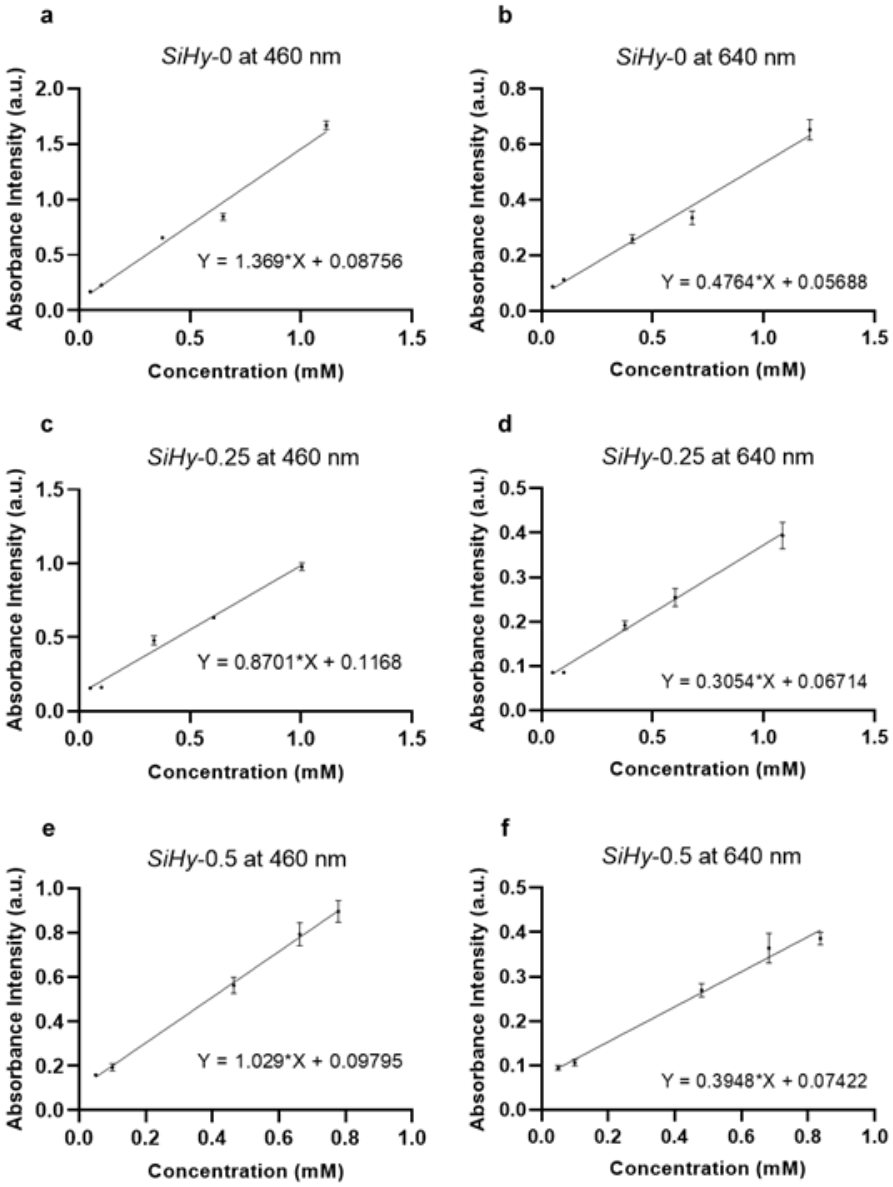

Figure 4.13 Calibration curves for absorbance at (a, c, e) 460 nm and (b, d, f) 640 nm, plotting with absorbance of HULK in DNs (SiHy-x, x = 0, 0.25 and 0.5) versus HULK concentrations in DNs (~ 0.05 mM, ~0.1 mM, ~0.45 mM, ~0.65 mM, and ~1 mM).

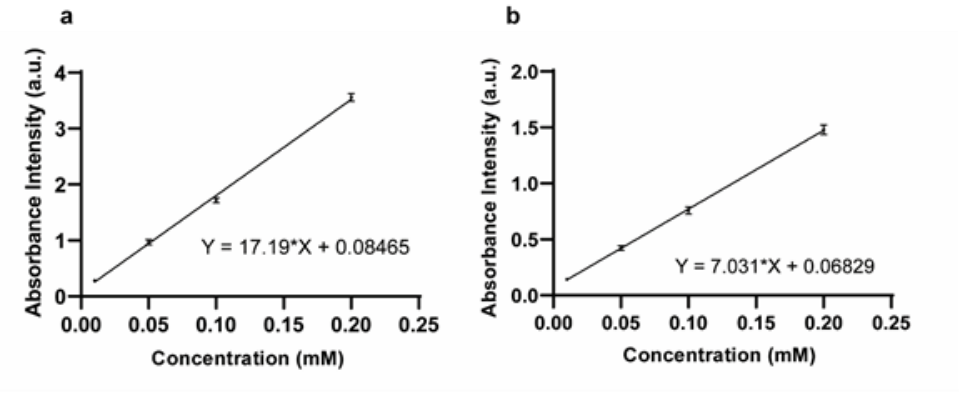

Figure 4.14 Calibration curves for absorbance at (a) 460 nm and (b) 640 nm, plotting with absorbance of HULK IPA solution versus HULK concentrations (0.01 mM, 0.05 mM, 0.1 mM and 0.2 mM).

Table 4.2 Sol content of both SNs and DNs for all compositions (*SiHy*-0, *SiHy*-0.25, and *SiHy*-0.5). (Data corresponds to that reported in Figure 4.4b.)

	SN	**DN**
SiHy-0	0.11 ± 0.06	0.27 ± 0.01
SiHy-0.25	0.13 ± 0.01	0.27 ± 0.01
SiHy-0.5	0.12 ± 0.02	0.28 ±0.01

Table 4.3 Contact angle (°) of *SiHy*-0, *SiHy*-0.25, and *SiHy*-0.5. (Data corresponds to that reported in Figure 4.7a.)

	0 min	**10 min**
SiHy-0	93.6 ± 3.1	60.9 ± 8
SiHy-0.25	100.7 ± 3.3	78.4 ± 4.2
SiHy-0.5	108.4 ± 2.4	84.7 ± 5.5

Table 4.4 H-index of *SiHy*-0, *SiHy*-0.25, and *SiHy*-0.5. (Data corresponds to that reported in Figure 4.7b.)

	H-index
SiHy-0	0.73 ± 0.01
SiHy-0.25	0.79 ± 0.03
SiHy-0.5	0.98 ± 0.03

Table 4.5 Glucose diffusion coefficient ($\times 10^{-6}$ cm^2s^{-1}) of *SiHy*-0, *SiHy*-0.25, and *SiHy*-0.5. (Data corresponds to that reported in Figure 4.7c.)

	At RT	**At 37 °C**
SiHy-0	1.9 ± 0.08	2.6 ± 0.01
SiHy-0.25	2.2 ± 0.09	3.3 ± 0.07
SiHy-0.5	1.9 ± 0.08	2.9 ± 0.01

Table 4.6 Compressive mechanical properties of *SiHy*-0, *SiHy*-0.25, and *SiHy*-0.5. (Data corresponds to that reported in Figure 4.8.)

	Strain (%)	**Modulus (MPa)**	**Strength (MPa)**	**Toughness (MJ/m^3)**
SiHy-0	54.5 ± 0.7	0.4 ± 0.03	2.1 ± 0.1	0.26 ± 0.02
SiHy-0.25	59.2 ± 1.7	0.26 ± 0.02	1.7 ± 0.2	0.23 ± 0.03
SiHy-0.5	88.1 ± 2.9	0.19 ± 0.02	2.7 ± 0.2	0.6 ± 0.06

5. CONCLUSIONS AND FUTURE WORK

5.1. Conclusion

This work was motivated by the realization of subcutaneously implanted optical glucose biosensors to improve diabetes management. On-the-market CGMs are primarily transcutaneous designs having limited lifetimes (7-14 days), primarily attributed to the FBR to the electrochemical sensors that resides in the subcutaneous tissue. An optical glucose sensor of reduced size would permit non-surgical implantation to the wrist, and also could be could be interrogated exclusively via a LED and photodiode pair on a smart-watches, allowing for the exclusion of skin-attached transmitters. The membrane used to construct such a sensor is paramount to success, but must address challenges related to fabrication, assay retention, glucose diffusivity, and minimizing the FBR. In this work, thermosensitive, DN hydrogel membranes were designed to successfully house optical glucose sensing assays. The designs were based on thermoresponsive NIPAAm, and included different charged and hydrophilic comonomers as well as covalent linkers. By precisely tuning the VPTT, membranes would be able to cyclically deswell/reswell with the temperature fluctuations (~ 1 ºC) known to occur in subcutaneous tissue. This "self-cleaning" process would minimize cellular adhesion, ultimately leading to a diminished FBR as confirmed in the previously studied first-generation membrane evaluated *in vivo* (rat model). In Chapter I, a perspective on the utility of hydrogels to house glucose sensors or sensing assays was presented, providing context to the work presented herein.

In Chapter II, the mesh size (ξ) of a thermoresponsive DN membrane was systematically reduced via incorporation of a comb architecture, towards eventual formation of a biosensor with a FRET-based glucose sensing assay. The mesh size of the membrane would have to be tuned to ~1-3 nm to afford glucose diffusion [D_h ~0.8 nm], but retain within a central cavity fluorescently-labeled PEGylated Concanavalin A (mPEG-TRITC-ConA) [D_h ~30 nm] and mannotetraose (APTS-MT) [D_h ~3 nm]. The DN-25% membrane (7 nm < ξ < 10 nm) was based on a negatively charged P(NIPAAm-*co*-AMPS) 1st network and a P(NIPAAm-*co*-AAm) 2nd network. Comb-DN-25% hydrogels were prepared by introducing PAMPS-MA (negatively charged), PEG-A (neutral), and PATAC-MA (positively charged) of varying concentration and length (n) during formation of the first network. When prepared with negatively charged PAMPS-MA combs, an increase in comb concentration led to a decreased mesh size. All comb lengths (n = 5, 10, 20) achieved the targeted mesh size (ξ < 3 nm), but a longer comb did so at a reduced relative concentration. Analogous comb-DN-25% hydrogels prepared with neutral or cationic combs were did not effectively reduce the mesh size: PEG-c-25% (n = 10) [4 nm < ξ < 10 nm] and PAPTAC-c-25% (n = 10) [7 nm < ξ < 10 nm]. The efficacy of negatively charged combs to reduce mesh size is attributed to electrostatic repulsive forces with the DN. PAMPS-c-25% (n = 10) was also shown to allow diffusion of glucose, indicating its mesh size to be ~1 < ξ < 3 nm. Based on its thermosensitivity, and mesh size as well as mechanical properties and cytocompatibility, this membrane is an excellent candidate for an implanted glucose biosensor membrane prepared with the FRET assay as well as for other sensors.

In Chapters III and IV, thermosensitive DN membranes were customized to directly embed a phosphorescence sensing assay based on an oxygen-sensitive metalloporphyrin ("HULK") and GOx. First, in Chapter III, the membrane's first network was prepared from NIPAAm and cationic APTAC (75:25 mol%). The second network was formed from a loosely crosslinked NIPAAm copolymerized with AAm to tune the VPTT. Anionic HULK was retained via electrostatic attraction to cationic moieties. The GOx enzyme was covalently bonded to the DN membranes by leveraging the AAm segments' primary amides, and also a glutaraldehyde linker's dialdehydes. HULK levels were systematically varied (0, 0.1, 0.3, and 0.5 mM) with retention the metalloporphyrin's absorbance profile. GOx levels were found to be critical to glucose sensitivity. For membranes formed with a high GOx concentration, the phosphorescent intensity plateaued at glucose levels >50 mg/dL. Attributed to reducing the rate of oxygen consumption, membranes formed with the lowest GOx levels exhibited an increase in phosphorescent intensity from 0 to 200 mg/dL. While demonstrating promising sensitivity in this lower glucose range, sensitivity up to 500 mg/dL is desirable. Thus, in Chapter IV,

a new thermosensitive DN membrane was prepared to improve oxygen permeability by incorporation of hydrophobic, silicone microdroplets. To modify the 1st network precursor solution, an ultrasonicate processor was used to disperse the silicone phase, consisting of 3-(methacryloyloxy)propyltris(trimethylsiloxy)silane (TRIS), methacryloxypropyl terminated polydimethylsiloxane (crosslinker), and photoinitiator. After UV cure of the 1st network, the P(NIPAAm-*co*-AAm) 2nd network was subsequently formed, resulting in DNs with the targeted VPTT. Membranes were prepared with three

molar concentrations of TRIS in the 1st network: *SiHy*-x (x = 0, 0.25 or 0.5, where x = TRIS concentration [M]). With the optimal concentration of silicone microdroplets, sensitivity was observed in concentrations from 100 to 300 mg/dL. The *SiHy*-0.25 membrane (i.e., intermediate silicone microdroplet levels) exhibited significantly greater phase separation as observed by SEM, leading to greater glucose diffusion and apparent oxygen permeability. This membrane showed widest glucose sensitivity range (100 to 300 mg/dL).

In summary, the design of thermosensitive DN membranes may be customized to effectively house different optical glucose sensing assays. Importantly, such modifications can be done while retaining the thermosensitivity associated desired for self-cleaning behavior. As UV-curable systems, fabrication of the membranes/formation of sensors is highly flexible in terms of final dimensions and geometry. As described in "Future Work", tailoring of the designs could further improve the biosensor functionality.

5.2. Future works

The next step for work discussed in chapter II, is to construct the biosensor with FRET sensing assay and characterize the sensitivity *in vitro*, in collaboration with Prof. Gerard Coté. To achieve this, comb DN *PAMPS*-*c*-25% (n = 10) will be used to fabricate the hollow cylinder membrane and polyampholyte hydrogels, which was reported with adhesive properties toward charged surfaces,[223] will be used to fabricate caps to enclose the cylinder ends.

For the future works based on studies in chapter III and IV, the biosensor comprised with HULK, GOx and silicone containing hydrogel matrix (*SiHy*-0.25) needs

to be subject to phosphorescence lifetime sensing tests *in vitro*, collaborating with Prof. Mike McShane.

The comb DN [*PAMPS*-*c*-25% (n = 10)] and silicone containing DN (*SiHy*-0.25) showed great potential to construct the implantable biosensor. Thus, *in vivo* material biocompatibility studies are necessary for both compositions. Rat subcutaneous model with 7-, 30- and 90-day implantation studies will be conducted, following with the histology analysis for healing status, and immunohistochemistry technics to analyze the inflammation cellular activities.

Furthermore, after the *in vitro* sensing tests, both of the biosensors will be tested on a rat model to characterize their *in vivo* functionality.

REFERENCES

1. Roglic, G.e., WHO Global report on diabetes: A summary. *Int. J. Non-Commun. Dis.* **2016,** *1*, 3.

2. Organization, W.H., Global report on diabetes. 2016.

3. Organization, W.H. *Global report on diabetes: executive summary*; World Health Organization: 2016.

4. Prevention, C.f.D.C.a. *National Diabetes Statistics Report*; Centers for Disease Control and Prevention, U.S. Dept of Health and Human Services: Atlanta, GA, 2020.

5. van Enter, B.J.; von Hauff, E., Challenges and perspectives in continuous glucose monitoring. *Chem. Commun.* **2018,** *54*, 5032-5045.

6. Joseph, J.I., Review of the long-term implantable senseonics continuous glucose monitoring system and other continuous glucose monitoring systems. *J. Diabetes Sci. Technol.* **2021,** *15*, 167-173.

7. Yu, Z.; Jiang, N.; Kazarian, S.G.; Tasoglu, S.; Yetisen, A.K., Optical sensors for continuous glucose monitoring. *Prog. Biomed. Eng.* **2021,** *3*, 022004.

8. Papatheodorou, K.; Papanas, N.; Banach, M.; Papazoglou, D.; Edmonds, M., Complications of Diabetes 2016. *J. Diabetes Res.* **2016,** *2016*, 6989453.

9. Nathan, D.M., Long-term complications of diabetes mellitus. *N. Engl. J. Med.* **1993,** *328*, 1676-1685.

10. Group, I.H.S., Minimizing hypoglycemia in diabetes. *Diabetes Care* **2015,** *38*, 1583-1591.

11. Cryer, P.E., The barrier of hypoglycemia in diabetes. *Diabetes* **2008,** *57*, 3169-3176.

12. Klonoff, D.C.; Ahn, D.; Drincic, A., Continuous glucose monitoring: A review of the technology and clinical use. *Diabetes Res. Clin. Pract.* **2017,** *133*, 178-192.

13. Bobrowski, T.; Schuhmann, W., Long-term implantable glucose biosensors. *Curr. Opin. Electrochem.* **2018,** *10*, 112-119.

14. Cappon, G.; Acciaroli, G.; Vettoretti, M.; Facchinetti, A.; Sparacino, G., Wearable continuous glucose monitoring sensors: a revolution in diabetes treatment. *Electronics* **2017,** *6*, 65.

15. Jernelv, I.L.; Milenko, K.; Fuglerud, S.S.; Hjelme, D.R.; Ellingsen, R.; Aksnes, A., A review of optical methods for continuous glucose monitoring. *Appl. Spectrosc. Rev.* **2019,** *54*, 543-572.

16. Mortellaro, M.; DeHennis, A., Performance characterization of an abiotic and fluorescent-based continuous glucose monitoring system in patients with type 1 diabetes. *Biosens. Bioelectron.* **2014,** *61*, 227-231.

17. Zimmerman, C.; Albanese-O'Neill, A.; Haller, M.J., Advances in type 1 diabetes technology over the last decade. *Eur. Endocrinol.* **2019,** *15*, 70-76.

18. Manavalan, D.; Wen, C.; Young, C.F.; Farhangi, V., Diabetes technology: the present and the future. *Prim. Care Rep.* **2021,** *27*.

19. Funtanilla, V.D.; Candidate, P.; Caliendo, T.; Hilas, O., Continuous glucose monitoring: a review of available systems. *Pharm. Ther.* **2019,** *44*, 550-553.

20. Scholten, K.; Meng, E., A review of implantable biosensors for closed-loop glucose control and other drug delivery applications. *Int. J. Pharm.* **2018,** *544*, 319-334.

21. Gerritsen, M.; Jansen, J.; Lutterman, J., Performance of subcutaneously implanted glucose sensors for continuous monitoring. *JNeth. J. Med.* **1999,** *54*, 167-179.

22. Welsh, J.B.; Thomas, R., Continuous glucose monitoring: an emerging standard of care. *Am J Manag Care* **2019,** *25*, Sp116-sp119.

23. Engler, R.; Routh, T.L.; Lucisano, J.Y., Adoption barriers for continuous glucose monitoring and their potential reduction with a fully implanted system: results from patient preference surveys. *Clin. Diabetes* **2018,** *36*, 50-58.

24. Nichols, S.P.; Koh, A.; Storm, W.L.; Shin, J.H.; Schoenfisch, M.H., Biocompatible materials for continuous glucose monitoring devices. *Chem. Rev.* **2013,** *113*, 2528-2549.

25. Valdes, T.; Moussy, F., In vitro and in vivo degradation of glucose oxidase enzyme used for an implantable glucose biosensor. *Diabetes Technol. Ther.* **2000,** *2*, 367-376.

26. Ward, W.K., A review of the foreign-body response to subcutaneously-implanted devices: the role of macrophages and cytokines in biofouling and fibrosis. *J. Diabetes Sci. Technol.* **2008,** *2*, 768-777.

27. Gerritsen, M.; Jansen, J.A.; Kros, A.; Vriezema, D.M.; Sommerdijk, N.A.J.M.; Nolte, R.J.M.; Lutterman, J.A.; Van Hövell, S.W.F.M.; Van der Gaag, A., Influence of inflammatory cells and serum on the performance of implantable glucose sensors. **2001,** *54*, 69-75.

28. Englert, K.; Ruedy, K.; Coffey, J.; Caswell, K.; Steffen, A.; Levandoski, L.; (DirecNet), D.R.i.C.S.G., Skin and adhesive issues with continuous glucose monitors: a sticky situation. *J. Diabetes Sci. Technol.* **2014,** *8*, 745-751.

29. Senseonics Long-term CGM System / Eversense Continuous Glucose Monitoring. https://www.eversensediabetes.com/eversense-cgm-system (accessed January 1).

30. Christiansen, M.P.; Klaff, L.J.; Brazg, R.; Chang, A.R.; Levy, C.J.; Lam, D.; Denham, D.S.; Atiee, G.; Bode, B.W.; Walters, S.J., A prospective multicenter evaluation of the accuracy of a novel implanted continuous glucose sensor: PRECISE II. *Diabetes Technol. Ther.* **2018,** *20*, 197-206.

31. Dautta, M.; Alshetaiwi, M.; Escobar, J.; Tseng, P., Passive and wireless, implantable glucose sensing with phenylboronic acid hydrogel-interlayer RF resonators. *Biosens. Bioelectron.* **2020,** *151*, 112004.

32. Kropff, J.; Choudhary, P.; Neupane, S.; Barnard, K.; Bain, S.C.; Kapitza, C.; Forst, T.; Link, M.; Dehennis, A.; DeVries, J.H., Accuracy and longevity of an implantable continuous glucose sensor in the PRECISE study: a 180-Day, prospective, multicenter, pivotal Trial. *Diabetes Care* **2017,** *40*, 63-68.

33. U.S. Department of Health & Human Services Class 2 Deivce Recall Eversense. https://www.accessdata.fda.gov/scripts/cdrh/cfdocs/cfres/res.cfm?id=176696 (accessed April 27).

34. Lin, R.; Brown, F.; James, S.; Jones, J.; Ekinci, E., Continuous glucose monitoring: A review of the evidence in type 1 and 2 diabetes mellitus. *Diabet. Med.* **2021,** *38*, e14528.

35. Xu, J.; Lee, H., Anti-biofouling strategies for long-term continuous use of implantable biosensors. *Chemosensors* **2020,** *8*, 66.

36. Joseph, J.I.; Eisler, G.; Diaz, D.; Khalf, A.; Loeum, C.; Torjman, M.C., Glucose sensing in the subcutaneous tissue: attempting to correlate the immune response with continuous glucose monitoring accuracy. *Diabetes Technol. Ther.* **2018,** *20*, 321-324.

37. Rigla, M.; Pons, B.; Rebasa, P.; Luna, A.; Pozo, F.J.; Caixàs, A.; Villaplana, M.; Subías, D.; Bella, M.R.; Combalia, N., Human subcutaneous tissue response to glucose sensors: macrophages accumulation impact on sensor accuracy. *Diabetes Technol. Ther.* **2018,** *20*, 296-302.

38. Klueh, U.; Frailey, J.T.; Qiao, Y.; Antar, O.; Kreutzer, D.L., Cell based metabolic barriers to glucose diffusion: macrophages and continuous glucose monitoring. *Biomaterials* **2014,** *35*, 3145-53.

39. Harris, J.M.; Reyes, C.; Lopez, G.P., Common causes of glucose oxidase instability in in vivo biosensing: a brief review. *J. Diabetes Sci. Technol.* **2013,** *7*, 1030-8.

40. Li, D.-J.; Ohsaki, K.; Ii, K.; Cui, P.-C.; Ye, Q.; Baba, K.; Wang, Q.-C.; Tenshin, S.; Takano-Yamamoto, T., Thickness of fibrous capsule after implantation of hydroxyapatite in subcutaneous tissue in rats. *J. Biomed. Mater. Res.* **1999,** *45*, 322-326.

41. Ward, W.K.; Slobodzian, E.P.; Tiekotter, K.L.; Wood, M.D., The effect of

microgeometry, implant thickness and polyurethane chemistry on the foreign body response to subcutaneous implants. *Biomaterials* **2002,** *23*, 4185-4192.

42. Irwin, E.F.; Saha, K.; Rosenbluth, M.; Gamble, L.J.; Castner, D.G.; Healy, K.E., Modulus-dependent macrophage adhesion and behavior. *J. Biomater. Sci. Polym. Ed.* **2008,** *19*, 1363-1382.

43. Klueh, U.; Kaur, M.; Montrose, D.C.; Kreutzer, D.L., Inflammation and glucose sensors: use of dexamethasone to extend glucose sensor function and life span in vivo. *J. Diabetes. Sci. Technol.* **2007,** *1*, 496-504.

44. Vallejo-Heligon, S.G.; Brown, N.L.; Reichert, W.M.; Klitzman, B., Porous, Dexamethasone-loaded polyurethane coatings extend performance window of implantable glucose sensors in vivo. *Acta Biomater.* **2016,** *30*, 106-115.

45. Jung, S.-K.; Wilson, G.S., Polymeric mercaptosilane-modified platinum electrodes for elimination of interferants in glucose biosensors. *Anal. Chem.* **1996,** *68*, 591-596.

46. Hetrick, E.M.; Schoenfisch, M.H., Reducing implant-related infections: active release strategies. *Chem. Soc. Rev.* **2006,** *35*, 780-789.

47. Yu, B.; Wang, C.; Ju, Y.M.; West, L.; Harmon, J.; Moussy, Y.; Moussy, F., Use of hydrogel coating to improve the performance of implanted glucose sensors. *Biosens. Bioelectron.* **2008,** *23*, 1278-1284.

48. Means, A.K.; Dong, P.; Clubb, F.J.; Friedemann, M.C.; Colvin, L.E.; Shrode, C.A.; Coté, G.L.; Grunlan, M.A., A self-cleaning, mechanically robust membrane for minimizing the foreign body reaction: towards extending the lifetime of sub-Q glucose biosensors. *J. Mater. Sci. Mater. Med.* **2019,** *30*, 79.

49. Bae, J.; Park, J.; Kim, S.; Cho, H.; Kim, H.J.; Park, S.; Shin, D.-S., Tailored hydrogels for biosensor applications. *J. Ind. Eng. Chem.* **2020,** *89*, 1-12.

50. Quinn, C.A.P.; Connor, R.E.; Heller, A., Biocompatible, glucose-permeable hydrogel for in situ coating of implantable biosensors. *Biomaterials* **1997,** *18*, 1665-1670.

51. Trzebinski , J.; Moniz, A.R.-B.; Sharma, S.; Burugapalli, K.; Moussy, F.; Cass, A.E.G., Hydrogel membrane improves natch-to-batch reproducibility of an enzymatic glucose biosensor. *Electroanalysis* **2011,** *23*, 2789-2795.

52. Locke, A.K.; Means, A.K.; Dong, P.; Nichols, T.J.; Coté, G.L.; Grunlan, M.A., A Layer-by-Layer approach to retain a fluorescent glucose sensing assay within the cavity of a hydrogel membrane. *ACS Appl. Bio Mater.* **2018,** *1*, 1319-1327.

53. Dong, P.; Schott, B.J.; Means, A.K.; Grunlan, M.A., Comb architecture to control the selective diffusivity of a double network hydrogel. *ACS Appl. Polym. Mater.* **2020,** *2*, 5269-5277.

54. Li, J.; Mooney, D.J., Designing hydrogels for controlled drug delivery. *Nat. Rev. Mater.* **2016,** *1*, 16071.

55. Annabi, N.; Tamayol, A.; Uquillas, J.A.; Akbari, M.; Bertassoni, L.E.; Cha, C.; Camci-Unal, G.; Dokmeci, M.R.; Peppas, N.A.; Khademhosseini, A., 25th Anniversary Article: Rational Design and Applications of Hydrogels in Regenerative Medicine. *Adv. Mater.* **2014,** *26*, 85-124.

56. Hoffman, A.S., Hydrogels for biomedical applications. *Adv. Drug Del. Rev.* **2012,** *64*, 18-23.

57. Helton, K.L.; Ratner, B.D.; Wisniewski, N.A., Biomechanics of the sensor-tissue interface-effects of motion, pressure, and design on sensor performance and foreign body response-part II: examples and application. *J. Diabetes. Sci. Technol.* **2011,** *5*, 647-56.

58. Akhtar, M.F.; Hanif, M.; Ranjha, N.M., Methods of synthesis of hydrogels: A review. *Saudi. Pharm. J.* **2016,** *24*, 554-559.

59. Oliva, N.; Conde, J.; Wang, K.; Artzi, N., Designing hydrogels for on-demand therapy. *Acc. Chem. Res.* **2017,** *50*, 669-679.

60. Ye, L.; Zhang, Y.; Wang, Q.; Zhou, X.; Yang, B.; Ji, F.; Dong, D.; Gao, L.; Cui, Y.; Yao, F., Physical cross-linking starch-based zwitterionic hydrogel exhibiting excellent biocompatibility, protein resistance, and biodegradability. *ACS Appl. Mater.*

Interfaces. **2016,** *8*, 15710-23.

61. Tang, Z.; Miao, Y.; Zhao, J.; Xiao, H.; Zhang, M.; Liu, K.; Zhang, X.; Huang, L.; Chen, L.; Wu, H., Mussel-inspired biocompatible polydopamine/carboxymethyl cellulose/polyacrylic acid adhesive hydrogels with UV-shielding capacity. *Cellulose (Lond)* **2021**, 1-14.

62. Yazdi, M.K.; Vatanpour, V.; Taghizadeh, A.; Taghizadeh, M.; Ganjali, M.R.; Munir, M.T.; Habibzadeh, S.; Saeb, M.R.; Ghaedi, M., Hydrogel membranes: a review. *Mater. Sci. Eng. C Mater. Biol. Appl.* **2020,** *114*, 111023.

63. Erol, O.; Pantula, A.; Liu, W.; Gracias, D.H., Transformer hydrogels: a review. *Adv. Mater. Technol.* **2019,** *4*, 1900043.

64. Fei, R.; George, J.T.; Park, J.; Means, A.K.; Grunlan, M.A., Ultra-strong thermoresponsive double network hydrogels. *Soft Matter* **2013,** *9*, 2912-2919.

65. Fei, R.; Means, A.K.; Abraham, A.A.; Locke, A.K.; Coté, G.L.; Grunlan, M.A., Self-Cleaning, thermoresponsive P(NIPAAm-co-AMPS) double network membranes for implanted glucose biosensors. *Macromol. Mater. Eng.* **2016,** *301*, 935-943.

66. Quinn, C.A.; Connor, R.E.; Heller, A., Biocompatible, glucose-permeable hydrogel for in situ coating of implantable biosensors. *Biomaterials* **1997,** *18*, 1665-70.

67. Quinn, C.P.; Pathak, C.P.; Heller, A.; Hubbell, J.A., Photo-crosslinked copolymers of 2-hydroxyethyl methacrylate, poly(ethylene glycol) tetra-acrylate and ethylene dimethacrylate for improving biocompatibility of biosensors. *Biomaterials* **1995,** *16*, 389-96.

68. Wang, C.; Yu, B.; Knudsen, B.; Harmon, J.; Moussy, F.; Moussy, Y., Synthesis and performance of novel hydrogels coatings for implantable glucose sensors. *Biomacromolecules* **2008,** *9*, 561-7.

69. Yu, B.; Wang, C.; Ju, Y.M.; West, L.; Harmon, J.; Moussy, Y.; Moussy, F., Use of hydrogel coating to improve the performance of implanted glucose sensors. *Biosens. Bioelectron.* **2008,** *23*, 1278-84.

70. Xie, X.; Doloff, J.C.; Yesilyurt, V.; Sadraei, A.; McGarrigle, J.J.; Omami, M.; Veiseh, O.; Farah, S.; Isa, D.; Ghani, S.; Joshi, I.; Vegas, A.; Li, J.; Wang, W.; Bader, A.; Tam, H.H.; Tao, J.; Chen, H.J.; Yang, B.; Williamson, K.A.; Oberholzer, J.; Langer, R.; Anderson, D.G., Reduction of measurement noise in a continuous glucose monitor by coating the sensor with a zwitterionic polymer. *Nat. Biomed. Eng.* **2018,** *2*, 894-906.

71. Patil, S.D.; Papadimitrakopoulos, F.; Burgess, D.J., Dexamethasone-loaded poly(lactic-co-glycolic) acid microspheres/poly(vinyl alcohol) hydrogel composite coatings for inflammation control. *Diabetes. Technol. Ther.* **2004,** *6*, 887-97.

72. Norton, L.W.; Tegnell, E.; Toporek, S.S.; Reichert, W.M., In vitro characterization of vascular endothelial growth factor and dexamethasone releasing hydrogels for implantable probe coatings. *Biomaterials* **2005,** *26*, 3285-97.

73. Norton, L.W.; Koschwanez, H.E.; Wisniewski, N.A.; Klitzman, B.; Reichert, W.M., Vascular endothelial growth factor and dexamethasone release from nonfouling sensor coatings affect the foreign body response. *J. Biomed. Mater. Res. A* **2007,** *81*, 858-69.

74. Abraham, A.A.; Fei, R.; Coté, G.L.; Grunlan, M.A., Self-Cleaning membrane to extend the lifetime of an implanted glucose biosensor. *ACS Appl. Mater. Interfaces* **2013,** *5*, 12832-12838.

75. Kajisa, T.; Sakata, T., Glucose-responsive hydrogel electrode for biocompatible glucose transistor. *Sci. Technol. Adv. Mater.* **2017,** *18*, 26-33.

76. Shang, J.; Yan, J.; Zhang, Z.; Huang, X.; Maturavongsadit, P.; Song, B.; Jia, Y.; Ma, T.; Li, D.; Xu, K.; Wang, Q.; Lin, Q., A hydrogel-based glucose affinity microsensor. *Sens. Actuators. B Chem.* **2016,** *237*, 992-998.

77. Dou, Q.; Hu, D.; Gao, H.; Zhang, Y.; Yetisen, A.K.; Butt, H.; Wang, J.; Nie, G.; Dai, Q., High performance boronic acid-containing hydrogel for biocompatible continuous glucose monitoring. *RSC Adv.* **2017,** *7*, 41384-41390.

78. Lai, J.; Yi, Y.; Zhu, P.; Shen, J.; Wu, K.; Zhang, L.; Liu, J., Polyaniline-based glucose biosensor: a review. *J. Electroanal. Chem.* **2016,** *782*, 138-153.

79. Zhai, D.; Liu, B.; Shi, Y.; Pan, L.; Wang, Y.; Li, W.; Zhang, R.; Yu, G., Highly sensitive glucose sensor based on pt nanoparticle/polyaniline hydrogel heterostructures. *ACS Nano* **2013,** *7*, 3540-6.

80. Al-Sagur, H.; Shanmuga Sundaram, K.; Kaya, E.N.; Durmuş, M.; Basova, T.V.; Hassan, A., Amperometric glucose biosensing performance of a novel graphene nanoplatelets-iron phthalocyanine incorporated conducting hydrogel. *Biosens. Bioelectron.* **2019,** *139*, 111323.

81. Liang, Z.; Zhang, J.; Wu, C.; Hu, X.; Lu, Y.; Wang, G.; Yu, F.; Zhang, X.; Wang, Y., Flexible and self-healing electrochemical hydrogel sensor with high efficiency toward glucose monitoring. *Biosens. Bioelectron.* **2020,** *155*, 112105.

82. Zhong, R.; Tang, Q.; Wang, S.; Zhang, H.; Zhang, F.; Xiao, M.; Man, T.; Qu, X.; Li, L.; Zhang, W.; Pei, H., Self-Assembly of Enzyme-Like Nanofibrous G-Molecular Hydrogel for Printed Flexible Electrochemical Sensors. *Adv. Mater.* **2018,** *30*, e1706887.

83. Ravichandran, R.; Martinez, J.G.; Jager, E.W.H.; Phopase, J.; Turner, A.P.F., Type I collagen-derived injectable conductive hydrogel scaffolds as glucose sensors. *ACS Appl. Mater. Interfaces.* **2018,** *10*, 16244-16249.

84. Chung, J.S.; Hur, S.H., A highly sensitive enzyme-free glucose sensor based on Co3O4 nanoflowers and 3D graphene oxide hydrogel fabricated via hydrothermal synthesis. *Sens. Actuators B Chem.* **2016,** *223*, 76-82.

85. Darvishi, S.; Souissi, M.; Kharaziha, M.; Karimzadeh, F.; Sahara, R.; Ahadian, S., Gelatin methacryloyl hydrogel for glucose biosensing using Ni nanoparticles-reduced graphene oxide: an experimental and modeling study. *Electrochim. Acta* **2018,** *261*, 275-283.

86. Egawa, Y.; Seki, T.; Takahashi, S.; Anzai, J.-i., Electrochemical and optical sugar sensors based on phenylboronic acid and its derivatives. *Mater. Sci. Eng. C* **2011,** *31*, 1257-1264.

87. Guan, Y.; Zhang, Y., Boronic acid-containing hydrogels: synthesis and their applications. *Chem. Soc. Rev.* **2013,** *42*, 8106-21.

88. Zhai, W.; Sun, X.; James, T.D.; Fossey, J.S., Boronic Acid-Based Carbohydrate Sensing. *Chem. Asian J.* **2015,** *10*, 1836-48.

89. Russell, R.J.; Pishko, M.V.; Gefrides, C.C.; McShane, M.J.; Coté, G.L., A fluorescence-based glucose biosensor using concanavalin A and dextran encapsulated in a poly(ethylene glycol) hydrogel. *Anal. Chem.* **1999,** *71*, 3126-32.

90. Bruen, D.; Delaney, C.; Chung, J.; Ruberu, K.; Wallace, G.G.; Diamond, D.; Florea, L., 3D printed sugar-sensing hydrogels. *Macromol. Rapid. Commun.* **2020,** *41*, e1900610.

91. Kasák, P.; Mosnáček, J.; Danko, M.; Krupa, I.; Hloušková, G.; Chorvát, D.; Koukaki, M.; Karamanou, S.; Economou, A.; Lacík, I., A polysulfobetaine hydrogel for immobilization of a glucose-binding protein. *RSC advances* **2016,** *6*, 83890-83900.

92. Qasemi, S.; Ghaemy, M., Highly sensitive and strongly fluorescent gum tragacanth based superabsorbent hydrogel as a new biosensor for glucose optical detection. *J. Mater. Chem. C* **2020,** *8*, 4148-4156.

93. Dong, P.; Ko, B.S.; Lomeli, K.A.; Clark, E.C.; McShane, M.J.; Grunlan, M.A., A glucose biosensor based on phosphorescence lifetime sensing and a self-cleaning membrane. *Sumitted* **2021**.

94. Dong, P.; Singh, K.A.; Soltes, A.M.; Ko, B.S.; Gaharwar, A.K.; McShane, M.J.; Grunlan, M.A., A self-cleaning silicone containing double network hydrogel membrane to enhance glucose sensing. *Submitted* **2021**.

95. You, Y.-H.; Biswas, A.; Nagaraja, A.T.; Hwang, J.-H.; Coté, G.L.; McShane, M.J., Multidomain-based responsive materials with dual-mode optical readouts. *ACS Appl. Mater. Interfaces* **2019,** *11*, 14286-14295.

96. Ham, J.; Yun, B.J.; Koh, W.-G., SERS-based biosensing platform using shape-coded hydrogel microparticles incorporating silver nanoparticles. *Sens. Actuators B: Chem.* **2021,** *341*, 129989.

97. Park, H.-I.; Park, S.-Y., Smart fluorescent hydrogel glucose biosensing microdroplets with dual-mode fluorescence quenching and size reduction. *ACS Appl.*

Mater. Interfaces **2018,** *10*, 30172-30179.

98. Li, Z.; Zhu, B.; Duan, X.; Tang, W., The imaging of local glucose levels in tumor periphery via peroxyoxalate chemiluminescent nanoparticle–glucose oxidase–doped alginate hydrogel. *Anal. Methods* **2019,** *11*, 2763-2768.

99. Van Vlierberghe, S.; Dubruel, P.; Schacht, E., Biopolymer-based hydrogels as scaffolds for tissue engineering applications: a review. *Biomacromolecules* **2011,** *12*, 1387-1408.

100. Wisniewski, N.; Reichert, M., Methods for reducing biosensor membrane biofouling. *Colloids Surf. B. Biointerfaces* **2000,** *18*, 197-219.

101. Caló, E.; Khutoryanskiy, V.V., Biomedical applications of hydrogels: A review of patents and commercial products. *Eur. Polym. J.* **2015,** *65*, 252-267.

102. Peppas, N.A.; Hilt, J.Z.; Khademhosseini, A.; Langer, R., Hydrogels in biology and medicine: from molecular principles to bionanotechnology. *Adv. Mater.* **2006,** *18*, 1345-1360.

103. Slaughter, B.V.; Khurshid, S.S.; Fisher, O.Z.; Khademhosseini, A.; Peppas, N.A., Hydrogels in Regenerative Medicine. *Adv. Mater.* **2009,** *21*, 3307-3329.

104. Tavakoli, J.; Tang, Y., Hydrogel based sensors for biomedical applications: an updated review. *Polymers* **2017,** *9*, 364.

105. Kim, S.W.; Bae, Y.H.; Okano, T., Hydrogels: swelling, drug loading, and release. *Pharm. Res.* **1992,** *9*, 283-290.

106. Lin, C.-C.; Metters, A.T., Hydrogels in controlled release formulations: network design and mathematical modeling. *Adv. Drug Del. Rev.* **2006,** *58*, 1379-1408.

107. Yamamoto, M.; Ikada, Y.; Tabata, Y., Controlled release of growth factors based on biodegradation of gelatin hydrogel. *J. Biomater. Sci., Polym. Ed.* **2001,** *12*, 77-88.

108. Cai, S.; Liu, Y.; Shu, X.Z.; Prestwich, G.D., Injectable glycosaminoglycan hydrogels for controlled release of human basic fibroblast growth factor. *Biomaterials* **2005,** *26*, 6054-6067.

109. Holland, T.A.; Tabata, Y.; Mikos, A.G., Dual growth factor delivery from degradable oligo (poly (ethylene glycol) fumarate) hydrogel scaffolds for cartilage tissue engineering. *J. Control. Release* **2005,** *101*, 111-125.

110. Zhu, J.; Marchant, R.E., Design properties of hydrogel tissue-engineering scaffolds. *Expert Rev. Med. Devices* **2011,** *8*, 607-626.

111. Geckil, H.; Xu, F.; Zhang, X.; Moon, S.; Demirci, U., Engineering hydrogels as extracellular matrix mimics. *Nanomedicine* **2010,** *5*, 469-484.

112. Yu, B.; Wang, C.; Ju, Y.M.; West, L.; Harmon, J.; Moussy, Y.; Moussy, F., Use of hydrogel coating to improve the performance of implanted glucose sensors. *Biosens. Bioelectron.* **2008,** *23*, 1278-84.

113. Seliktar, D., Designing cell-compatible hydrogels for biomedical applications. *Science* **2012,** *336*, 1124-1128.

114. Canal, T.; Peppas, N.A., Correlation between mesh size and equilibrium degree of swelling of polymeric networks. *J. Biomed. Mater. Res.* **1989,** *23*, 1183-1193.

115. Amsden, B., Solute Diffusion within Hydrogels. Mechanisms and Models. *Macromolecules* **1998,** *31*, 8382-8395.

116. Axpe, E.; Chan, D.; Offeddu, G.S.; Chang, Y.; Merida, D.; Hernandez, H.L.; Appel, E.A., A multiscale model for solute diffusion in hydrogels. *Macromolecules* **2019,** *52*, 6889-6897.

117. Richbourg, N.R.; Peppas, N.A., The swollen polymer network hypothesis: Quantitative models of hydrogel swelling, stiffness, and solute transport. *Prog. Polym. Sci.* **2020,** *105*, 101243.

118. Hadjiev, N.A.; Amsden, B.G., An assessment of the ability of the

obstruction-scaling model to estimate solute diffusion coefficients in hydrogels. *J. Control. Release* **2015,** *199*, 10-16.

119. Am Ende, M.; Hariharan, D.; Peppas, N., Factors influencing drug and protein transport and release from ionic hydrogels. *React. Polym.* **1995,** *25*, 127-137.

120. Jimenez‐Vergara, A.C.; Lewis, J.; Hahn, M.S.; Munoz‐Pinto, D.J., An improved correlation to predict molecular weight between crosslinks based on equilibrium degree of swelling of hydrogel networks. *J. Biomed. Mater. Res. B* **2018,** *106*, 1339-1348.

121. Collins, M.C.; Ramirez, W.F., Transport through polymeric membranes. *J. Phys. Chem.* **1979,** *83*, 2294-2301.

122. Stringer, J.L.; Peppas, N.A., Diffusion of small molecular weight drugs in radiation-crosslinked poly(ethylene oxide) hydrogels. *J. Control. Release* **1996,** *42*, 195-202.

123. Hickey, A.S.; Peppas, N.A., Mesh size and diffusive characteristics of semicrystalline poly (vinyl alcohol) membranes prepared by freezing/thawing techniques. *J. Membr. Sci.* **1995,** *107*, 229-237.

124. Browning, M.B.; Wilems, T.; Hahn, M.; Cosgriff-Hernandez, E., Compositional control of poly(ethylene glycol) hydrogel modulus independent of mesh size. *J. Biomed. Mater. Res. A* **2011,** *98*, 268-73.

125. Peppas, N.; Bures, P.; Leobandung, W.; Ichikawa, H., Hydrogels in pharmaceutical formulations. *Eur. J. Pharm. Biopharm.* **2000,** *50*, 27-46.

126. Munoz-Pinto, D.J.; Samavedi, S.; Grigoryan, B.; Hahn, M.S., Impact of secondary reactive species on the apparent decoupling of poly (ethylene glycol) diacrylate hydrogel average mesh size and modulus. *Polymer* **2015,** *77*, 227-238.

127. Liao, H.; Munoz-Pinto, D.; Qu, X.; Hou, Y.; Grunlan, M.A.; Hahn, M.S., Influence of hydrogel mechanical properties and mesh size on vocal fold fibroblast extracellular matrix production and phenotype. *Acta Biomater.* **2008,** *4*, 1161-71.

128. Munoz-Pinto, D.J.; Bulick, A.S.; Hahn, M.S., Uncoupled investigation of scaffold modulus and mesh size on smooth muscle cell behavior. *J. Biomed. Mater. Res. A* **2009,** *90*, 303-16.

129. Pedron, S.; Pritchard, A.M.; Vincil, G.A.; Andrade, B.; Zimmerman, S.C.; Harley, B.A., Patterning three-dimensional hydrogel microenvironments using hyperbranched polyglycerols for independent control of mesh size and stiffness. *Biomacromolecules* **2017,** *18*, 1393-1400.

130. Hoare, T.R.; Kohane, D.S., Hydrogels in drug delivery: Progress and challenges. *Polymer* **2008,** *49*, 1993-2007.

131. Mauri, E.; Rossi, F.; Sacchetti, A., Tunable drug delivery using chemoselective functionalization of hydrogels. *Mater. Sci. Eng. C* **2016,** *61*, 851-857.

132. Zhong, T.; Jiang, Z.; Wang, P.; Bie, S.; Zhang, F.; Zuo, B., Silk fibroin/copolymer composite hydrogels for the controlled and sustained release of hydrophobic/hydrophilic drugs. *Int. J. Pharm.* **2015,** *494*, 264-270.

133. He, C.; Kim, S.W.; Lee, D.S., In situ gelling stimuli-sensitive block copolymer hydrogels for drug delivery. *J. Control. Release* **2008,** *127*, 189-207.

134. Vinogradov, S.V.; Bronich, T.K.; Kabanov, A.V., Nanosized cationic hydrogels for drug delivery: preparation, properties and interactions with cells. *Adv. Drug Del. Rev.* **2002,** *54*, 135-147.

135. Huang, Y.; Yu, H.; Xiao, C., pH-sensitive cationic guar gum/poly (acrylic acid) polyelectrolyte hydrogels: Swelling and in vitro drug release. *Carbohydr. Polym.* **2007,** *69*, 774-783.

136. Drury, J.L.; Mooney, D.J., Hydrogels for tissue engineering: scaffold design variables and applications. *Biomaterials* **2003,** *24*, 4337-4351.

137. Zhu, J., Bioactive modification of poly (ethylene glycol) hydrogels for tissue engineering. *Biomaterials* **2010,** *31*, 4639-4656.

138. Lin, C.-C.; Anseth, K.S., PEG hydrogels for the controlled release of biomolecules in regenerative medicine. *Pharm. Res.* **2009,** *26*, 631-643.

139. Cummins, B.M.; Garza, J.T.; Coté, G.L., Optimization of a Concanavalin A-based glucose sensor using fluorescence anisotropy. *Anal. Chem.* **2013,** *85*, 5397-5404.

140. Locke, A.K.; Cummins, B.M.; Abraham, A.A.; Coté, G.L., PEGylation of Concanavalin A to improve its stability for an in vivo glucose sensing assay. *Anal. Chem.* **2014,** *86*, 9091-9097.

141. Cummins, B.M.; Li, M.; Locke, A.K.; Birch, D.J.; Vigh, G.; Coté, G.L., Overcoming the aggregation problem: A new type of fluorescent ligand for ConA-based glucose sensing. *Biosensors Bioelectron.* **2015,** *63*, 53-60.

142. Schultz, S.G.; Solomon, A., Determination of the effective hydrodynamic radii of small molecules by viscometry. *J. Gen. Physiol.* **1961,** *44*, 1189-1199.

143. Zhou, Y.; Liedberg, B.; Gorochovceva, N.; Makuska, R.; Dedinaite, A.; Claesson, P.M., Chitosan-N-poly(ethylene oxide) brush polymers for reduced nonspecific protein adsorption. *J. Colloid Interface Sci.* **2007,** *305*, 62-71.

144. Nishimoto, A.; Watanabe, M.; Ikeda, Y.; Kohjiya, S., High ionic conductivity of new polymer electrolytes based on high molecular weight polyether comb polymers. *Electrochim. Acta* **1998,** *43*, 1177-1184.

145. Ju, H.K.; Kim, S.Y.; Lee, Y.M., pH/temperature-responsive behaviors of semi-IPN and comb-type graft hydrogels composed of alginate and poly(N-isopropylacrylamide). *Polymer* **2001,** *42*, 6851-6857.

146. Kaneko, Y.; Sakai, K.; Kikuchi, A.; Yoshida, R.; Sakurai, Y.; Okano, T., Influence of freely mobile grafted chain length on dynamic properties of comb-type grafted poly(N-isopropylacrylamide) hydrogels. *Macromolecules* **1995,** *28*, 7717-7723.

147. Annaka, M.; Matsuura, T.; Kasai, M.; Nakahira, T.; Hara, Y.; Okano, T., Preparation of comb-type N-isopropylacrylamide hydrogel beads and their application for size-selective separation media. *Biomacromolecules* **2003,** *4*, 395-403.

148. Annaka, M.; Sugiyama, M.; Kasai, M.; Nakahira, T.; Matsuura, T.; Seki, H.; Aoyagi, T.; Okano, T., Transport properties of comb-type grafted and normal-type N-isopropylacrylamide hydrogel. *Langmuir* **2002,** *18*, 7377-7383.

149. Ivopoulos, P.; Sotiropoulou, M.; Bokias, G.; Staikos, G., Water-soluble hydrogen-bonding interpolymer complex formation between poly (ethylene glycol) and poly (acrylic acid) grafted with poly (2-acrylamido-2-methylpropanesulfonic acid). *Langmuir* **2006,** *22*, 9181-9186.

150. Hou, Y.; Schoener, C.A.; Regan, K.R.; Munoz-Pinto, D.; Hahn, M.S.; Grunlan, M.A., Photo-cross-linked PDMSstar-PEG hydrogels: synthesis, characterization, and potential application for tissue engineering scaffolds. *Biomacromolecules* **2010,** *11*, 648-656.

151. Gacasan, E.G.; Sehnert, R.M.; Ehrhardt, D.A.; Grunlan, M.A., Templated, macroporous PEG‐DA hydrogels and their potential utility as tissue engineering scaffolds. *Macromol. Mater. Eng.* **2017,** *302*, 1600512.

152. Armstrong, J.K.; Wenby, R.B.; Meiselman, H.J.; Fisher, T.C., The hydrodynamic radii of macromolecules and their effect on red blood cell aggregation. *Biophys. J.* **2004,** *87*, 4259-4270.

153. Shiraishi, Y.; Akiyama, M.; Sato, T.; Hattori, M.; Komatsu, T., Size-dependent dextran loading in protein nanotube with an interior wall of concanavalin A. *Polym. Adv. Technol.* **2014,** *25*, 1247-1251.

154. Hannoun, B.J.M.; Stephanopoulos, G., Diffusion coefficients of glucose and ethanol in cell-free and cell-occupied calcium alginate membranes. *Biotechnol. Bioeng.* **1986,** *28*, 829-835.

155. Teixeira, J.A.; Mota, M.; Venâncio, A., Model identification and diffusion coefficients determination of glucose and malic acid in calcium alginate membranes. *Chem. Eng. J. Biochem. Eng. J.* **1994,** *56*, B9-B14.

156. Sharkawy, A.A.; Klitzman, B.; Truskey, G.A.; Reichert, W.M., Engineering the tissue which encapsulates subcutaneous implants. I. Diffusion properties. *J. Biomed. Mater. Res.* **1997,** *37*, 401-412.

157. Gong, J.P., Why are double network hydrogels so tough? *Soft Matter* **2010,** *6*, 2583-2590.

158. Prevention, C.f.D.C. *National diabetes statistics report, 2020*; Centers for Disease Control Prevention, US Department of Health Human Services: Atlanta, GA, 2020.

159. Battelino, T.; Dovc, K.; Bode, B.W., Continuous and intermittent glucose monitoring in 2019. *Diabetes Technol. Ther.* **2020,** *22*, S3-s16.

160. Edelman, S.V.; Argento, N.B.; Pettus, J.; Hirsch, I.B., Clinical implications of real-time and intermittently scanned continuous glucose monitoring. *Diabetes Care* **2018,** *41*, 2265-2274.

161. Rodbard, D., Continuous glucose monitoring: a review of successes, challenges, and opportunities. *Diabetes Technol. Ther.* **2016,** *18*, S2-3-S2-13.

162. Ajjan, R.; Slattery, D.; Wright, E., Continuous glucose monitoring: A brief review for primary care practitioners. *Adv Ther* **2019,** *36*, 579-596.

163. Foster, N.C.; Beck, R.W.; Miller, K.M.; Clements, M.A.; Rickels, M.R.; DiMeglio, L.A.; Maahs, D.M.; Tamborlane, W.V.; Bergenstal, R.; Smith, E.; Olson, B.A.; Garg, S.K., State of type 1 diabetes management and outcomes from the T1D exchange in 2016-2018. *Diabetes Technol. Ther.* **2019,** *21*, 66-72.

164. Tanenbaum, M.L.; Hanes, S.J.; Miller, K.M.; Naranjo, D.; Bensen, R.; Hood, K.K., Diabetes device use in adults with type 1 diabetes: barriers to uptake and potential intervention targets. *Diabetes Care* **2017,** *40*, 181-187.

165. Mujeeb-U-Rahman, M.; Nazari, M.H.; Sencan, M.; Antwerp, W.V., A novel needle-injectable millimeter scale wireless electrochemical glucose sensing platform for artificial pancreas applications. *Sci. Rep.* **2019,** *9*, 17421.

166. Hsiao, K.-L., What drives smartwatch adoption intention? Comparing Apple and non-Apple watches. *Library Hi Tech* **2017,** *35*, 186-206.

167. Chuah, S.H.-W.; Rauschnabel, P.A.; Krey, N.; Nguyen, B.; Ramayah, T.; Lade, S., Wearable technologies: The role of usefulness and visibility in smartwatch adoption. *Computers in Human Behavior* **2016,** *65*, 276-284.

168. Canhoto, A.I.; Arp, S., Exploring the factors that support adoption and sustained use of health and fitness wearables. *Journal of Marketing Management* **2017,** *33*, 32-60.

169. Russell, R.J.; Pishko, M.V.; Gefrides, C.C.; McShane, M.J.; Coté, G.L., A Fluorescence-based glucose biosensor using concanavalin A and dextran encapsulated in a poly(ethylene glycol) hydrogel. *Anal. Chem.* **1999,** *71*, 3126-3132.

170. Sawayama, J.; Okitsu, T.; Nakamata, A.; Kawahara, Y.; Takeuchi, S., Hydrogel glucose sensor with in vivo stable fluorescence intensity relying on antioxidant enzymes for continuous glucose monitoring. *iScience* **2020,** *23*, 101243.

171. Yetisen, A.K.; Jiang, N.; Fallahi, A.; Montelongo, Y.; Ruiz-Esparza, G.U.; Tamayol, A.; Zhang, Y.S.; Mahmood, I.; Yang, S.-A.; Kim, K.S.; Butt, H.; Khademhosseini, A.; Yun, S.-H., Glucose-sensitive hydrogel optical fibers functionalized with phenylboronic acid. *Adv. Mater.* **2017,** *29*, 1606380.

172. Collier, B.B.; McShane, M.J., Dynamic windowing algorithm for the fast and accurate determination of luminescence lifetimes. *Anal. Chem.* **2012,** *84*, 4725-4731.

173. Na, R.; Stender, I.-M.; Henriksen, M.; Wulf, H.C., Autofluorescence of human skin is age-related after correction for skin pigmentation and redness. *Journal of investigative dermatology* **2001,** *116*, 536-540.

174. Kollias, N.; Zonios, G.; Stamatas, G.N., Fluorescence spectroscopy of skin. *Vib. Spectrosc* **2002,** *28*, 17-23.

175. Colvin, L.; Dong, P.; Means, A.K.; Grunlan, M.; Coté, G. In *Assessment of wavelengths with skin tones for an implantable FRET-based glucose biosensor*, SPIE BiOS, SPIE: 2019; 108850Y.

176. Collier, B.B.; McShane, M.J., Time-resolved measurements of luminescence. *J. Lumin.* **2013,** *144*, 180-190.

177. Collier, B.; Long, R.; McShane, M. In *Dual-probe luminescence lifetime measurements for the oxygen compensation in enzymatic biosensors*, SENSORS, 2009 IEEE, 25-28 Oct. 2009; 2009; 703-706.

178. Bornhoeft, L.R.; Biswas, A.; McShane, M.J., Composite hydrogels with engineered microdomains for optical glucose sensing at low oxygen conditions. *Biosensors* **2017,** *7*, 8.

179. Biswas, A.; Bornhoeft, L.R.; Banerjee, S.; You, Y.-H.; McShane, M.J., Composite Hydrogels Containing Bioactive Microreactors for Optical Enzymatic Lactate Sensing. *ACS Sensors* **2017,** *2*, 1584-1588.

180. Falohun, T.; McShane, M.J., An optical urate biosensor based on urate oxidase and long-lifetime metalloporphyrins. *Sensors* **2020,** *20*, 959.

181. Collier, B.B.; McShane, M.J., Dynamic Windowing Algorithm for the Fast and Accurate Determination of Luminescence Lifetimes. *Anal. Chem.* **2012,** *84*, 4725-4731.

182. Collier, B.B.; McShane, M.J., Temperature Compensation of Oxygen Sensing Films Utilizing a Dynamic Dual Lifetime Calculation Technique. *IEEE Sens. J.* **2014,** *14*, 2755-2764.

183. Wisniewski, N.; Moussy, F.; Reichert, W., Characterization of implantable biosensor membrane biofouling. *J. Anal. Chem.* **2000,** *366*, 611-621.

184. Geckil, H.; Xu, F.; Zhang, X.; Moon, S.; Demirci, U., Engineering hydrogels as extracellular matrix mimics. *Nanomed. J.* **2010,** *5*, 469-484.

185. Werner, J.; Buse, M., Temperature profiles with respect to inhomogeneity and geometry of the human body. *J. Appl. Physiol.* **1988,** *65*, 1110-1118.

186. Montgomery, L.D.; Williams, B.A., Effect of ambient temperature on the thermal profile of the human forearm, hand, and fingers. *Ann. Biomed. Eng.* **1976,** *4*, 209-219.

187. Bolles, R.C.; Duncan, P.M., Daily course of activity and subcutaneous body temperature in hungry and thirsty rats. *Physiol. Behav.* **1969,** *4*, 87-89.

188. Shido, O.; Sakurada, S.; Kohda, W.; Nagasaka, T., Day—Night changes of body temperature and feeding activity in heat-acclimated rats. *Physiol. Behav.* **1994,** *55*, 935-939.

189. Swinehart, D.F., The beer-lambert law. *J. Chem. Educ.* **1962,** *39*, 333.

190. Ye, G.; Li, X.; Wang, X., Diffraction grating of hydrogel functionalized with glucose oxidase for glucose detection. *ChemComm* **2010,** *46*, 3872-3874.

191. Kalisz, H.M.; Hecht, H.-J.; Schomburg, D.; Schmid, R.D., Effects of carbohydrate depletion on the structure, stability and activity of glucose oxidase from Aspergillus niger. *Biochim. Biophys. Acta, Protein Struct. Mol. Enzymol.* **1991,** *1080*, 138-142.

192. Bankar, S.B.; Bule, M.V.; Singhal, R.S.; Ananthanarayan, L., Glucose oxidase — an overview. *Biotechnol. Adv.* **2009,** *27*, 489-501.

193. Sigma-Aldrich Enzymatic assay of glucose oxidase. https://www.sigmaaldrich.com/technical-documents/protocols/biology/enzymatic-assay-of-glucose-oxidase.html (accessed 10-11-2021).

194. Bergmeyer, H.U.; Gawehn, K.; Grassl, M., *Methods of enzymatic analysis* Second ed.; Academic Press Inc., New York, 1974; Vol. I, 457-458.

195. Kang, S.I.; Bae, Y.H., A sulfonamide based glucose-responsive hydrogel with covalently immobilized glucose oxidase and catalase. *J. Controlled Release* **2003,** *86*, 115-121.

196. Zhu, H.; Srivastava, R.; Brown, J.Q.; McShane, M.J., Combined physical and chemical immobilization of glucose oxidase in alginate microspheres improves stability of encapsulation and activity. *Bioconjugate Chem.* **2005,** *16*, 1451-1458.

197. Xing, W.; Yin, M.; Lv, Q.; Hu, Y.; Liu, C.; Zhang, J., 1 - Oxygen solubility,

diffusion coefficient, and solution viscosity. In *Rotating electrode methods and oxygen reduction electrocatalysts*, Xing, W.; Yin, G.; Zhang, J., Eds. Elsevier: Amsterdam, 2014; pp 1-31.

198. Feil, H.; Bae, Y.H.; Feijen, J.; Kim, S.W., Effect of comonomer hydrophilicity and ionization on the lower critical solution temperature of N-isopropylacrylamide copolymers. *Macromolecules* **1993,** *26*, 2496-2500.

199. Abraham, R.J.; Eivazi, F.; Pearson, H.; Smith, K.M., π–π Aggregation in metalloporphyrins: causative factors. *ChemComm* **1976**, 699-701.

200. Pasternack, R.F.; Francesconi, L.; Raff, D.; Spiro, E., Aggregation of nickel(II), copper(II), and zinc(II) derivatives of water-soluble porphyrins. *Inorg. Chem.* **1973,** *12*, 2606-2611.

201. Kiparissides, C.; Seferlis, P.; Mourikas, G.; Morris, A.J., Online optimizing control of molecular weight properties in batch free-radical polymerization reactors. *Ind. Eng. Chem. Res.* **2002,** *41*, 6120-6131.

202. Sugimura, A.; Asai, M.; Matsunaga, T.; Akagi, Y.; Sakai, T.; Noguchi, H.; Shibayama, M., Mechanical properties of a polymer network of Tetra-PEG gel. *Polym. J.* **2013,** *45*, 300-306.

203. Biswas, A.; Nagaraja, A.T.; You, Y.-H.; Roberts, J.R.; McShane, M.J., Cross-linked nanofilms for tunable permeability control in a composite microdomain system. *RSC Adv.* **2016,** *6*, 71781-71790.

204. Unruh, R.M.; Roberts, J.R.; Nichols, S.P.; Gamsey, S.; Wisniewski, N.A.; McShane, M.J., Preclinical Evaluation of Poly(HEMA-co-acrylamide) Hydrogels Encapsulating Glucose Oxidase and Palladium Benzoporphyrin as Fully Implantable Glucose Sensors. *J Diabetes Sci Technol* **2015,** *9*, 985-92.

205. Roberts, J.R.; Park, J.; Helton, K.; Wisniewski, N.; McShane, M.J., Biofouling of polymer hydrogel materials and its effect on diffusion and enzyme-based luminescent glucose sensor functional characteristics. *J Diabetes Sci Technol* **2012,** *6*, 1267-75.

206. Real-world safety of an implantable continuous glucose sensor over multiple cycles of use: A post-market registry study. **2020,** *22*, 48-52.

207. Sheng, T.; Offringa, R.; Kerr, D.; Clements, M.; Fischer, J.; Parks, L.; Greenfield, M., Diabetes healthcare professionals use multiple continuous glucose monitoring data indicators to assess glucose management. *J. Diabetes Sci. Technol.* **2019,** *14*, 271-276.

208. Sanchez, P.; Ghosh-Dastidar, S.; Tweden, K.S.; Kaufman, F.R., Real-world data from the first U.S. commercial users of an implantable continuous glucose sensor. *Diabetes Technol. Ther.* **2019,** *21*, 677-681.

209. Battelino, T.; Danne, T.; Bergenstal, R.M.; Amiel, S.A.; Beck, R.; Biester, T.; Bosi, E.; Buckingham, B.A.; Cefalu, W.T.; Close, K.L.; Cobelli, C.; Dassau, E.; DeVries, J.H.; Donaghue, K.C.; Dovc, K.; Doyle, F.J.; Garg, S.; Grunberger, G.; Heller, S.; Heinemann, L.; Hirsch, I.B.; Hovorka, R.; Jia, W.; Kordonouri, O.; Kovatchev, B.; Kowalski, A.; Laffel, L.; Levine, B.; Mayorov, A.; Mathieu, C.; Murphy, H.R.; Nimri, R.; Nørgaard, K.; Parkin, C.G.; Renard, E.; Rodbard, D.; Saboo, B.; Schatz, D.; Stoner, K.; Urakami, T.; Weinzimer, S.A.; Phillip, M., Clinical targets for continuous glucose monitoring data interpretation: recommendations from the international consensus on time in range. *Diabetes Care* **2019,** *42*, 1593.

210. McNichols, R.J.; Coté, G.L., Optical glucose sensing in biological fluids: an overview. *J. Biomed. Opt.* **2000,** *5*, 5-16.

211. Oliver, N.S.; Toumazou, C.; Cass, A.E.; Johnston, D.G., Glucose sensors: a review of current and emerging technology. *Diabet. Med.* **2009,** *26*, 197-210.

212. Onuki, Y.; Bhardwaj, U.; Papadimitrakopoulos, F.; Burgess, D.J., A review of the biocompatibility of implantable devices: current challenges to overcome foreign body response. *J. Diabetes Sci. Technol.* **2008,** *2*, 1003-1015.

213. Ngo, B.K.D.; Grunlan, M.A., Protein resistant polymeric biomaterials. Lett., A. M., Ed. ACS Publications: 2017.

214. Jesmer, A.H.; Wylie, R.G., Controlling experimental parameters to improve characterization of biomaterial fouling. *Front. Chem.* **2020,** *8*, 604236-604236.

215. Hou, Y.; Matthews, A.R.; Smitherman, A.M.; Bulick, A.S.; Hahn, M.S.; Hou, H.; Han, A.; Grunlan, M.A., Thermoresponsive nanocomposite hydrogels with cell-releasing behavior. *Biomaterials* **2008,** *29*, 3175-3184.

216. Wu, S.; Zhang, X.; Sun, Y.; Yang, H.; Lin, B.; Han, X.; Chen, P., Study on the influence of crosslinking density and free polysiloxan chain length on oxygen permeability and hydrophilicity of multicomponent silicone hydrogels. *Colloid Polym. Sci.* **2021**.

217. Wu, B.; Wiseman, M.E.; Seitz, M.E.; Tomić, K.; Heise, A.; Brougham, D.F.; Litvinov, V.M., Impact of morphology on O_2 permeability in silicone hydrogel membranes: new insights into domain percolation from experiments and simulations. *J. Membr. Sci.* **2021,** *621*, 118970.

218. Lamberti, A.; Marasso, S.L.; Cocuzza, M., PDMS membranes with tunable gas permeability for microfluidic applications. *RSC Adv.* **2014,** *4*, 61415-61419.

219. Caló, E.; Khutoryanskiy, V.V., Biomedical applications of hydrogels: A review of patents and commercial products. *Eur. Polym. J.* **2015,** *65*, 252-267.

220. Jacob, J.T., Biocompatibility in the development of silicone-hydrogel lenses. *Eye & Contact Lens* **2013,** *39*.

221. Keir, N.; Jones, L., Wettability and Silicone Hydrogel Lenses: A Review. *Eye & Contact Lense* **2013,** *39*, 100-108.

222. Frassica, M.T.; Jones, S.K.; Diaz-Rodriguez, P.; Hahn, M.S.; Grunlan, M.A., Incorporation of a silicon-based polymer to PEG-DA templated hydrogel scaffolds for bioactivity and osteoinductivity. *Acta Biomater.* **2019,** *99*, 100-109.

223. Roy, C.K.; Guo, H.L.; Sun, T.L.; Ihsan, A.B.; Kurokawa, T.; Takahata, M.; Nonoyama, T.; Nakajima, T.; Gong, J.P.J.A.m., Self‐Adjustable Adhesion of Polyampholyte Hydrogels. **2015,** *27*, 7344-7348.